L-Università ta' Malta
Faculty of Engineering

MASTER OF SCIENCE IN ENGINEERING DISSERTATION

Development of an Intent Interpretation System for a Minimal Anthropomorphic Prosthetic Hand

RACHEL CAUCHI

Supervised by:

PROF. DR ING. KENNETH P. CAMILLERI

Co-supervised by:

PROF. DR ING. MICHAEL A. SALIBA

DR JESMOND ATTARD

A dissertation submitted in partial fulfilment of the requirements for the degree of Master of Science in Engineering

by the

Faculty of Engineering

July 2021

L-Università ta' Malta
Faculty of Engineering

Copyright Notice

1) Copyright in text of this dissertation rests with the Author. Copies (by any process) either in full, or of extracts may be made only in accordance with regulations held by the Library of the University of Malta. Details may be obtained from the Librarian. This page must form part of any such copies made. Further copies (by any process) made in accordance with such instructions may not be made without the permission (in writing) of the Author.

2) Ownership of the right over any original intellectual property which may be contained in or derived from this dissertation is vested in the University of Malta and may not be made available for use by third parties without the written permission of the University, which will prescribe the terms and conditions of any such agreement.

3) Publication rights over the academic and/or research results presented in this dissertation are vested jointly in both the Author and his/her academic Supervisor(s), and unless such rights are explicitly waived in writing, both parties must be listed among the authors in any academic publication that is derived substantially from this work. Furthermore, any other public communication / disclosure of any form that focuses on the project must acknowledge that this work has been carried out by the Author and the Supervisor(s) (named explicitly) through the University of Malta.

Dedication

I dedicate this dissertation to Ing. Vince Rapa, who taught me so much in so little time. I only wish to be as resilient and as fearless in the pursuit of fulfilling my wildest dreams. Your laugh still echoes in my mind and your energy still resonates in my heart.

Abstract

Upper-limb amputation brings about its challenges, including loss of identity as well as independence. Several prosthetic hands have been developed to aid amputees with regaining normal function following their traumatic experience, however, acceptance of such foreign body extensions is challenging. This is especially true when the chosen artificial limb poses a number of operational limitations whilst feeling unnatural. This results in a reduction of the overall experience whilst posing the risk of device rejection.

In order to satisfy the end user with an innovative intent interpretation system to be used with an anthropomorphic prosthetic hand, the ultimate objective of this research project was to carry out a systematic exercise to seek a practical solution for the framework which best addresses a trade-off problem between simplicity, dexterity and usability. This problem was mainly addressed by investigating surface electromyography signal acquisition methods in relation to isometric and anisometric contractions which led to the choice of using transient signals for motion identification and steady-state signals for force estimation.

The intent interpretation framework was also developed with the ability of reliably detecting movement phases from no movement phases, only triggering a classifier to make a motion prediction with true movement detection. A classifier was designed to distinguish between four specifically chosen motions from a rest or neutral state, providing the amputee with the capability of performing a large percentage of activities of daily living. Most importantly, the system was set to recognise human instructions in the most simple and intuitive manner to humans.

The intent interpretation framework was designed to be user-specific and five normal limbed subjects and two transradial amputees performed offline, episodic experiments which resulted in successful statistical results on the movement detection and identification performance of the system. Successful inter-session performance, as well as force estimation performance results were also obtained through further episodic, continuous and force estimation tests performed by a smaller subject pool.

A successful maximised trade-off between the three important attributes was achieved through this framework, which is capable of exploiting the natural human sense of intuition, whilst still providing the end-user with the capability of performing a vast majority of daily tasks in a reliable and practical way.

Acknowledgements

This dissertation would not have been possible without the help and support of several individuals, who all deserve my sincere gratitude.

My first thanks go to my supervisor, Prof. Dr Ing. Kenneth P. Camilleri for sharing his wisdom on the subject as well as providing the necessary and crucial guidance to continue moving forward and achieve the targeted goals.

Thanks also to my co-supervisor Prof. Dr Ing. Michael A. Saliba, who is also the primary investigator of the MAProHand project of which this work forms part, for his continuous high-level guidance that was crucial to the success of this research.

I would also like to thank my other co-supervisor Dr Jesmond Attard, for his crucial insights into practical amputee-related issues in the field, and his help in recruiting amputee volunteers for the experiments.

A heartfelt thanks also goes to the faculty staff, especially to the staff at the Biomedical Engineering Laboratory and the Robotic Systems Laboratory who have always been so patient and helpful whenever required.

A special thanks also goes to all the subjects who have voluntarily participated in these experiments. Without your participation, this study would not have been possible.

My appreciation also goes towards the Malta Council for Science & Technology and the FUSION Research and Innovation programme for funding the research.

Finally, my greatest thanks go to my family and friends who have been supportive throughout this journey. Your constant presence has been indispensable.

Oliver – your patience, reassurance, help and support were always my fuel at my lowest. Thank you for being you.

Table of Contents

List of Figures

List of Tables

List of Abbreviations

ADL	Activity of Daily Living
AR	Autoregressive
BLE	Bluetooth Low Energy
BPM	Beats Per Minute
CNN	Convolution Neural Network
CNS	Central Nervous System
DOFs	Degrees of Freedom
EMD	Electromechanical Delay
EMG	Electromyography
ECOC	Error-Correcting Output Codes
FC	Fuzzy Clustering
FD	Frequency-Domain
FN	False Negative
FP	False Positive
GUI	Graphical User Interface
IED	Interelectrode Distance
IEMG	Integrated EMG
KNN	K-Nearest Neighbour
LD	Log Detector
LDA	Linear Discriminant Analysis
MAProHand	Development of the Mechanical and Control Framework for a Minimal Anthropomorphic Prosthetic Hand
MAV	Mean Absolute Value
MAVS	Mean Absolute Value Slope
MD	Mahalonobis Distance
MLP	Multi-layer Perceptron
MU	Motor Unit
MUAPT	Motor Unit Action Potential Train
MVC	Maximum Voluntary Contraction
NLR	Non-linear Logistic Regression
NN	Neural Network
PC	Principal Component
PG	Proto-Gesture

PM	Proto-Motion
Q-Q	Quantile-Quantile
RFN	Regulatory Feedback Network
RMS	Root Mean Square
RMSE	Root Mean Squared Error
SDK	Software Development Kit
sEMG	Surface Electromyography
SENIAM	Surface Electromyography for the Non-Invasive Assessment of Muscles
SSC	Slope Sign Changes
SVM	Support Vector Machine
TD	Time-Domain
TF	Time-Frequency
TMG	Tactile Myography
TMR	Targeted Muscle Reinnervation
TN	True Negative
TP	True Positive
UM	University of Malta
VAR	Variance
WAMP	Willison's Amplitude
WL	Waveform Length
ZC	Zero Crossings

Glossary of Symbols and Notations

D	Feature Vector Dimension
$\delta_k(\boldsymbol{x})$	Linear score function of Class k
F_s	Sampling Frequency
γ	Regularisation Term
$\mathbf{I}$	Identity Matrix
μ	Mean
$\boldsymbol{\mu_k}$	Mean of the Training Feature Vectors for Class k
$\boldsymbol{M}$	Coding Design Matrix
$\phi(\boldsymbol{x})$	Fixed feature space transformation
$p(C_k)$	Class prior for Class k
$p(C_k\|\boldsymbol{x})$	Posterior Probability for Class k
$p(\boldsymbol{x}\|C_k)$	Conditional Probability Density Function for Class k
P_{THmax}	Desired upper boundary
P_{THmin}	Desired lower boundary
PC_i	Proportional Control Output given Grasp i
σ	Standard Deviation
$\boldsymbol{\sigma}(a)$	Logistic Sigmoid
$\boldsymbol{\Sigma}$	Covariance Matrix
$\|\boldsymbol{\Sigma}\|$	Determinant of the Covariance Matrix
$\widehat{\boldsymbol{\Sigma}}$	Pooled-in Covariance Matrix
$\widehat{\boldsymbol{\Sigma}}_{\boldsymbol{\gamma}}$	Regularised Covariance Matrix
θ	Angle
$TH_{max,i}$	The upper bound of Grasp i
$TH_{min,i}$	The lower bound of Grasp i
$\boldsymbol{w}$	Vector containing the coefficients which define an orthogonal vector to the hyperplane
W_T	Window used to determine Movement Detection validity
WL_M	Window Length used to determine the EMG RMS Maxima for every Channel
WL_{RMS}	Window Length used as a Sliding Window RMS computation
$x_{i,j,k}^{Tr}$	The RMS of the Training Data from Grasp i, Channel j and Computation Window k

$x_{Min,i}^{Tr}$	The minimum computed RMS value from the Training Data for Grasp *i*
$x_{Max,i}^{Tr}$	The maximum computed RMS value from the Training Data for Grasp *i*
ξ	Slack Variable

1. Introduction

Upper limb loss is perceived as a devastating occurrence, totally changing a person's lifestyle whilst affecting the individual's social and private life [1]. This impairment adversely affects an amputee's quality of life, reducing the overall interaction capability and decline in performance of activities of daily living success rates. Approximately 4,000 persons a year suffer from an upper-limb amputation in Italy, whilst 20% of all amputations in the USA are of the upper-limb type [2].

Due to these numbers, the interest in prosthetics is outstanding, with the field having gained various interested researchers to work on ongoing research projects. In fact, a remarkable number of papers regarding upper-limb prosthetics research have been published in the last twenty years, with figures showing that approximately 4,000 publications in relation to this field were available until 2010, 70% of which having been published between 2001 and 2010 [3]. With further innovative technologies, materials, methods and ideas, the publication numbers continue to increase. However, due to the complexity that comes along with the development of a prosthetic hand, the studies that are carried out are widely spread, aimed at targeting different problems. This thus leads to difficulty for most researchers to stay up to date with all developed prosthetic systems and their different capabilities. This has led to market and research achievements to remain disconnected [4]. Furthermore, even though the technical and clinical advancements made from the initiation of upper-limb prosthetics have been game changing, several limitations are still present within the prosthetics industry. These limitations include, and are not limited to, noisy prosthetics due to the number and operation of actuators, lack of sensory feedback provided to the amputee and the lack of intuition and reliability in the prosthetic control aspect [2].

A problem that has been identified at the University of Malta (UM) in the recent years [5] [6] is the difficulty of achieving a balance between three very important attributes related to prosthetics, namely, *simplicity*, *dexterity* and *usability*. While it is understood that the optimisation of the trade-off between these three attributes is difficult to obtain due to their conflicting natures when it comes to design, a sensible balance is essential for a device to be successfully effective and accepted by the amputee community. However, this problem has to date been mostly identified from a mechanical design point of view. Nevertheless, this study aims to find a solution to satisfy this three-attribute trade-off solely from a prosthetic action intent point of view for its eventual integration with the mechanical device currently being developed concurrently at UM.

Both this study and the mechanical device are being carried out as part of the project entitled *The Development of the Mechanical and Control Framework for a Minimal Anthropomorphic Prosthetic Hand* (MAProHand [7]) at UM and with the collaboration of the company Orthopaedic Centre Malta. The MAProHand project is financed by the Malta Council for Science & Technology through FUSION: The R&I Technology Development Programme 2018 [1].

Therefore, the primary research objective of this research project was identified to be a systematic exercise to seek a practical solution for the control system of a minimal anthropomorphic artificial hand which best addresses the common trade-off problem between simplicity, dexterity and usability. In this work, a control system or framework refers to the analysis of input signals for the recognition of prosthesis action intent, which has also been termed as an intent interpretation system. Thus, in this context, a control system does not refer to a system having a mathematical relationship between its input and output with feedback logic.

To reach this trade-off objective, the aim was to satisfy a balance between these three attributes which have been defined as follows:

- A *simple* system mainly focusing on a simple command system which is intuitive to use (as is our normal hand) and does not require the amputee to re-learn the fundamentals of limb operation. This aims to reduce the learning curves that come with most prosthetic hands whilst promoting a more natural sense of control;
- *A dexterous* system having appropriate hand capability with a sufficient degree of freedom allowance for the user to be capable of performing a vast majority of the most common activities of daily living. This mostly relates to the kind of gestures and grasps that are made available to the user;
- A *usable* system with a reliable and practical intent interpretation system which has a large resemblance to normal human hand functionality. This relates to how reliably the user can utilise the prosthesis and how intelligent the system is with extracting different user intentions.

These definitions go hand-in-hand with the claim that the ultimate goal in upper-limb prostheses research and development is to have a system which functions as closely as possible to an actual human hand, with all its capabilities, giving back the amputee the

[1] Contract Number R&I-2017-028T.

experience of functionality which they had prior to limb loss [8] [9].

The umbrella term of *intuition* has been chosen to be the most important aspect when it comes to this above-mentioned research objective, since this will be the most important element for the design and development of the action intent recognition of the prosthesis. This is so since the lack of intuition provided within the currently available devices is seen as an overall limitation; affecting the general user experience and requiring extensive re-learning training [2]. This choice is also believed to allow us to successfully balance the three above-mentioned attributes. In fact, an intent interpretation interface via surface electromyography (sEMG) has been chosen to facilitate the exploitation of the human sense of intuition, to our own advantage. The sEMG phenomenon is the extraction of myoelectric signals formed by physiological changes in muscle fiber membrane states in response to instructions sent to motor units by the Central Nervous System (CNS). This information is gathered non-invasively through surface electrodes which may then be manipulated to aid with the determination of naturally intended hand movements [10] [11].

The broad primary research objective was therefore split into smaller milestones to be tackled throughout the course of this dissertation and may be identified as follows:

- Identification of various prosthetic control systems which have been researched and implemented through a thorough literature review to identify which measures shall contribute to the three-attribute trade-off satisfaction;
- Familiarisation with the relationships that exist between sEMG signals and different muscle contractions for intuitive action intent system development;
- Development of an intent interpretation system based on the sEMG signals recorded during the performance of different motions, as well as force exertion in different grasps for eventual user-intended prosthetic hand control;
- Testing of the system by normal-limbed subjects as well as amputees to determine its performance in ideal, laboratory conditions.

The next chapters of this dissertation explore these different objectives accordingly. Firstly, Chapters 2 and 3 are literature review chapters which identify the different prosthetic systems that have been investigated, leading to specific decisions contributing to our system design. Chapter 4 explores the relationships that may be obtained between sEMG signal features and changes in velocities and forces. This chapter gives an insight into what kind of sEMG signals may be used to extract specific

information, which were then used in the intent interpretation system design as explained in Chapter 5. Chapter 6 discusses the testing methodologies and the data processing methodologies used. Chapter 7 then presents all the results obtained which are also analysed and discussed. Finally, the dissertation is concluded with Chapter 8.

2. Hand Prostheses Control Review

It is known that the majority of upper-limb loss cases are due to trauma following work and road related accidents, as well as war injuries. However, illnesses and other medical conditions such as cancer, tumours, diabetes and vascular complications are also cause for amputation [12]. The amputee demographic also includes those with congenital limb deficiencies who are born with deformed or missing limbs, at times still requiring surgery or amputation [13].

There are various anatomic levels at which the hand may be amputated, including transhumeral amputation, transradial amputation, partial-hand amputation and shoulder, elbow and wrist disarticulations [14]. Four of these levels are shown in Figure 2.1. While it is generally said that the longer the remaining limb is, the better it is for the patient to be fitted with a prosthesis due to more joints remaining intact [15], the most common amputation levels are transradial, at 65% [14]. Transradial amputations take place between the wrist and elbow and due to these high figures, this work will solely focus on prosthetic hands for transradial amputees.

Beasley [16] describes how an amputee goes through three stages following his amputation, which are similar to grieving stages; such that the first stage is disbelief, followed by realisation and finally, adaptation. The most important stage from these three is the realisation stage since this is the point at which the amputee is faced with the opportunity to start with the process of mentally accepting this loss and to start adapting accordingly. Therefore, it is crucial that during this stage, the amputee is offered an optional aid, such as a prosthetic limb, to help with this transition. Failure of mental acceptance at this stage may lead to rehabilitation failures, which is why it is important that the prosthetic hands offered to the patient are appealing and provide the user with satisfactory results.

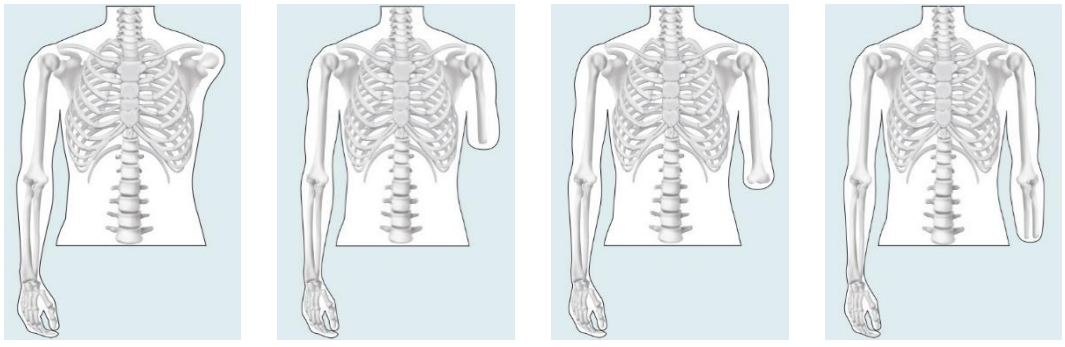

(a) (b) (c) (d)

Figure 2.1 - (a) Shoulder Disarticulation, (b) Transhumeral Amputation, (c) Elbow Disarticulation and (d) Transradial Amputation Levels [17].

The prosthetic devices field is a multidisciplinary one, consisting of many subdivisions which ultimately need to merge together. Knowledge with regard to human physiology and anatomy is required in order to be able to design a functional system using several software, electrical and electronic designs and mechanical designs, amongst others [18]. Since the human hand is a very powerful tool to any human being whilst also being a sophisticated means for physical and social interaction, there are a lot of aspects that one needs to figure out with regard to its anatomy and functionality. The hand allows us to accomplish many movements, ranging from very powerful to utterly precise tasks which are only possible due to the available Degrees of Freedom (DoFs) which amount to more than 20, and thumb opposition dynamics [1]. Having said that, even though the technical and clinical advancements made from the initiation of upper-limb prosthetics have been game changing, several limitations are still present within the prosthetics industry. From an intent interpretation point of view, these limitations are mostly due to the lack of intuitivism as well as low reliability of the overall system [2]. This leads us to perform a review of the different prosthetic systems that exist on the market in order to determine which kind of control system would be best to implement to obtain a system which maximally balances the simplicity, dexterity and usability attributes mentioned in Chapter 1.

2.1. Upper-Limb Prosthetic Systems

There are various types of upper-limb prostheses which are commercially available or have been developed for research purposes. A brief hierarchy of the most important prosthetic classes is as shown in Figure 2.2. The most basic distinction between some of the available prostheses is whether they are simply used as passive accessories or active tools and the following sub-sections delve into the differences of the listed prostheses types.

2.1.1. Passive Prostheses

There are two types of passive prostheses, cosmetic and functional. Cosmetic prostheses, as shown in Figure 2.3, offer no functionality and are simply seen as an aesthetic substitution to the lost limb. This substitution also provides aesthetic and psychological support to the amputee who opts to wear it. Meanwhile, functional prosthetic devices have very specific purposes, developed with the aim of facilitating some kind of activity, usually sport or work related [1] [4], as shown in Figure 2.4.

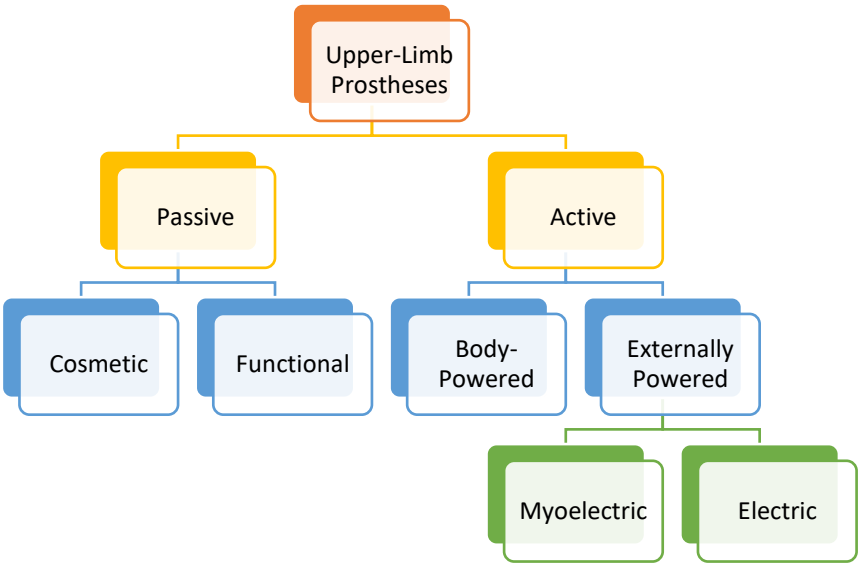

Figure 2.2 - Upper-Limb Prostheses Classifications [2].

Figure 2.3 - Lifelike Cosmetic Prostheses [19].

Figure 2.4 - A Functional Prosthesis used for Sports [20].

2.1.2. Active Prostheses

For body-powered prostheses, energy is harnessed from other body muscles in order to operate a cable through a link, as shown in Figure 2.5. While such upper-limb prosthetics are known to be difficult for some to operate due to the required body power whilst also lacking in cosmetic appeal, such systems are essentially lower in cost than other prostheses whilst proving to be less expensive to repair [1].

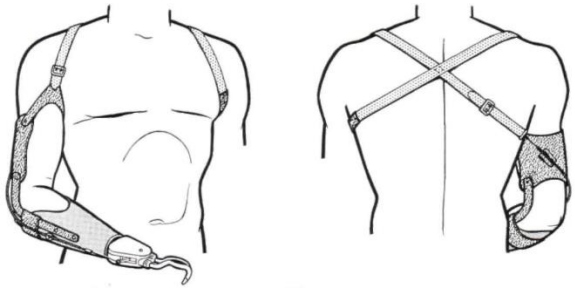

Figure 2.5 - Body Powered Prostheses [21].

Meanwhile, externally powered prostheses use external power sources such as batteries rather than using energy generated by their body. According to Geethanjali [18], externally powered prostheses are more desirable by amputees than body-powered prostheses due to their cosmetic appearance. These externally powered prostheses are then usually classified into electric and myoelectric prostheses [1] [18].

While body-powered hands are known to require strenuous shoulder efforts in order to operate the prosthetic devices, one can still argue that such systems give a better feel to the user with regard to the position as well as exerted forces [22]. Meanwhile, myoelectric hands do not give the user such an advantage, unless having an in-built sensory system which feeds back some sensory information back to the amputee.

2.1.2.1. Electric Prostheses

Electric prostheses are operated electrically, using, for example, batteries, and are known to be heavy and expensive to buy and repair. Such electric devices may be pressure signal, strain gauge and switch signal operated, amongst others [18]. According to Cordella et al. [1], such electric protheses are most suitable for persons who suffer from phocomelia and are born with short and malformed limbs, since it gives them the ability to control the device through external buttons.

2.1.2.2. Myoelectric Prostheses

Myoelectric prostheses work on the idea of reading and utilising EMG signals which are generated in skeletal muscles, reflecting the user's intention, through surface electrodes. For prosthetic hand control, these signals need to be recorded from any viable residual muscle/s following amputation, in accordance to the intent interpretation system chosen. The introduction of reading the user's intent gives these kinds of prostheses an edge over all others in terms of the ability of 'natural control'.

One is to note that the information that is conveyed by myoelectric signals obtained from surface electrodes may only be a subset of the total information delivered to the muscles by the motor neurons. Therefore, the measured signals at the skin's surface provide us with less spatial and temporal information that is actually provided to the neuromuscular system and thus, the action intent signals sent through the central nervous system are impossible to fully extract through myoelectric signals. This is especially true when utilising surface electrodes.

Whilst sEMG electrodes have been chosen as the method to be used for data collection for this work, one is to note that other myoelectric control sensor alternatives or combinations have also been used in the literature. Such sensor modalities include accelerometers, ultrasound, touchpads, force and slip sensors, finger position encoders and grip chips, amongst others [2] [3] [4]. Targeted Muscle Reinnervation (TMR) is another way of obtaining signals to control the prosthesis through the restoration of function of the arm nerves by rewiring them to different, more accessible, muscle sets. This technique, however, requires surgical interventions [4] [18] [23]. Other multi-modal sensing techniques such as Tactile Myography (TMG) have also been explored [24] [25].

Atzori and Müller [4] and Dwivedi et al. [26] both agree that sEMG is the most commonly used interface in both research and commercial products since it facilitates movement execution. This is in relation to other intent interpretation interfaces such as brain or nerves which are known to be invasive. Therefore, since these claims are backed by numerous papers that have utilised this method whilst also providing us with the capability of providing some kind of intuitive command control to the user, the myoelectric system route was chosen as a way forward for this project. This leads us to the next sections which underline the different myoelectric control systems that have been implemented.

2.2. Myoelectric Prostheses Control Systems

For the design of a myoelectric prosthetic system, developers usually follow a model which may be split into three stages, as shown in Figure 2.6. This includes a pre-processing stage, an intent interpretation stage and an output stage, starting from signal capture instances to signal outputs to the actuators [3].

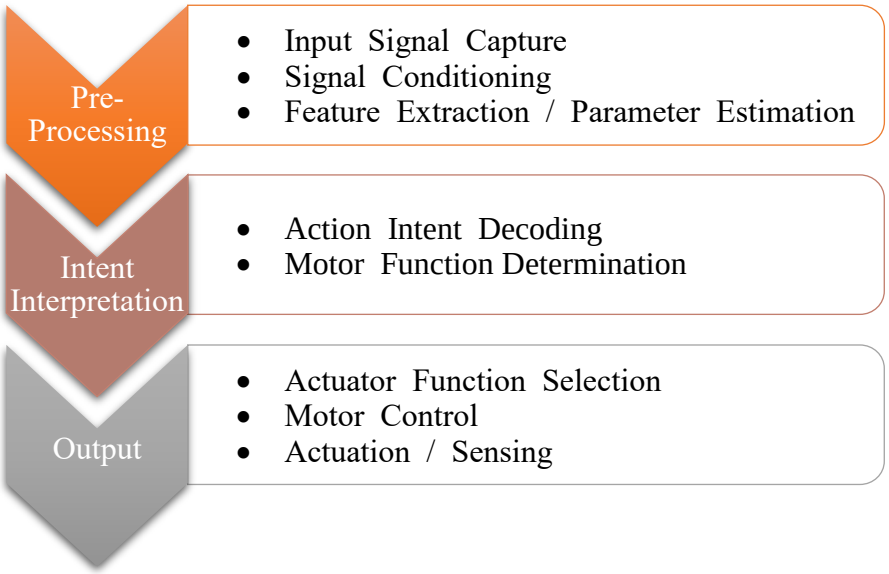

Figure 2.6 - Prostheses Control Model as explained by Fougner et al. [3].

The *pre-processing* stage of the model includes the acquisition of the signal from sEMG electrodes which provide qualitative and quantitative information to be able to process an output. This step includes all signal filtering and amplification methods which may be required to produce reliable signals for further computation of required features and parameters. Therefore, in this stage, the important information is extracted from the subject's muscles which is in turn processed as a quantitative value to be used for the eventual outputs.

The *intent interpretation* part of the model includes the analysis of the signal features obtained from the previous section of the model, according to the type of outputs used and EMG sites provided. These features are then decoded and mapped to a specific output, with the final step of this decoding usually being voltage levels for the targeted motors. This is seen as the most important part within this model since the information gathered is interpreted as the high-level control, as eventually experienced by the subject.

The final stage of this model is the *output* stage which translates the different motor functions, such as the various different grips, into setpoints that the actuators are to follow. The motors are then controlled according to the defined setpoints and sensed feedback. In the case where there is feedback included in the system, the outputs of the motors are corrected according to information recorded from the sensors. Therefore, this stage implements the decisions made in the preceding stage [3].

2.2.1. Control Schemes

There are numerous control schemes which have been investigated and implemented for myoelectric prostheses. In this context, a control scheme refers to a paradigm by which the user actuates the prosthesis. The most popular and widely used schemes are the 'On-Off Control', 'Agonist/Antagonist Control', 'Proportional Control', 'Finite State Machine Control' and 'Machine Learning and Pattern Recognition Techniques'. In the sections below, the differences between these control schemes will be underlined within the scope of myoelectric prosthetics.

2.2.1.1. On-Off Control

On-Off control, also known as 'bang-bang control', 'binary control' and 'crisp control' is one type of simple prosthesis control. The functional ability of the prosthesis is turned either on or off as soon as the amplitude of the EMG signal, usually calculated using the Mean Absolute Value (MAV) or Root Mean Square (RMS), exceeds the set thresholds. In principle, this method provides the user with very limited functions which can either be activated or deactivated without any other user control and usually requires an electrode site for every single available grasping function. Even though highly unnatural, due to its simplicity, such controlled prostheses still occupy a good share of the market [2] [3] [18].

2.2.1.2. Agonist/Antagonist Control

This control method is simple and robust and is implemented on the basis of analysing electrode signals on agonist and antagonist muscle pairs. Upon contraction of one of the muscles in the pair, the hand opens while upon contraction of the other muscle, the hand closes. Meanwhile, co-contraction allows for switching between the different available grasping functions whilst all mechanical movements are done at a singular speed [2] [27]. A slight deviation from this control system is the two-channel amplitude-coded control system [8] [23] [28]. This system requires two control muscles (a flexor and a corresponding extensor) for each prosthetic degree of freedom. An example is provided in Figure 2.7 which illustrates how, if a muscle is active above a pre-set cut off threshold, its associated limb function is selected. Therefore, in this case, if *S1* exceeds the set threshold, the prosthetic hand opens while if *S2* exceeds the threshold, the hand closes. With co-contraction, the control system takes no action.

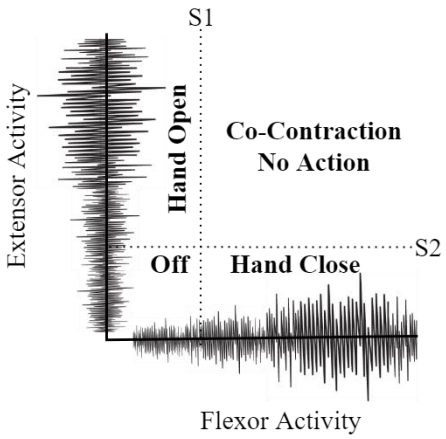

Figure 2.7 - Two-channel amplitude-coded myoelectric control where S1 and S2 are switching thresholds for flexor and extensor activity. Adapted from [8].

2.2.1.3. Proportional Control

An important disclaimer is that this proportional control scheme does not relate in any way to the feedback controllers which generate a control signal proportional to the error signal within a closed loop, which are known as proportional controllers [3].

Battye et al. [29] were the pioneers who put forward the proposal to utilise recorded EMG signals for proportional control systems into action in 1955 [3] [22]. Fougner et al. [3] define the term proportional control for this application as follows: "Proportional control is exhibited by a prosthesis system if and only if the user can control at least one mechanical output quantity of the prosthesis (e.g., force, velocity, position, or any function thereof) within a finite, useful, and essentially continuous interval by varying his/her control input within a corresponding continuous interval." Therefore, the relationship in proportional control prostheses between the controller output and their input is continuous, with the control system reacting accordingly. This definition also comprises the fact that the end user should be able to vary the output signal at a continuous rate with acceptable efforts from their end. Varied EMG amplitudes obtained during either flexion or extension could thus be mapped to pre-set voltages according to the contraction intensities. Therefore, the speed and the force of the prosthetic device can be made to vary in proportion to the amplitude of the EMG signal [8] [30].

Since Battye et al.'s first system in 1955, there were various advancements in the myoelectric control field which ultimately led researchers to utilise several EMG features in relation to muscle force for information extraction. These EMG features are now more commonly known as Time-Domain (TD) feature sets, Frequency-

Domain (FD) feature sets and Time-Frequency (TF) domain sets [3].

2.2.1.4. Finite State Machine Control

A finite state machine system is designed to cater for different possible states and the transitions are pre-defined and fixed for a set number of grasps. Such control systems can also be designed to take multiple inputs from different sensors, such as force sensors, into consideration before taking the next decision and reaching the next state. Another type of state machine system includes one which has a mechanical system incorporated within the prosthesis to be able to switch from one state to the next, manually. A slight deviation to this includes systems which record co-contractions of antagonistic muscles and change state accordingly [3] [31].

2.2.1.5. Machine Learning and Pattern Recognition Techniques

With advancements in machine learning, researchers have since preferred to shift their focus to machine learning solutions and pattern recognition techniques. With machine learning techniques, two widely used approaches are the classification and regression methods where the former reaches a decision with regard to what the user's intended task is, while the latter results in continuous human motion estimation. Since continuous motion is difficult to decode, most pattern recognition techniques lead with regard to discrete control of the prosthesis [26].

For different human contractions, it has been noted that repeatable signal patterns usually contain control information within their intrinsic features, allowing the formation of a pattern feature vector [32]. Therefore, pattern recognition control includes feature extraction of the raw myoelectric signals obtained in the TD, FD and/or TF domains. TD features usually contain the signal amplitude information, the FD features provide the signal power spectral density while the TF features provide a combination of both. The feature set is to be chosen in a way that best separates the desirable output classes such that as soon as the signals are processed and the necessary features are extracted, these features could then be classified accordingly. Therefore, information is essentially identified from the extracted features, outputting class labels which represent the desired prosthetic movements [8] [9] [18] [26] [32].

In such intent interpretation systems, multiple electrodes are used to detect several myoelectric signals for information extraction at several muscle sites. This leads to the

processing and acquisition of the above-mentioned feature set which serves to discriminate between different movement classes. The chosen classifier would then need to exploit this information to determine the intended prosthesis action [8]. Therefore, the total number of functions that may be included within a prosthesis will only be limited by the number of distinct patterns that may be generated by the subject, sometimes also depending on the total number of electrodes used [32].

However, due to the very complicated nature of forearm muscles and their synergistic movements, the displacement of the muscles during contractions, cross talk due to multiple muscle layers detected at a single surface point and arm posture modifications, performance of such pattern recognition techniques is affected [2].

2.2.2. Myoelectric Prostheses on the Market

With a variety of myoelectric prosthetic hands on the market, it is essential to take note of what kinds of control systems are being used to drive these mechanical hands. A comparison between four different myoelectric prosthetic hands provided in Figure 2.8 was carried out by Atzori and Müller [4] to compare and contrast the different functionalities of the different systems. A comparison table as drawn-up by the authors is provided in Table 2.1, focusing on the control capabilities of the different hands. One is to note that since this publication, the Bebionic hand has been acquired by Ottobock.

From this table, it can be noted how a large number of grip patterns are available for the user with a very limited number of EMG electrodes to provide the action intent commands with. It has also been observed that different control schemes may be used within the same prosthetic device for different functionalities. With the use of sequential schemes, signal triggers, as well as the use of mobile phone applications, it is specifically clear that the movement commands that these prosthetic hands require are completely unintuitive, requiring multiple activation of different sEMG electrodes for co-contraction as well as double and triple signal impulses, amongst others. Therefore, these prostheses' control systems require unnatural intent instructions, unlike the use of intuitive pattern recognition techniques.

(a) (b) (c) (d)

Figure 2.8 - (a) Touch Bionics' i-limb Quantum [33], (b) Ottobock's Michelangelo with Axon Bus Technology [34], (c) Steeper's Bebionic v3 [35] and (d) Vincent GmbH's Evolution 2 [36].

Table 2.1 - A table showing the most important control features for the four considered prosthetic hands, adapted from [4]; Touch Bionics' i-limb Quantum [33], Ottobock's Michelangelo with Axon Bus Technology [34], Steeper's Bebionic v3 [35] and Vincent GmbH's Evolution 2 [36].

Company Name	Touch Bionics	Ottobock	Steeper	Vincent GmbH
Prosthesis Model	i-limb Quantum	Michelangelo with Axon Bus Technology	Bebionic v3	Evolution 2
Grip Patterns	7	7	11	20
Proportional Control	Yes	Yes	Yes	Yes
Number of Electrodes	1-2	1-2-3	1-2	1-2 wired
Movement Control Type	Movement Triggers, Mobile App, Bluetooth Grip Chips, Favourite Environment, Gesture Control	Sequential, 4-Channel Control	Sequential, Morph RFID GRIP Selection Compatible	Single Trigger or Vincent Morse Code
Movement Command	Hold Open, Double Impulse, Triple Impulse, Co-Contraction	Different Switching Modes Available	Co-Contraction / Open-Open Signal	Hold Signal, Double Signal, Co-Contraction, Alternating Signal

Furthermore, while 'sophisticated' systems such as those controlled through mobile phone applications and Bluetooth grip chips are attractive to researchers, the actual

usability of such systems are questionable when one requires to use such a system in the real-world whilst performing day-to-day activities.

Regardless of the fact that a lot of research has been recently focused on pattern recognition techniques, it is well known that the widely available myoelectric prosthetic hands still use simple, unintuitive intent interpretation systems, with the general idea being that pattern recognition techniques provide unreliable performance in real-life environments. Whilst it has been proven time and time again from different scientific studies [37] [38] [39] [40] [41] that pattern recognition control is capable of obtaining very high accuracies, even greater than 95%, it is also known that such systems still lack representation on the market.

However, a few prosthetic pattern recognition systems have been introduced into the market in the recent years. The first pattern recognition system which was commercially released was the Coapt system, in 2014 [1] [4], followed by Ottobock's Myo Plus system which can only be used with compatible Ottobock prosthetic models [42]. The release of such systems confirms that real-life use of prosthetics controlled by sEMG pattern recognition, is in fact possible and successful. This provides a new market to upper extremity amputees who are capable of performing distinguishable and most importantly, intuitive hand movements for less mind-burdening prosthetic control.

2.2.3. Controlled Actuator States

A movement intent does not solely depend on the final position or posture but may also include velocity at which the movement is performed, and force required to be exerted. A case in point is during a grasp motion where the movement can be divided into two parts, namely the reaching and the grasping. A feature which predominantly varies during the reach phase is the speed at which the hand closes, until contact is made with the object. Following this, grasping follows where speed is no longer quantified and force increases or decreases, according to the object being grasped and its characteristics. As shown in Figure 2.9, there is a loop that one goes through with regard to position, speed and force when opting to grasp something, such as, in this case, an apple [3]. This is very important since these experienced states make the movements feel natural. The higher the resemblance of the system to the actual human hand's behaviour, the higher the usability of the prosthetic device.

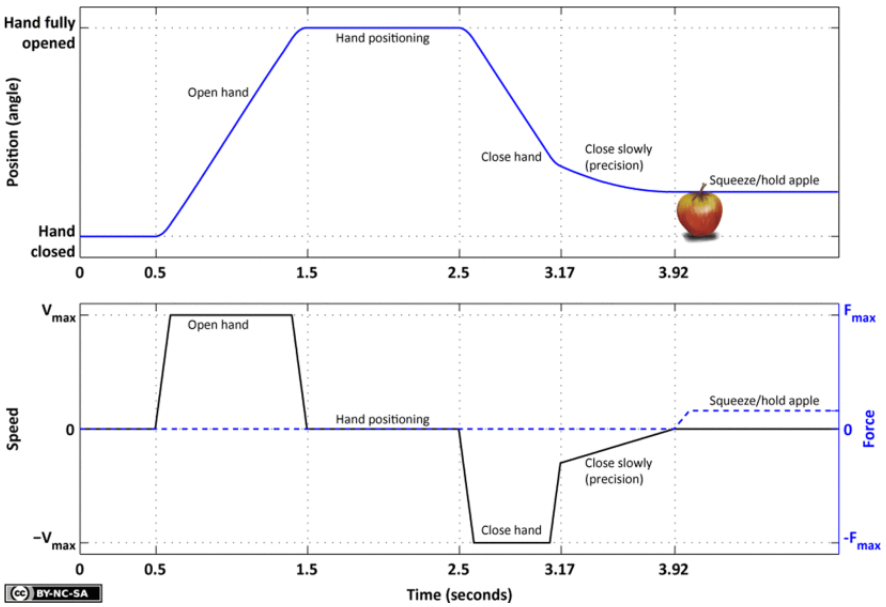

Figure 2.9 - The interconnection between hand position, speed and exerted force [3].

2.2.4. Myoelectric User Training

For successful prosthetic use, regardless of the myoelectric control scheme used to instruct the intent of the mechanical hand, user training is critical. User training involves the training of any patient who is to start utilising a prosthetic hand. It is important that an amputee fully understands how to wear and essentially correctly operate the prosthetic hand, with the ultimate focus on improving the patient's performance to the best possible, in the least amount of time. Such training is known to potentially aid an amputee's confidence, comfort and competence whilst using their new 'addition to the body'. Myoelectric user training is typically composed of three stages; namely signal, control and functional training [9].

In signal training, the raw signals obtained from the patients in real time are on display in order for them to learn activation and relaxation movement requirements as well as isolation of the different muscles for co-contraction avoidance. The second step, control training, is more advanced, using systems such as simulators and video games in order to gauge whether the patient can exert the required signals for an eventual prosthetic fitting and also to teach the patients on how to generate the correct signals for the best prosthetic utility. The final step, functional training, is carried out with the actual fitted prosthetic device, to learn how to perform movements utilised during activities of daily living. Such movements usually start off with the most basic, leading to the most advanced. This step is very important since the ability to repetitively perform muscular commands in the same manner is crucial for a reliable performance,

in turn resulting in better prosthetic usability. However, our aim for this project is to also have a system which is so intuitively easy for the amputee to use, that both the intensive and training time aspects that are usually experienced during training, are reduced.

2.2.5. Myoelectric Control Schemes Choice for this Project

In order to be successful in developing a system which is simple while still highly usable, controlled actuator states as mentioned in Section 2.2.3 are important to be given attention. Therefore, from the control schemes listed in Section 2.2.1, pattern recognition techniques, as well as proportional control techniques were chosen to be the best collaborative choice for our intent interpretation system. Through pattern recognition techniques, the hand's motion decisions would be based on the user's intuitive motions and thus, the user would be in charge of controlling the hand's joint movements towards a specific direction, as required. By using such an intent interpretation system, the user will be provided with an intuitive hand control solution, with no requirement of large amounts of re-learning and re-mapping of the brain's usual intent.

In the meantime, by using proportional control, the speed and force intentions of the user when approaching an object and grasping it could also be quantitatively extracted from the sEMG signals. These values, or levels, could then be utilised by the developed intent interpretation system to proportionally instruct the actuators to increase or decrease speed or force, accordingly. Since this part of the system gives the user further control on the prosthetic hand's operation, the resemblance to normal hand functionality is increased, which should result in a more usable system.

This work gives the highest importance to motion identification since it is the first step towards having a reliable prosthetic action intent system. Thus, a more detailed literature review on this scheme is provided in the next chapter, paving the way towards the intent interpretation framework implementation.

3. Myoelectric Pattern Recognition Review

As has been mentioned in Section 2.2.1.5, with myoelectric pattern recognition schemes, different EMG channels are used to extract intent information. The information extracted from the different channels is then combined to recognise the intended hand movement. The signal patterns obtained for separate gestures are all unique. Therefore, by using this technique, the intuition of normal hand motion may be retained [43]. In addition, such pattern recognition systems can also exploit any consistent cross-talk and muscle coactivation related to specific hand movements, also improving the recognition of the intended movement [44].

The main steps which are typically followed for pattern recognition based prosthetic classifiers as demonstrated in Figure 3.1, are as follows [45]:

1. Raw EMG data collection from all the EMG channels in specified time windows;
2. Signal processing and feature extraction;
3. Features input into the classifier;
4. Selection of output class;
5. Post processing performed on output classes to improve robustness;
6. Actuation of DOFs dictated by the final output decision. Signals are passed to controllers driving the prosthesis mechanical motion.

Different methodologies chosen for the above steps affect the final outcome. Due to the large number of study-dependent variables, comparisons between different studies is not straight-forward, though the movement classification accuracy is usually a comparable outcome. The variables known to hinder comparisons between studies include the electrode types, sizes and placements, the amplification hardware, filtering strategies, data analysis parameters, experimental protocols, type of classifier developed and training data set compositions, amongst others [45] [46].

Figure 3.1 - Pattern Recognition Classifier Prosthetics Flow.

3.1. Data Collection and Pre-Processing

There are various variables which concern data collection and pre-processing, namely electrode types, electrode sizes, method of electrode placements, number of electrodes, parts of the total captured signal which will be utilised, type and size of processing windows and data reduction techniques. The most important parameters shall thus be discussed in the following sections.

3.1.1. sEMG Electrode Configurations

The muscles in the forearm, whether superficial or deep, have different responsibilities, mostly differing from wrist to finger movements. Some muscles are responsible for multiple actions, resulting in co-activation of multiple muscles, however, those muscles which are not situated towards the surface are more difficult to obtain clear signals from. The anatomy of the forearm muscles and their responsibilities are clearly shown in Figure 3.2 and Table 3.1. Therefore, if one wants to specifically monitor a particular muscle, this must be correctly located, accordingly. Otherwise, symmetric electrode positioning may be implemented, such that no specific muscles are located, aiming towards targeting a larger area of muscle activity.

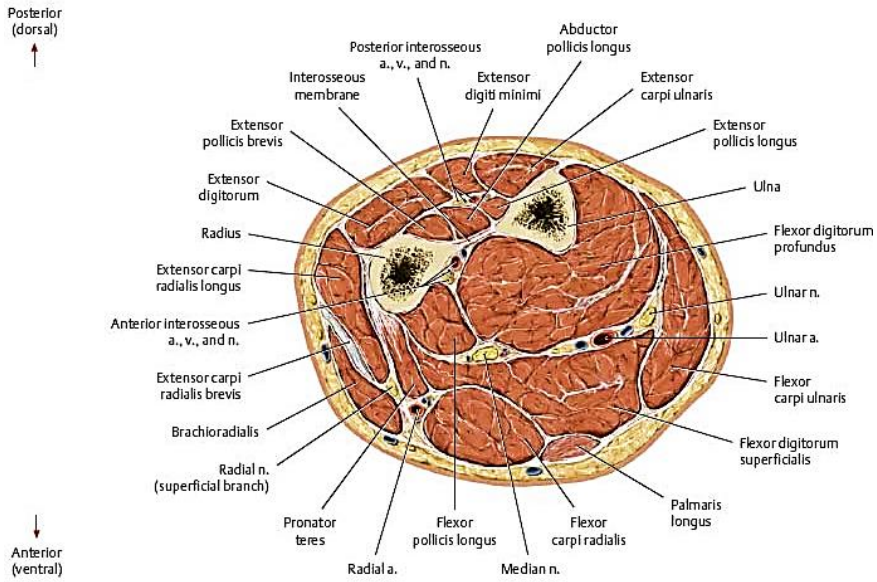

Figure 3.2 - A forearm cross section clearly showing all the muscles in the different compartments [47]. The Posterior compartment of the forearm is responsible for wrist and finger extension while the Anterior compartment of the forearm is responsible for wrist and finger flexion.

Table 3.1 - All the muscles acting on the wrist and fingers highlighting their actions and whether they are located on the anterior or posterior compartment of the forearm. The shaded muscles are superficial muscles while the others are deep muscles. 'Pr' refers to the muscle as being the prime mover of the action. Recreated from [48].

	Acting Muscles	Actions at the Wrist				Actions on the Fingers	
		Flexion	**Extension**	**Abduction**	**Adduction**	**Flexion**	**Extension**
Anterior Compartment	Flexor Carpi Radialis	✓ (Pr)		✓			
	Palmaris Longus	✓ (Weak)					
	Flexor Carpi Ulnaris	✓ (Pr)			✓		
	Flexor Digitorum Superficialis	✓ (Pr)				✓	
	Flexor Pollicis Longus					✓ (Thumb)	
	Flexor Digitorum Profundus	✓				✓	
Posterior Compartment	Extensor Carpi Radialis Longus and Brevis		✓	✓			
	Extensor Digitorum		✓				✓ (Pr & Abducts)
	Extensor Carpi Ulnaris		✓		✓		
	Abductor Pollicis Longus			✓		(Abducts Thumb)	
	Extensor Pollicis Longus and Brevis						✓ (Thumb)
	Extensor Indicis		✓ (Weak)				✓ (Index Finger)

It is very evident in the literature that different researchers opt for different methods of electrode placements, also varying the number of electrodes used. Whilst clinical setting practicality favours untargeted electrode placement due to simpler implementation [45] [46], it has also been shown that classification accuracy sensitivity to electrode shifts is higher when using selective placement rather than symmetrical [46] [49]. Targeted electrode placement requires the researcher to locate the required muscle bellies which is known to be challenging, since anatomical landmarks may differ for different people. This is a problem when experimental repeatability is required and consistency in electrode placements is crucial [50]. Furthermore, studies have also shown that by targeting specific muscles for pattern recognition control, no significant improvements are deduced in classification outputs when compared to symmetrically placed electrodes [45] [51].

A non-targeted approach is also ideal for signal detection on amputated limbs, since specific target muscles from the residual limb may not always be available. The extremity of this issue will then depend on the muscle states following the amputation which may, in turn, affect the required EMG signal's quality [52]. Due to this, it was concluded that untargeted surface electrodes implementation is the best method due to the least cost, invasiveness and complications introduced in socket fabrication.

Therefore, it has come as no surprise that more researchers have opted for symmetrical electrode placements rather than targeted placements when pattern recognition classification of certain gestures was the aim. In fact, there are abundant studies [45] [46] [53] [54] [55] [56] utilising symmetrical electrode positions, which aid in developing algorithms which are independent on specific electrode locations. In these cases, varying numbers of electrodes were used, ranging from four to 12 electrodes. In the majority of studies, the electrode pairs are usually placed a few (2-5) centimetres below the elbow whilst keeping an approximate equal distance between each electrode pair.

The optimal number of electrodes used for pattern recognition systems has also been studied by several researchers [54] [56]. From the study by Li et al. [54], it was deduced that the original 12 electrode channels used to detect ten different wrist and hand classes may be reduced to 6 to 8 channels instead. Furthermore, when the motion classes were reduced to six, the classification accuracy plateaued at 4-6 electrodes.

Meanwhile, Hargrove et al.'s study [56] displayed classification accuracies resulting from subsets (symmetrical or optimal) of the 16 channels placed around the forearm to detect ten gestures. It was observed that as the number of channels used increased, the classification accuracy quickly increased up to a high value followed by a smaller further increase in accuracy, as shown in Figure 3.3.

Different electrode specifications have also been listed in the literature, in accordance to different guidelines. Since two electrodes are required to obtain a single sEMG signal, apart from the electrode's material, their recording areas as well as the electrode distance between them is to be specified. Several studies have used recording diameter and interelectrode distance values as recommended by Surface Electromyography for the Non-Invasive Assessment of Muscles (SENIAM) [57] for bipolar electrodes, these being 1 cm diameter recording areas as well as a 2 cm interelectrode distance (IED) [45] [53] [55]. Larger IEDs have also been found to yield performance improvement [49], however, the possibilities of using such distances depends on the subject's residual limb's length.

Thus, it may be concluded that untargeted symmetric electrode positioning is the most beneficial, in comparison to targeted electrodes whilst a maximum of eight electrodes are envisaged to provide the best results. Meanwhile, IED is to be specified in accordance to electrode equipment limitations as well as stump length.

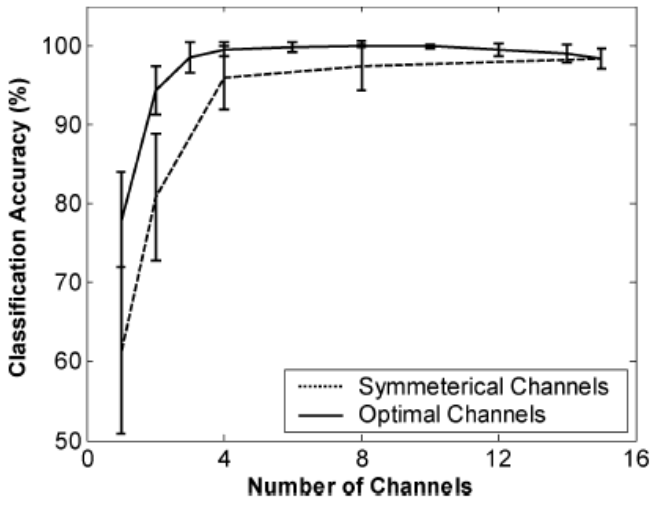

Figure 3.3 - Classification Accuracy increased with respect to the number of channels with symmetrical and optimal electrode channel subsets [56] © 2007 IEEE.

3.1.2. Signal Windowing

Studies have shown that EMG time window lengths of at least 100 ms to at most 300 ms provide the highest information content. Nevertheless, for prosthetic pattern recognition, the optimal window length is suggested to be between 150 ms and 250 ms and should be chosen as a trade-off between the class information that it may hold and the feature estimated error [32] [44] [46] [58] [59]. Nevertheless, window length and processing time for prosthetic application should never exceed 300 ms due to the user's perceived lag and thus, adequate window sizes should be chosen in accordance to feature variance and contribution to the best system performance [32] [40] [44] [60]. Therefore, the ultimate trade-off that is to be balanced is between the system's accuracy and the overall response time.

These extraction windows may be either disjoint from each other or overlapping one another. With an overlapping analysis window, a dense decision stream is obtained and is usually the most preferred for prosthetic classification since disjoint segments result in an idle processor for large segment portions [40] [58] [60]. Feature extraction windows implemented in the literature are varied, ranging from overlapping windows of 200 ms in length with overlap periods of 50 ms [41] [46] [61] to 256 ms windows with 32 ms overlaps [56], to 150 ms windows with 50 ms overlaps [54] [55].

3.2. Pattern Recognition Classifiers and Feature Sets

Abundant research has been done by using different technologies and techniques to identify the best performing classifier and the most appropriate set of features, as will be discussed in Sections 3.2.1 and 3.2.2.

Different combinations of feature sets and classifiers, in addition to other signal processing decisions are known to provide different levels of robustness. Nevertheless, the Linear Discriminant Analysis (LDA) classifier combined with a four time-domain feature set (made up of the MAV, Waveform Length (WL), number of Zero Crossings (ZC) and number of Slope Sign Changes (SSC)) is commonly known as a benchmark system. This is due to its balance between computational efficiency and algorithm performance, providing implementation simplicity, especially for implementation on microcontrollers [40] [43] [44] [58] [59] [62] [63].

3.2.1. Pattern Recognition Algorithms

Several pattern recognition algorithms have been implemented to determine performance, reliability and robustness for use in prosthetic hand systems. These include the K-Nearest Neighbour (KNN), Support Vector Machine (SVM), Neural Network (NN), Fuzzy Clustering (FC), Mahalonobis Distance (MD), Multi-layer Perceptron (MLP), Regulatory Feedback Network (RFN), Non-linear Logistic Regression (NLR), Convolutional Neural Network (CNN) and Linear Discriminant Analysis (LDA) [40] [41] [46] [61] [62] [63] [64]. From studies which have compared classification results between different pattern recognition algorithms, the majority have concluded [41] [46] [61] [63] [64] that the LDA classifier was either the best performer, or showed no statistical difference when compared to others.

While others have found that the LDA is inferior in direct comparison to others [62], LDA classifiers based on time domain feature sets have been the most preferred in the field. This is due to their satisfactory classification accuracies obtained for both static conditions [40] and dynamic movements [41] and for both offline and real-time classifications. LDA uses labelled data samples to learn a linear discriminant function to discriminate between the different classes and is generally considered a very suitable classifier for prosthetic use due to its high performance as well as ease of implementation, simplicity, speed and accuracy, making it ideal for real-time classification [41] [58] [59].

Meanwhile, pattern recognition testing on amputated arms rather than intact limbs have shown to lower classification accuracies by a significant amount [54]. Therefore, while satisfactory tests on normal limbed subjects might be easier to obtain, the challenge of reaching suitable classification accuracies for amputees is a critical requirement. However, while the absolute accuracy values are fairly different between normal limbed subjects and amputees, different classifiers are known to rank in the same ways when tested with amputees and when tested with normal limbed subjects. This suggests that the choice of classifiers made for normal limbed subjects may be considered to still be an appropriate choice for amputees [44].

Since the LDA has often been found to be either the best classifier or a suitable classifier for this task, this suggests that it would be a good classifier to start deploying for such problems. However, these results also suggest that a linear discriminator may

not always be sufficient, depending on the conditions of the hand movement classification, in which case, more complex classifiers may need to be studied.

3.2.2. Signal Features

There is a variety of signal features which may be utilised for hand movement classification, with the main feature sets being the Time-Domain (TD) features, Frequency-Domain (FD) features, Time-Frequency (TF) domain features, Autoregressive (AR) model coefficients and Wavelet features, amongst others [45] [53] [58].

Ortiz-Catalan et al. [46] provided a non-exhaustive list of signal features which have been employed in different literature targeting pattern recognition for prosthetic control whilst also explaining how no generalised consensus has ever been reached on which features or groups lead to the best results. This list also highlights the fact that the most widely used TD features are the MAV, WL, ZC and SSC, since their resultant values provide information regarding the frequency, duration and amplitude of the captured signals. These features may also be recorded in a time-constrained scenario as in prosthetics [46] [53] [54] [55] [62] whilst providing computational simplicity, stability against varying segment length, high classification accuracy rates as well as low alteration over repeated sessions [58].

Other popular TD features apart from those mentioned above are the Mean Absolute Value Slope (MAVS), Willison's Amplitude (WAMP), Variance (VAR) and the Log Detector (LD) [41]. Additionally, the RMS feature is also a common feature extracted by some researchers for basic amplitude information, in addition to other feature sets mentioned above [45] [65] [66].

While TD features are usually chosen for prosthetic implementation due to their low complexity [41] [62], others [45] [58] have highlighted how TD and AR coefficient feature sets have been shown to outperform accuracies obtained from TD features only but at the expense of much larger processing overheads, which are not desirable in such applications. AR features are known to be a non-practical real-time feature in the scope of clinical embedded system implementation [41].

Studies have also investigated the ideal number of features to be used in combination with classifiers. While high dimensional features have been found to result in the lowest classification errors [41], other studies [53] [67] deduced that the larger the

number of features used, the slower the process is, whilst obtaining lower or stabilised classification accuracy.

With contradictory outcomes with regard to the number of feature sets as well as the feature types that are best to be used for such classification applications, it can be said that the standard group of MAV, WL, ZC and SSC features is still the most popular. The most important attribute of such features is the ease of computation in time-constrained scenarios, unlike other features such as the high performing AR feature. Nevertheless, studies initiating their systems with a singular feature are not uncommon [37] [65] [68], which always provide a good, simple starting point, requiring further feature set experimentation once a stable system is established.

3.3. Post-Processing

Post-processing algorithms are sometimes implemented in order to improve the system's real-time stability by providing smooth transitions between gestures and removing misclassifications. Typical post-processing algorithms include the Majority Voting algorithm and the Buffer Output algorithm. The former algorithm filters any sporadic misclassifications by acting on the most active classification predictions, usually leading to slower response times. The latter algorithm uses a percentage threshold to determine whether classes have been consistently predicted instead of choosing the most active class [32] [46] [58] [40].

These methods are implemented such that the output is not based on the most recent decision but is rather taken more intelligently by choosing which class has appeared most in the previous class decisions. This helps to increase robustness [46].

3.4. Experimental Methodologies

Different researchers have opted for different methodologies when it comes to experimental design based on user intent classification. The differences between experiments could be noted in the different hand gestures/grasps tested and studied, the number of trials gathered, the number of subjects, gesture/grasp repetitions, contraction times and instructions provided to the participants.

Firstly, the number of hand and wrist gestures that are usually performed to train classifiers for prostheses varies, with some solely focusing on wrist gestures, others only on hand gestures, and others combining both. The choice of the types of gestures

as well as the number of these gestures that are distinguished by a classifier are important to note, especially when comparing studies to each other.

Wrist movements are known to be produced by easily detectable muscles on the forearm which are more dominant than the larger number of hand muscles which act together to produce a movement [69]. In fact, Li et al. [54] concluded that accuracy rates decreased when only considering hand gesture classification, in comparison to both wrist and hand gestures.

Nevertheless, the most popular gestures that have been implemented in most studies are a combination of the following: wrist flexion, wrist extension, pronation, supination, open hand (extension of all fingers), close hand (flexion of all fingers), palmar grasp, radial deviation, ulnar deviation, lateral grasp, power grasp, pointing posture, side grip, fine grip and thumb up, amongst others [45] [46] [53] [54] [56].

It is also important to note how subjects were usually asked to remain in a comfortable posture, also allowing gravity to return their hand to a natural position following any hand movement, whilst providing the necessary rest times between movements [45] [54] [56] [59] [64]. It was also the norm that since data was usually extracted from the steady-state signals, whilst the subjects contracted their muscles in a specific hand grasp posture, the subjects had to be asked to hold their contractions at either specific force levels [56] [59] or at comfortable force levels [45] [54] [55]. Consistency in the performance of these force levels was usually required and expected, such that classifiers could be trained with consistently performed data [32] [54] [55]. However, Scheme et al. [69] have mentioned how the performance of ramp contractions has been found to improve classification robustness when compared to singular force contractions.

It is also known that when a classifier is trained on sets gathered from different persons, classification accuracy diminishes. Therefore, user-dependent classification is usually encouraged, requiring intensive training sets for every patient [64].

This shows how the ideal scenario is usually set up in order to obtain the first results from any devised classification system, prior to obtaining real-time results for less than ideal, but more realistic, set ups. This is done by allowing the subjects to be comfortable in a singular position whilst performing consistent hand/wrist gesture repetitions. Furthermore, the choice of hand/wrist gestures depends on the researchers' objectives and thus, the number and types of movements are always to be decided at

design stage. Meanwhile, systems are typically trained to cater for individual subjects, focussing on user-dependent classification.

3.5. Offline vs Real Time Classification

Initial pattern recognition algorithm implementations are done in an offline environment where testing and benchmarking are carried out by solely using recorded sessions. Training and validation sets are used during the learning process of the classifier. After this process, testing sets are then used to assess the system's performance with unseen data [46]. This provides classification accuracy values based on offline data gathered. In order to deduce whether a trained classifier is suitable and usable in real-life applications, its real-time performance would then need to be tested. It is known that high offline accuracies provide a false sense of high reliability which may not be reflected in real-time classifications [46], thus, this step is important to conclude whether a classifier is in fact, up to standard.

In prosthetic research, such real-time testing would be carried out either with the use of an actual prosthetic arm [37] or by using a virtual prosthesis where a simulation of a prosthetic device or a normal hand is used to show decisions made by a system, in real-time, on a screen or through a virtual reality device [39] [54].

3.6. Signal Phase Selection

The motion of the hands can be split into dynamic and static contractions, relating to transient and steady-state EMG signals. Dynamic contractions relate to hand contractions during movement while static contractions relate to hand contractions held in a static position [38]. For example, in order to quantify a hand operation such as grasping an object, the required hand motion can be described to go through two different phases, which are the movement (dynamic) phase and the force (static) phase. The movement phase can be described to be the movement occurring in the time span where the fingers are approaching the object to be grasped, starting from an initial posture, until contact is made. This movement phase can be performed at different velocities, in accordance to the subject's requirements. Subsequently, as soon as contact is made with the object to be grasped, the force phase is entered whereby the fingers apply the required force to the object.

The transient and steady-state EMG signals corresponding to these dynamic and static

contraction phases have different signal characteristics, since muscle recruitment is performed dynamically in accordance to contraction type, as well as muscle type [38]. The scope of this work is to utilise these characteristics to determine motion instruction, and force estimation, separately, in the most intuitive manner possible to the end-user.

From the literature, as noted in Section 3.4, the transient signal phases are usually neglected, focusing only on the use of steady-state signals, which correspond to static grasp contractions, for both motion and force intent interpretation. In such studies, data is usually collected from static contractions at different grasping positions for motion classifier training. Such systems usually also implement continuous classifiers, whereby feature sets are continuously extracted from the incoming signal streams, leading to a classification decision with every time step [40] [54]. Nevertheless, while most pattern recognition systems have been based on steady-state signals, some researchers have also opted to train their classifiers by using both transient and steady-state signals [32] [38] [39] [45] [46] [53] [62]. This, however, usually means that the proportion of the steady state feature to transient feature is not balanced, with the transient signal features being sparse when compared to the steady state features [70].

According to Gopura et al. [60], the preference of the steady-state phase in many EMG systems is justified by the large variations in transient phase signals, in comparison to the steady-state. There was also a time where it was believed that no valuable information could be extracted from transient signals, which Hudgins et al. [32] proved wrong. However, the use of transient signals was still eventually neglected due to the difficulties of switching between different gesture classes without always initiating a contraction from rest [40]. Nevertheless, for this work, this claim is not envisaged to be a limitation.

Furthermore, Kanitz et al. [37] have argued that the belief of obtaining repeated steady-state EMG signals with repeated static muscular contractions is, in fact, a common misconception. This is since these kinds of contractions require continuous muscle fiber recruitments and firing patterns. Also, EMG continuous classifiers that make use of the static phase for motion detection are problematic in terms of class prediction stability, requiring additional post-processing, thus affecting the overall system responsiveness.

Due to these conflicting arguments, there are only a few available papers on sEMG pattern recognition systems using solely transient signals for hand grasping classification. One recent study is by Kanitz et al. [37], where a system was implemented such that as soon as a movement from rest was detected, 300 ms of consecutive MAV values from the transient phase were collected and fed to a classifier to predict the movement class. Following the classifier's prediction, proportional velocity control was used to control the prosthetic's rate of opening and closing.

Due to the conflicting arguments within the literature, most of which supporting the discrimination of different motions through steady-state signals, it was envisaged that experiments were to be devised on a major muscle to identify the differences in sEMG signals with different contractions. For these experiments, a singular major muscle was chosen to test the general concept using a simple muscle, which could later be applied in the context of forearm muscles used for the intent interpretation system. This exercise aims to identify whether the two types of EMG signals are capable of contributing information with relation to their contraction type (dynamic or static) as well as identify signal aspects which best characterise the different contractions. These experiments are described and discussed in Chapter 4.

From these experiments, it could then be concluded which signals would best provide the most intuitive type of intent interpretation during both motion instruction, as well as force level instruction, ultimately leading to suitable action intent system implementation resulting in the simplicity, dexterity and usability trade-off.

3.7. Conclusion

The literature review discussion in the above chapters has laid out the different kinds of prosthetic control systems and schemes that are available on the market, as well as the systems that have been researched, including their advantages as well as limitations. By keeping the ultimate goal of this research in mind, i.e. that of achieving a balance between the simplicity, dexterity and usability attributes for a prosthetic action intent system, an active myoelectric prosthetic intent interpretation system which uses musculoskeletal signals as commands was to be developed. Furthermore, it had already been stated that providing the users with the ability to use their intuition would be most beneficial when it comes to maximising this design trade-off. This led to the choice of using a pattern recognition control system, capable of detecting different gestures, followed by proportional control. As has been discussed, there are

many variables that need to be taken into consideration when constructing such a system, including the classifier type, feature extraction windowing type, signal processing choices, and extracted features.

Based on the literature reviewed, for this work, eight electrodes, symmetrically placed around the forearm, on the muscular bulge will be used to sense the muscle recruitment whilst an LDA classifier will be used to classify the intended hand gesture. The choices regarding the sEMG features as well as windowing and any requirement of post-processing were to be decided with the implementation of the system, as will be discussed in Chapter 5.

Furthermore, it has been discussed that a very important choice lies in the signal phases that are to be used for motion classification as well as force estimation. Due to the contradictory views on this topic, it was decided that further experimentation on a major muscle is required to aid with this decision.

4. sEMG to Joint Velocity and sEMG to Joint Force Relationships

As has been discussed in Section 3.6, there have been many conflicting arguments regarding the use of transient or steady-state sEMG signals to determine user intention. In order to conclude whether sEMG signals contain information relating to the different contraction types, specific experiments were devised accordingly. The variable features which may be related to transient and steady-state contractions are velocity and force, respectively. Therefore, the aim of these experiments was to determine whether sEMG features have a relationship to the exerted force and to the velocity, thus concluding whether the different signals may both provide discriminatory information.

These experiments were carried out on the large biceps muscle such that the best sEMG signal acquisition procedures could first be tested on easily located muscles with minimal crosstalk. Relationships obtained from such a straightforward muscle also do not need any further consideration with regard to multiple synergistic muscles which aid in the different contraction types, as is the case with muscles controlling the hand. Therefore, the biceps muscle was chosen as a simpler alternative to the synergistic hand muscles as an initial test of the general concept. Thus, sEMG features could firstly be related to elbow flexion velocities and force exertion at the wrist.

In order to properly prepare for these experiments, the first step was to study the literature as to which contraction types should be used, how sEMG signals behave with anatomical differences and what relationships other researchers have found for similar studies. These topics will be discussed below.

4.1. EMG Relationships with Anatomical Differences and Contractions

For muscle force generation, the first link in the chain that initiates the process is nerve stimulation. Through afferent pathways, sensory input from the muscle travels to the Central Nervous System (CNS), promoting Motor Unit (MU) recruitment which stimulate muscle fibers, in turn resulting in muscle strength generation. The MU, known to be the muscle's functional unit, consists of an alpha motor neuron and numerous fibers (depending on the muscle's required overall strength and control) which are innervated by it. These muscle fibers contract when action potentials are activated in the motor unit that supplies these fibers. These fibers are also known to be

either of the ‘slow’ type or the ‘fast’ type. MU firing combinations and mechanisms operate in a way which differs for small and larger muscles due to being controlled by different schemes of recruitment and activation. In fact, an sEMG signal is composed of multiple Motor Unit Action Potential Trains (MUAPTs) generated from several motor units within a muscle [71] [72]. These processes are shown in Figure 4.1. According to Mustard and Lee [73], velocity, amplitude and force variations of a limb movement may be produced by altering the way the motor units activate and work, described by the authors as the ‘motor program’, resulting in adjustments in EMG burst characteristics.

In order to understand the way muscles work during movement, muscle forces are required to be known, however, such forces cannot be measured directly from human muscle, but such forces may only be modeled, calculated or assessed [71]. As explained by Disselhorst-Klug et al. [74] and De Luca [75], the direct measurement of the force exerted by a skeletal muscle is difficult to be found and assigned, mostly due to the fact that one muscle is usually part of a larger group of muscles acting as either agonists, antagonists or synergists. Having said that, while certain relationships for specific muscles with sEMG features may be highly reproducible, the same relationships are not usually found for other muscles and thus, differently curved relationships are uniquely found for every muscle which may be caused by the muscles’ length and their structured organisation.

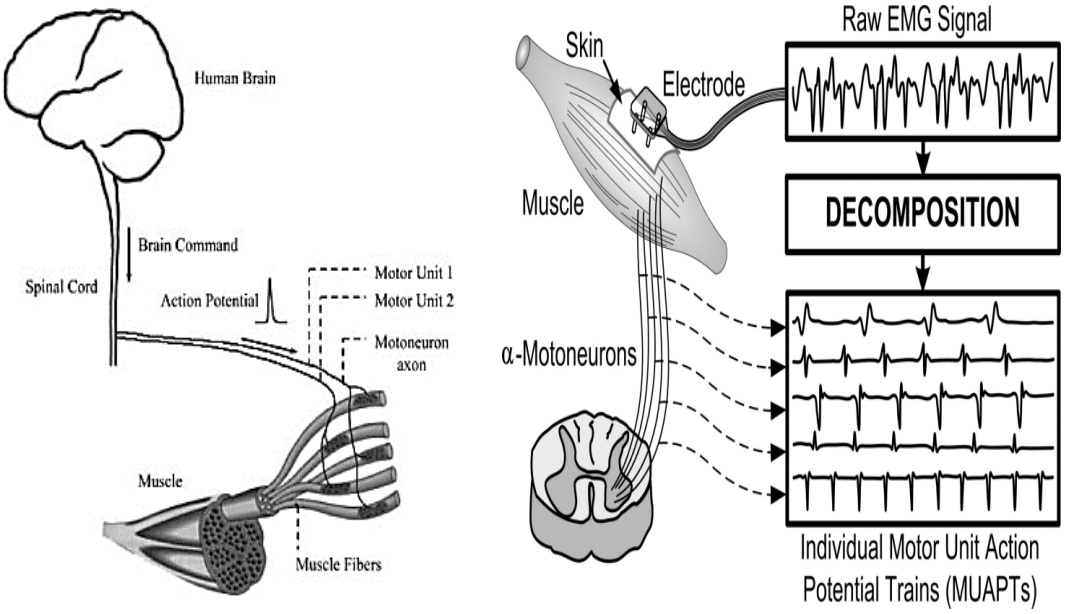

(a) (b)

Figure 4.1 - (a) Illustrations of the human nervous system and muscle activation. Reprinted from [76] with permission from Elsevier. (b) EMG pattern read from an activated muscle with permission from [77], [78], [79].

4.1.1. The Different Types of Limb Contractions

There are various contractions that humans can exert with their limbs. The most prominent contractions are namely *isometric*, *isotonic* and *isokinetic* contractions. *Isometric* contractions are generated whenever a force is exerted at a constant muscle length. Therefore, *isometric* contractions are carried out in a static position such that the joint angle and the muscle length are not varied during force generation. Meanwhile, *isotonic* contractions generate force whilst changing the muscle length in a *concentric* or *eccentric* manner. *Concentric* contractions occur when the muscle shortens while the energy is fluctuating while during *eccentric* contractions, muscles elongate in response to a greater opposing force. A more visual description is provided in Figure 4.2. Meanwhile, *isokinetic*/*isovelocity* contractions are similar to *isotonic* contractions, however, in this case, constant paced movements are performed. Therefore, the movement speed is controlled and paced while the muscle length shortens and lengthens according to the movements carried out by the limb [80].

Thus, in order to obtain sEMG-force and sEMG-velocity relationships, *isometric* and *isokinetic* contractions were decided to be performed, respectively. For *isokinetic* contractions, the velocity is usually kept constant with the help of isokinetic dynamometers, however, in this work, as will be mentioned in Section 4.2.4, the subject was only given an audio indication of these velocities. Since subjects are not as consistent with performing movements at specified set velocities, we follow the literature [72] [81] in referring to these contractions as *anisometric* instead.

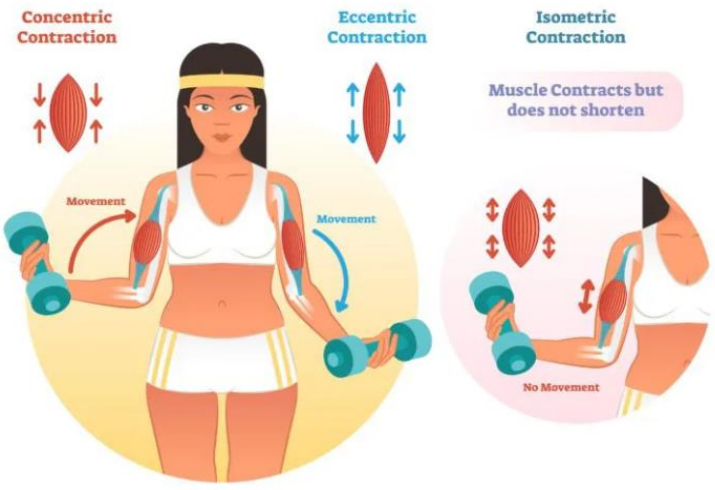

Figure 4.2 - Isometric, Concentric and Eccentric Contractions [82].

4.1.2. The EMG-Force Relationship

It has been previously suggested that sEMG amplitude is not directly proportional to force, however, it is also known that sEMG activity does reflect the amount of force exerted by any muscle, to a certain extent. Therefore, it is believed that when an sEMG signal is rectified and smoothed, the resulting amplitude can be qualitatively related to force measured at a joint, albeit providing an intangible quantitative relationship whose accuracy is questionable [75] [83]. This relationship has been studied by various researchers throughout the years [84] who have also found variability between subjects and experiments.

The elusiveness of the relationships obtained from sEMG signals is known to be due to sEMG signals being complicated signals which are affected by numerous technical, anatomical and physiological factors, as De Luca [75] extensively describes, which may not be easily detected and disentangled. These factors have been grouped into three categories, namely: causative, intermediate and deterministic factors.

In brief, causative factors are known to have a direct and elemental effect on the signal which may be divided into extrinsic or intrinsic factors. Extrinsic causative factors, unlike the intrinsic factors, may be controlled to achieve the expected results. This is since intrinsic factors are linked to anatomical, physiological and biochemical muscle characteristics. Even though intrinsic factors cannot be controlled, knowledge of these factors aids with EMG interpretation accuracy [85]. Meanwhile, intermediate factors are influenced by causative factors which in turn influence the deterministic factors. These intermediate factors are physiological and physical phenomena which take place due to various activities within the muscle, such as the crosstalk phenomenon [71] [75]. Meanwhile, deterministic factors which represent physical characteristics of EMG action potentials, directly affect the EMG signal information that may be extracted and the resultant force. Therefore, in order to fully understand the EMG signal, fundamental understanding of human physiology aspects is required [86] [87].

sEMG-force relationships for different muscles are known to vary due to their recruitment properties, muscle firing rates and other anatomical aspects such that smaller muscles usually result in quasi-linear relationships unlike larger muscles, such as the biceps and triceps muscles, which are known to produce a relationship which is more curvilinear. For mixed fiber type muscles, the sEMG-force relationship results to be curvilinear in contrast with muscles consisting of a singular muscle type [83].

In fact, various experimental protocols were devised in several studies in order to obtain this sEMG-force relationship from *isometric* contractions. These protocols included various experimental setups, numerous subjects, differing resting and contraction times and also differing contraction directions and postures. For studies targeting the biceps muscle, contractions have been exerted at singular static angles, specifically at 90 º in some cases [88] [89] with other researchers analysing different elbow angles [90] [91] [92]. Importantly, all studies specified adequate resting periods in order to prevent fatigue, which is a vital factor for force exertion studies [88] [89] [90] [91] [92]. Finally, all these different studies have agreed on the fact that with an increase in force exertion, an increase in sEMG features is obtained.

4.1.3. The EMG-Velocity Relationship

The most investigated contraction is the isometric contraction, however most tasks in daily life involve dynamic contractions. These latter contractions are more challenging to study since during such contractions, muscle fibers change length whereas sEMG electrodes remain affixed to the original skin location. Thus, the relationship between the electrode and the muscle fibers is continuously changing, adversely affecting the sEMG signal [75].

Furthermore, the factors mentioned in Section 4.1.2 are not only noticeable when obtaining a relationship between the EMG signal and force values but also when trying to obtain a relationship with contraction velocities. Therefore, relationships are expected to vary with changes in electrode placement, anisometric test values, differences in the range of limb motion, experiment duration, statistical analysis and the muscles investigated [89] [93]. The human motor variability phenomenon is an additional factor affecting such relationships since repetitive movements almost never result in identical sEMG signals [73] [94].

Differences in muscle postures and movements are also known to affect these relationships due to the changes in the way the muscle has to work, with linearity being dependent on the number of roles played by the muscle during the movement [95].

There were several studies which carried out research to obtain relationships between sEMG features and different velocities. Exponential trend lines were obtained to describe relationships between maximum EMG RMS values and their respective maximum velocity and acceleration values for bicep curls performed over three

velocity ranges [96]. In the meantime, for forearm movements in a horizontal space and with a pronated hand, a quadratic relationship was obtained between Integrated EMG (IEMG) and velocity [95], where the IEMG is a subset of the procedure of obtaining the average rectified value with the difference that the average rectified value is divided by the number of samples over which the calculation has been carried out [97] [98]. In this case, the electrical activity of the biceps was examined from the start of the movement until the angular forearm velocity reached its peak, therefore during the first phase of acceleration.

This technique of using only a section of the movement's signals was also used for wrist movements where the EMG's area was only calculated for the period containing the first agonist EMG burst, leading to the claim that for an increase in movement velocity, an almost linear increase in the first agonist burst area was obtained [73]. This leads to the fact that several authors opted to find EMG relationships by solely considering specific parts within the EMG signals. Gielen et al. [99] have also published their choice to calculate the IEMG activity for the duration of its burst rather than the whole movement's duration. From horizontal forearm flexions, a linear relationship was found with respect to a range of peak velocities. Furthermore, these researchers found quadratic relationships between EMG excitation levels versus peak velocities for horizontal arm movements at two different inertial loads.

Therefore, these studies all confirm that with an increase in velocity, an increase in the chosen EMG feature is expected, as was the case with the force feature.

4.2. Isometric and Anisometric Experiment Methodology

Keeping in mind all the relevant procedures followed by other researchers as mentioned in Section 4.1 as well as the aim of the experiments, the two experimental procedures required to obtain the two defined relationships were carefully devised. The experiments required were split into two, namely *Isometric Contraction Experiments* and *Anisometric Contraction Experiments.* For the *Isometric Contraction Experiments*, the forearm and upper arm muscles were required to be kept at a constant length whilst performing a specific force value against an immovable object. The *Anisometric Experiments* were based on the concept of *Isovelocity* or *Isokinetic* movements which consisted of concentric and eccentric movements performed at various constant set speeds, without changing the exerted force value.

While it had been initially decided that a minimum of five subjects were required for these experiments to obtain the required relationships, due to the disruptions caused by the COVID-19 pandemic, only three subjects had managed to participate before the laboratory was closed down due to precautionary restrictions. Furthermore, one of these subjects had participated prior to final posture decisions were made and thus, it was decided that this subject's results would not be used due to the experimental discrepancies from the other two. Therefore, the results discussed here shall be based on two different subjects, referred to as *Subject 0* and *Subject 2*.

The two participants were a 23-year-old male and a 24-year-old female. Both subjects did not do physical training on a regular basis since this was an exclusion criterion which was set to retain subjects within the norm. The subjects were both right-hand dominant and the required relationships were obtained for this same dominant arm. All subjects also declared that they did not have any history of musculoskeletal pain or injury in their upper limb or muscles before recruitment and consented to participating in these experiments, which were in line with the University of Malta's research ethics guidelines.

4.2.1. Subject Pose, Orientation and Movement Features

Since both *isometric* and *anisometric* experiments were performed by the same subjects on their same experimental day in order to have the same conditions for both experiments, a specific arm orientation was chosen which enabled exertion of constant force contractions as well as constant velocity movements. It was decided that the subjects were to be standing up with their right arm at a 90 ° shoulder flexion with the wrist in a natural position (i.e. the thumb is upwards). By providing a way to rest their elbow, the subjects were free to move their forearm in a lateral (external from the chest) and medial (internal towards the chest) manner, by adjusting the elbow joint. These movements shall be referred to as extension and flexion of the elbow joint, respectively. An adjustable tripod was chosen to perpendicularly secure the elbow to the chest.

This posture with medial and lateral movements was chosen rather than proximal and distal joint rotations due to the effects of the gravitational pull that would have otherwise been imposed during the flexions of the dynamic experiments.

Since the participants were not strapped and restrained as has been found in some literature [88] [89] [90] [91], the subjects were made aware to keep a straight posture and a lunge posture for the *anisometric* and *isometric* experiments, respectively. The lunge posture was chosen to enable the subjects to exert their actual maximum force in a steadier posture without risk of toppling over. The participants were also required to minimize unnecessary shoulder and upper arm movements such that the biceps brachii muscle remained the main activator throughout both experiments.

The upper arm was not restrained, so as not to deform the upper arm muscles from which the myoelectric signals were to be acquired from by using electromyographic electrodes. The subjects' arm postures and movements from front and top views can be seen in Figure 4.3.

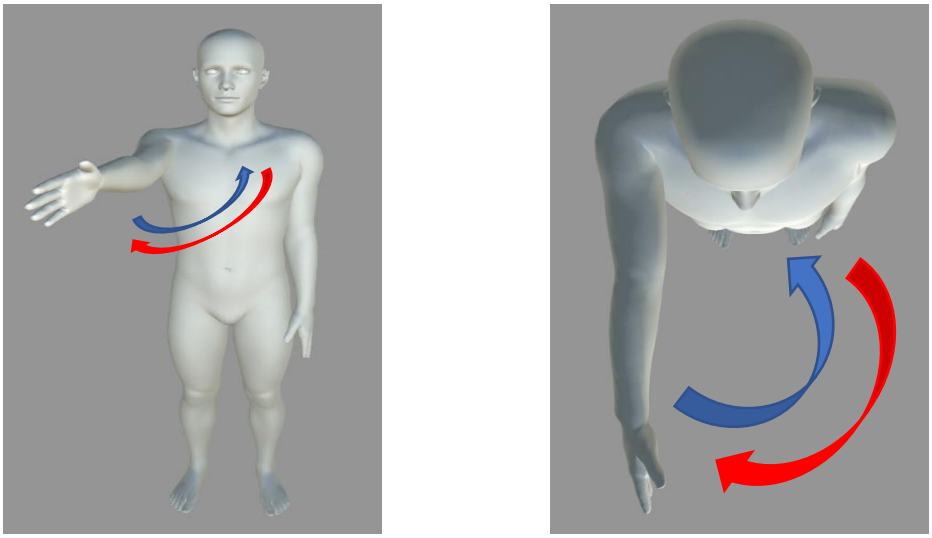

(a) (b)

Figure 4.3 - (a) Front and (b) Top views of the subjects' arm posture. The images show the fully extended arm at a 90 º shoulder flexion. The blue and red arrows refer to the direction of forearm movement from the elbow joint in flexion and extension, respectively.

4.2.2. The Setup

In order to carry out the experiments, the whole setup consisted of the following:

- A tripod adjusted and levelled according to the subject's height such that the elbow could rest on it, in a perpendicular orientation to the rest of the body. The tripod was utilised as a resting base for the elbow for both the *isometric* and *anisometric* experiments;
- A screen showing the Graphical User Interface (GUI) developed for the *isometric* experiment;
- A MARK-10's M5-500 Force Gauge Model dynamometer [100] mounted on

an aluminium profile which in turn, was mounted to a brick wall. This aluminium profile also included a mounted pulley, situated underneath the dynamometer with both pulley and dynamometer having the ability to be adjusted upwards or downwards, according to the subject's height. The pulley was required in order to direct a rope which was attached to the subject's wrist, to the dynamometer in a perpendicular manner. The rope was attached to a Velcro band which could be easily strapped to the subject's wrist. A setsquare was also used in order to ensure that the rope and the subject's forearm were perpendicular to each other. This part of the setup was only utilised for the *isometric* experiments and can be seen in Figure 4.4;

- A metronome to produce varying speed guidelines to the subjects for the *anisometric* experiments. A metronome website accessed through a smart phone was found to be suitable to provide these beats for this application;
- A TSD130B twin-axis goniometer [101] attached to the subject by attaching one end of the sensor to the upper arm and the other end of the sensor to the forearm by using double sided tape for elbow joint angle data. Medical tape was also used to secure the goniometer to the subject's arm. Since this sensor was not giving accurate values at the flexion ends, the readings from it were used to detect the static elbow angle during the *isometric experiments* as well as a tool to synchronise the Vicon motion captured angle data obtained (as will be mentioned below) with the sEMG signals;
- A singular channel from the wireless, ZeroWire sEMG system [102] which allows digital transmission of the EMG signal to a receiver device. The wireless bipolar electrode module was used to record bicep sEMG data with the use of two 8 mm, pre-gelled silver/silver chloride (Ag/AgCI) disposable electrodes, as shown in Figure 4.5.
- The Vicon Nexus motion capture system [103] and MP150 BIOPAC acquisition system [104] connected with all required sensors. By using these two systems, proper kinesiological analysis could then be possible. Angle and force sensors as well as EMG data could be synchronously recorded from the BIOPAC system which provided kinematic, kinetic and electromyography data, using a sampling rate of 1 kHz. This was done by using the UIM100C [105] and DA100C [106]. The subject's anthropometric data as well as elbow angle values could be obtained from the Vicon system, using a sampling rate of 100 Hz.

(a) (b)

Figure 4.4 - (a) The height adjustable dynamometer and pulley mounted on an aluminium profile and (b) a Velcro strapped wrist exerting force on the dynamometer through the rope with the setsquare showing a perpendicular angle between the forearm and the rope.

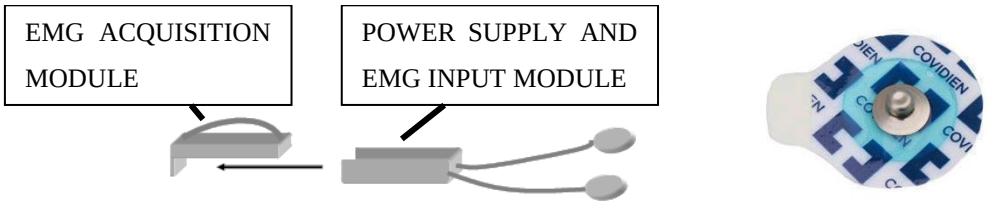

(a) (b)

Figure 4.5 - (a) The ZeroWire, wireless sEMG module [102] and (b) the 8 mm diameter Ag/AgCI, pre-gelled adhesive back with non-irritating gel, disposable surface electrodes [107].

For the Vicon motion capture system, in order to gather the right amount of data whilst not overwhelming the subjects with the number of optical motion markers, in addition to the other sensors which had to be attached to their arm; twelve markers were used. During post-processing, these twelve markers were eventually split into four segments, namely the Left Arm Segment (L_A), Right Arm Segment (R_A), Right Leg Segment (R_L) and Left Leg Segment (L_L). By obtaining data from these four segments, the posture of the subjects during experimentation periods was then able to be deduced. The most critical segment for the required results was the Right Arm Segment; most specifically, the shoulder, elbow and wrist markers. These markers were used to calculate the elbow angle values for the a*nisometric experiments.* Figure 4.6 (a) shows some of the markers as placed on the body for an *anisometric experiment* posture while Figure 4.6 (b) shows all the markers captured by the motion capture system.

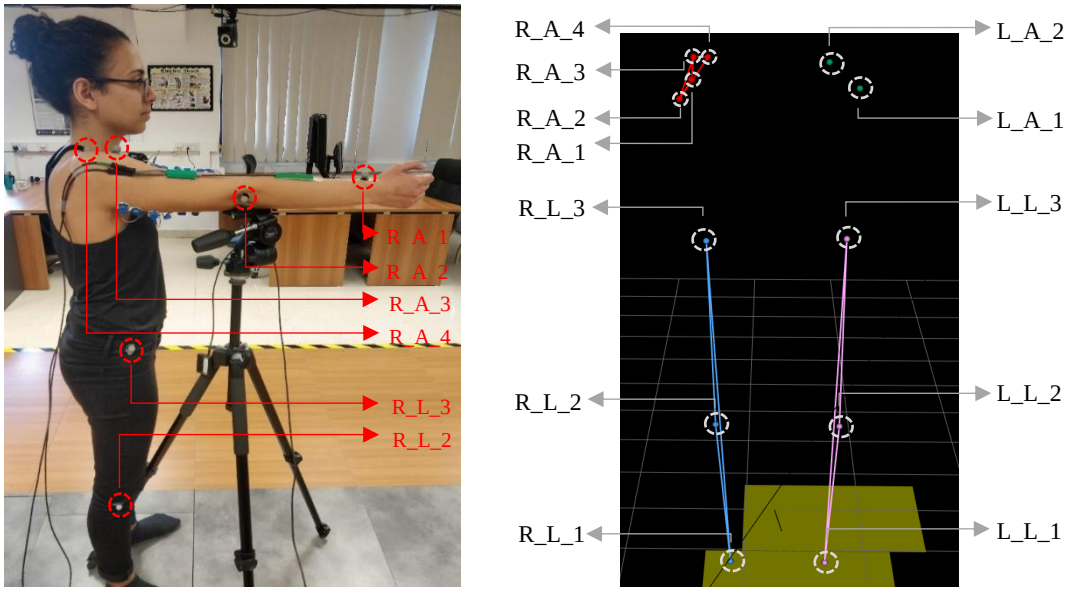

(a) (b)

Figure 4.6 - (a) Six of the twelve markers as attached to the subject during experimentation and (b) the twelve markers as captured from the Vicon system at a fully extended arm position during Anisometric Experiments. The green, red, blue and pink segments are the Left Arm, Right Arm, Right Leg and Left Leg Segments respectively.

4.2.3. Skin Preparation and Electrode Sensor Configurations

For the best sEMG signal characterisation, maximal care had to be taken during skin preparation and electrode sensor positioning. Electrode-skin impedance and noise reduction, proper electrode fixation and overall better sEMG recordings are obtained from appropriate skin preparation, thus, the standards listed by Hermens et al. [108], in line with SENIAM guidelines were followed. Therefore, during skin preparation, the subjects' skin was shaved, abraded and cleaned with alcohol wipes.

Since for biceps experiments, the muscle under analysis is not covered by other muscles or bones, skin surface electrodes were noted to be sufficient to obtain the necessary myoelectric information. Such surface electromyography electrodes are non-invasive, unlike needle or fine-wire electrodes. Furthermore, the use of wet-gel disposable electrodes, as were used in these experiments (Section 4.2.2) are known for their best hygienic aspects whilst also being easier and quicker to handle.

The Ag/AgCI disposable electrodes had an 8 mm diameter conductive area and following adjacent electrode placements, the inter-electrode distance was 24 mm, in line with SENIAM guideline recommendations [10] [57] [108].

4.2.3.1. Biceps-Brachium Electrodes Placement

At least three muscles contribute to the force output during bicep movement, namely the biceps brachii, brachialis and brachioradialis [90] [109]. While it is not feasible to separate forces into the component forces of each muscle of the group, it was concluded that the relationships between the joint torque and the myoelectric signals for the separate muscles are dependent during isometric conditions [109]. Thus, the joint torque may essentially be written as a function of the myoelectric signal from any one of the three muscles. Since the signals from the brachioradialis and the brachialis cannot be reliably obtained using surface electrodes, the best muscle to examine is the biceps brachium, as was done for these experiments.

Positioning of the electrodes was also made in accordance to the SENIAM guidelines, ensuring that the electrodes remained on the active muscle mass during movements, also targeting the most dominant middle portion of the muscle belly by placing them on the line between the medial acromion and the fossa cubit at a third from the fossa cubit as shown in Figure 4.7 [57]. The electrodes were placed in parallel to the muscle fibers and in the centre of the mass in a longitudinal arrangement [110]. Despite some sources [90] [109] [111] suggesting a transversal arrangement instead, the SENIAM guidelines were still followed for this project, as do most studies [49] [50] [112].

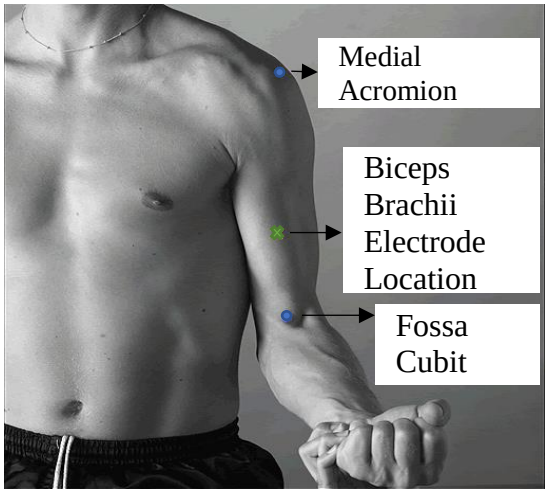

Figure 4.7 - Biceps Brachii electrode location as per SENIAM guidelines [57].

4.2.4. Anisometric Contractions Experiment Procedure

The focus of the *Anisometric Experiments* was for the subjects to perform forearm flexions and extensions at a constant velocity, to the best of their ability, for five repetitions, at five different reference beats, namely 50, 85, 120, 155 and 190 beats per minute (BPM). The speed guidelines were provided to the subject by a metronome, and necessary resting times were indicated clearly whenever required. Flexions were initiated at a 0 ° elbow joint angle (wrist in line with the shoulder) and halted when the hand reached the chest at an approximate elbow joint angle of 120 ° and vice-versa for extensions. The subjects were to move their arm as naturally as possible without the fear of striking themselves since this would lead to bias of the results obtained and were also instructed to have a relaxed fist such that no unnecessary gripping takes place. While extensions were not to be analysed, these were included for the subject to keep up a constant pace between repetitions.

A visual process of the above experimental procedure is provided in Figure 4.8. A minimum of a five-minute rest time was granted to the subjects between the *Anisometric* and *Isometric Experiments*.

4.2.5. Isometric Contraction Experiments Procedure

For the *Isometric Experiments,* the main aim was to obtain an sEMG signal relative to different force values exerted by the biceps during static contractions. Therefore, isometric contractions were exerted at a 90 ° elbow joint angle while the force was applied at the wrist to ensure that the biceps and triceps muscles were primarily involved. Real-time goniometer readings aided with elbow joint angle monitoring.

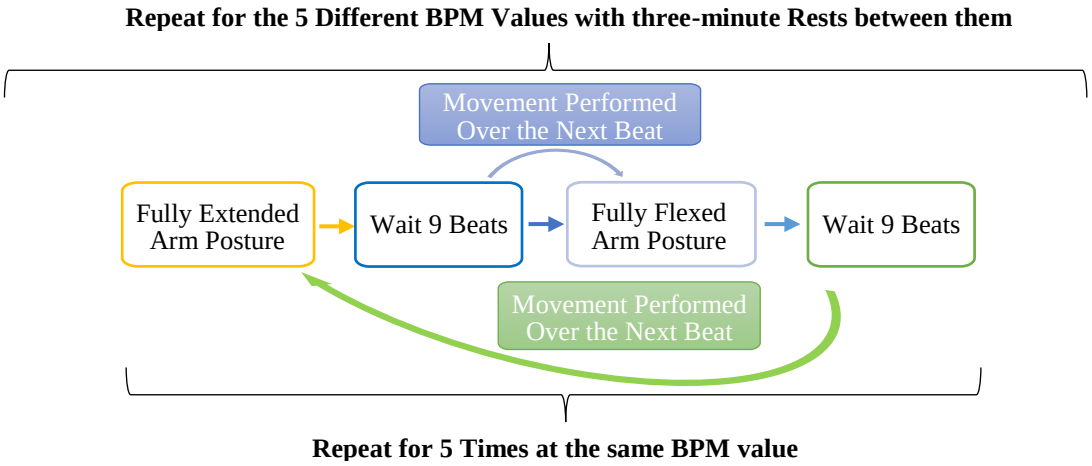

Figure 4.8 - The Anisometric Experimental Flow.

The subjects were required to exert five levels of force for five seconds each. These force levels were determined in accordance to the greatest Maximum Voluntary Contraction (MVC) performed by the subject such that other prescribed sub-maximal forces were exerted at approximately 20%, 40%, 60%, 80% and 100% of the MVC, using the display of a dynamometer as feedback. All contractions were to be performed in non-fatigued conditions, thus, suitable resting times were provided between trials.

The subject was instructed to follow the procedure indicated by a Graphical User Interface (GUI) projected on a screen. This clearly indicated the actions required from the subject as well as the required force levels to be exerted. Through the GUI, the subject and experimenter were notified when the subject was to get ready for the next contraction, the instant when the contraction was to start and when the subject was to release the contraction and rest. The followed procedure in conjunction with the GUI visual and sound cues, as well as manual inputs, are provided in Figure 4.9.

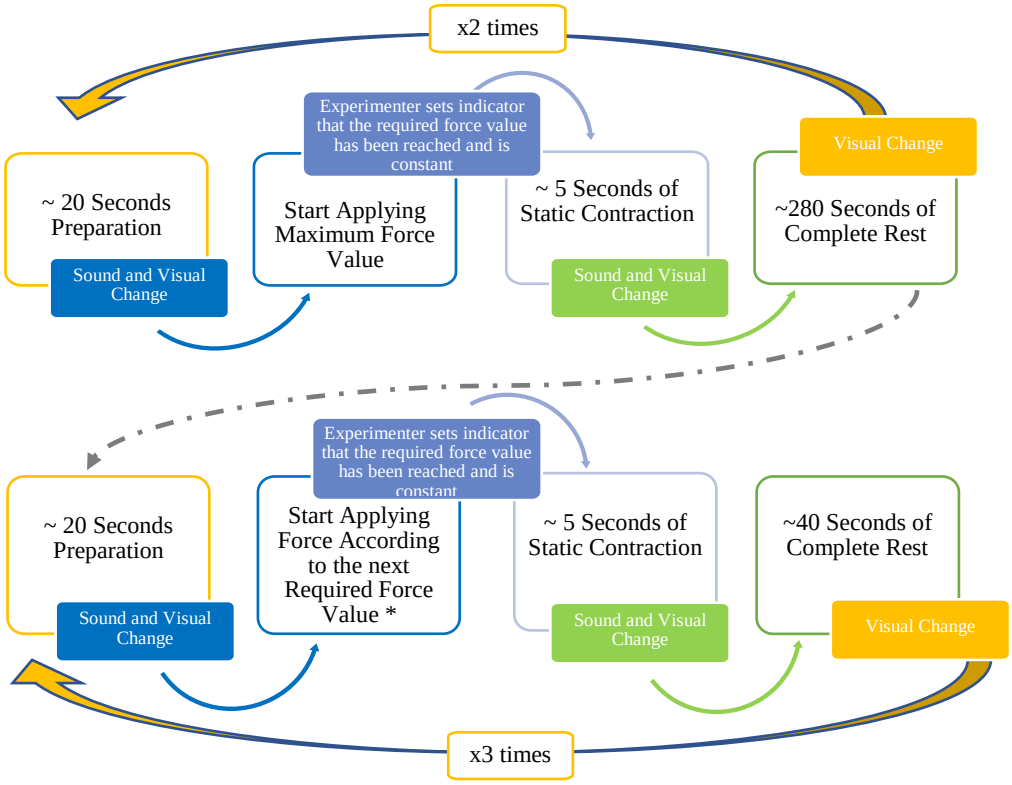

* The force to be applied is set to 20%, 40%, 60% and 80% of the maximum MVC value respectively

Figure 4.9 - The Isometric Experiment Flow as followed by the subjects. The text shown in the shaded boxes are inputs to or outputs from the GUI to aid the subject and experimenter during acquisition. The yellow parts of the flow depict the state where the subject was asked to start getting ready for the next contraction; The blue parts depict the initial contraction stage before the required contraction force is reached and kept steady; The purple parts depict the five seconds of required contraction; The green parts depict the subject's rest state.

4.3. Signal Processing Methodologies

Due to their nature, recorded raw EMG signals need to be properly processed before being used for further analysis. There are several methods and steps involved with suitably processing these signals, depending on the nature of the signals as well as the nature of contractions. Some of these techniques are explained below.

Since the EMG baseline quality determines the signal's noise and offset when at rest [10], for this work, the sEMG signals were chosen to first be detrended by eliminating these offset or DC levels on which the signals were mounted.

4.3.1. Filtering

It is known that EMG electrodes, apart from the wanted and useful EMG data, also pick up noise, therefore creating signal distortions. Noise mixed with the pure EMG signal is obtained from various sources and as explained by De Luca [97], may be caused by ambient noise, motion artefacts, signal instability and electronic component inherent noise, amongst others. Nevertheless, while the EMG signal is limited from 10 to 500Hz, the dominant energy is that between 50 and 150Hz. Stegemen and Hermens [113] state that while 95% of sEMG power is provided for by the harmonics up to 400Hz, low-pass cut-off frequencies are to be close to 500Hz while high-pass filtering should have a cut-off frequency between 10 and 20Hz, in order to preserve the most important sEMG frequencies. Meanwhile, whilst ambient noise is known to be a great contributor to noise whilst analysing an EMG signal, some researchers opt to include a notch-filter at this frequency, which is dominant at the mains power frequency (50Hz or 60Hz in most cases). Nevertheless, such filters will not only remove the unwanted power line frequencies but also adjacent dominant frequency components and thus, it is not always advisable [97].

For these experiments, EMG signals were filtered using a 4^{th} order Butterworth filter, having cut-off frequencies at 10Hz and 450Hz. The filter was implemented using the 'filtfilt' *Matlab* function such that no lag was introduced to the original signal. This filtering was done on the raw EMG signals, following their detrending.

4.3.2. Normalization

EMG normalization is commonly used where an electrical signal value at any point in time is expressed as a percentage of the muscle's activity recorded at a specific calibrated contraction. In order to be able to compare such signals to each other, a referencing point such as the MVC that one can exert is useful. In fact, there are guidelines regarding subject positions and exercises that are to be followed in order to obtain the actual MVC value. The most important part of the MVC exercise is very good fixation and contraction against rigid resistance [10] [114].

For this work, the results from the *isometric* experiments shall be presented in accordance to the normalization to these MVC values. Meanwhile for *anisometric* data, there was no subject-specific maximum velocity value, therefore the largest velocity measured across all trials and subjects was found and an upper bound of 240 °/s was used for velocity normalization.

4.3.3. sEMG Feature Choice for Analysis

The several features mentioned in Section 3.2.2, all allow a researcher to obtain different quantitative data from EMG signals. However, it has been argued [72] [97] that the RMS feature has a physical meaning regarding the power of the signal, which is why it is preferred when obtaining relationships of this kind. This is usually done in comparison to the popular MAV feature which simply provides the area under the signal without a specific physical meaning. The RMS feature is also said to show less variability when compared to MAV over successive *isometric* time windows, which results in the RMS feature having the capability of detecting smaller signal changes [115]. Conversely, no such claims were found regarding which feature is best for characterising EMG signals with respect to movement velocity relationships, although the IEMG feature is one of the most commonly used [95] [99]. However, this feature is simply a subset of the MAV procedure [97] [98]. Thus, it was decided that the relationships that were to be obtained from these experiments were to be found with respect to the sEMG RMS value.

4.4. Data Processing and Analysis

Following data collection, several post-processing scripts were created on *Matlab* such that dynamic relationships between average velocities and sEMG RMS, as well as

relationships between the forces exerted by every subject and their respective sEMG RMS values could be obtained.

4.4.1. Data Processing for the Anisometric Experiments

Due to the fact that for every subject's *anisometric experiment*, five repetitions of lower arm flexions and extensions per metronome trial were performed, 25 different flexion instances and another 25 different extension instances were obtained. Since the biceps is the main muscle acting on the flexion movements rather than extension movements, only the former contraction instances were analysed for this experiment. A flow chart showing the process that the collected data was processed through in order to achieve the RMS values for their respective flexion average velocities is provided in Figure 4.10.

Since the goniometer was unreliable with correctly recording the higher end of the angle spectrum, the motion capture marker data were used to determine the elbow joint angle, θ, by using Equation (4.1), where $\overrightarrow{SE}$ and $\overrightarrow{EW}$ are the two-dimensional vectors obtained from the shoulder (S) and elbow (E) markers, and the elbow (E) and wrist (W) markers, respectively. This relates to Figure 4.11.

$$\cos\theta = \frac{\overrightarrow{SE}\cdot\overrightarrow{EW}}{\left|\overrightarrow{SE}\right|\left|\overrightarrow{EW}\right|} \tag{4.1}$$

Since the Vicon and BIOPAC systems were not hardware synchronised, the joint angle motion data was manually aligned to the sEMG data using the goniometer data since the latter two are hardware synchronised through the BIOPAC system.

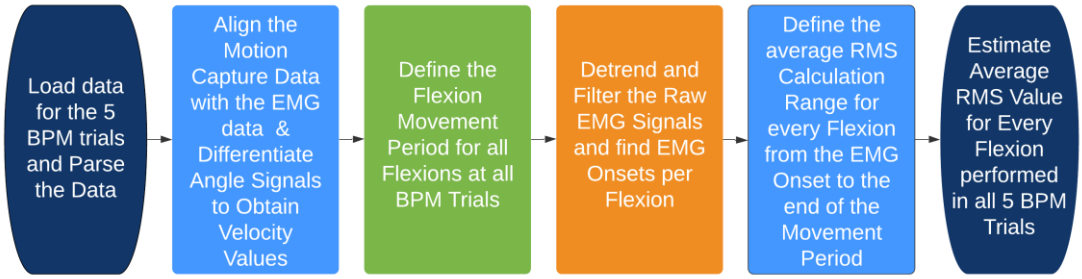

Figure 4.10 - A flow chart showing the data processing for the Anisometric Experiments.

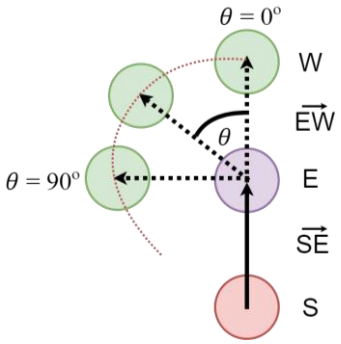

Figure 4.11 - The motion markers on the Shoulder (S), Elbow (E), and Wrist (W) and their resultant vectors used for elbow joint angle calculation.

The flexion movement period was defined as that interval where the calculated velocity exceeded 5% of the peak velocity of that specific flexion. The average velocity of each flexion was calculated by dividing the change in the joint angle during this interval by its duration.

Meanwhile, for every flexion trial, the sEMG onsets were determined using the single-threshold method [116]. In this method the resting mean, μ_{rest}, and standard deviation, σ_{rest}, were estimated and a suitable value for c was chosen manually to ensure proper onset detection. The threshold, T, was set using:

$$T = \mu_{rest} + (c * \sigma_{rest}). \quad (4.2)$$

The average RMS value for each flexion trial was therefore estimated starting from the sEMG signal onset up till the end of the movement period as illustrated in Figure 4.12. The estimated RMS values therefore considered all agonistic bursts within the single joint movement triphasic sEMG pattern, which usually consists of the initial agonist muscle burst, followed by an antagonist and several smaller agonistic bursts [73]. For this work, this was considered to be the best representation of the average velocity contraction [117], in contrast to some of the literature listed in Section 4.1.3, where only the initial sEMG agonistic burst was considered.

4.4.2. Data Processing for the Isometric Experiments

Following data gathering from the different subjects, the data analysis process carried out for the *isometric experiments* was according to the flow chart shown in Figure 4.13.

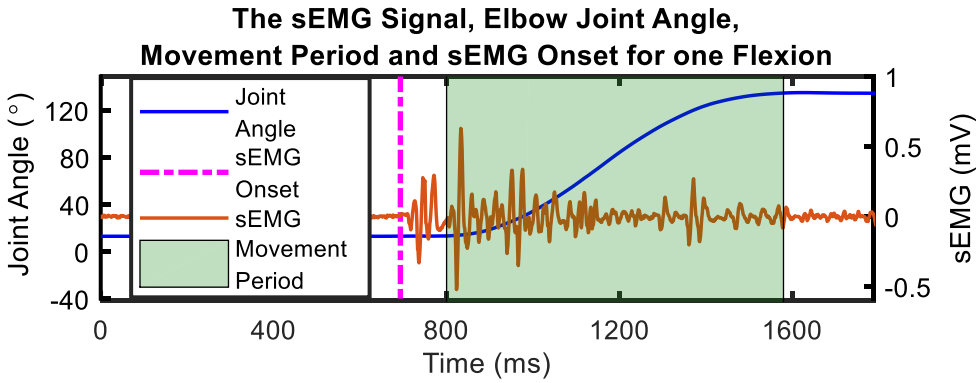

Figure 4.12 - The recorded elbow joint angle and sEMG signal from a flexion during an anisometric experiment, as well as the determined sEMG onset instance and the movement period. The average RMS value was estimated from the sEMG onset up till the end of the movement period whilst the average velocity was calculated by dividing the change in joint angle of the movement period by its duration.

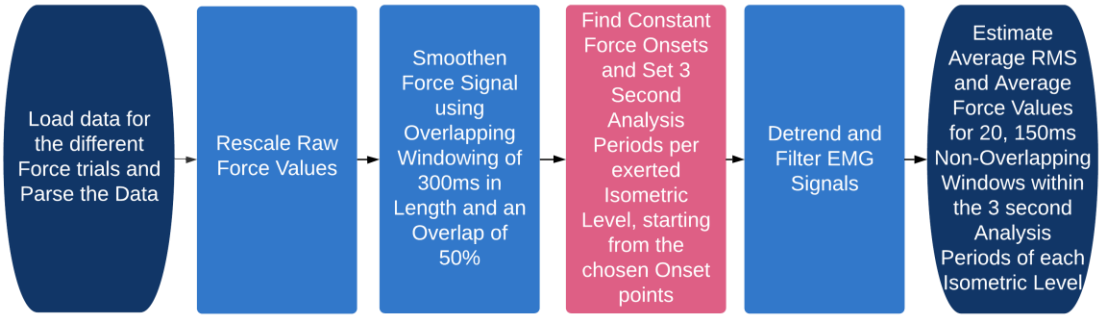

Figure 4.13 - A flow chart showing the data processing for the Isometric Experiments.

Since the force values were recorded by the MP150 data acquisition system as a raw voltage value from the dynamometer, a re-scaling, calibrating relationship between this raw voltage to the actual exerted force (as shown on the dynamometer screen) was required. Following a systematic calibration experiment, a linear relationship was obtained between the received raw voltage input and the actual force value, with a correlation coefficient of 1, as follows:

$$f(x) = -0.0004468x + 0.01348 \tag{4.3}$$

where x is the force value in Newtons and $f(x)$ is the raw voltage input.

This force data was then smoothened using a 300 ms averaging window with a 50% overlap. The single thresholding method was applied to the signal to detect those segments where the prescribed force levels were reached and remained stable for at least three seconds. For each isometric contraction level, sEMG RMS features and average force levels were computed from 20, 150 ms non-overlapping windows, yielding 100 sEMG RMS values and their corresponding average force values.

4.5. Results and Discussion

Matlab's built-in *Curve Fitting* application was utilised to find the optimal relationship for each subject's *isometric* and *anisometric* results, where the final best fit decision was taken based on the fitted curve shape, the square of correlation (R^2), the adjusted R^2, and the Root Mean Squared Error (RMSE) resulting from every fit. For better curve fitting results, any obvious outliers were removed and excluded from the curve fitting process.

Following the curve fitting process carried out for all the obtained results, the best fitting relationship between EMG RMS and average velocities was found to be that of a first order exponential as shown in Equation (4.4) whilst the best fitting relationship between EMG RMS and exerted force was found to be a second order polynomial as provided in Equation (4.5).

$$f(x) = ae^{bx} \tag{4.4}$$

$$f(x) = ax^2 + bx + c \tag{4.5}$$

where,

$f(x)$ is the EMG RMS amplitude;

x is the velocity or force value in (4.4) and (4.5), respectively;

a, *b* and *c* are coefficient constants.

For ease of comparison, curve fitting was performed on the normalized data for both experiments. The constant values as well as the square of correlation (R^2), the adjusted R^2, and the Root Mean Squared Error (RMSE) for the separately fitted curves are provided in Table 4.1 and Table 4.2 for both subjects' *anisometric* and *isometric* fits, respectively.

Meanwhile, plots showing the data and their respective fitted curve are provided in Figure 4.14 and Figure 4.15 for *Subject 0* and *Subject 2*, respectively.

Table 4.1 - The First Order Exponential Constants obtained from curve fitting the normalized anisometric data obtained for Subjects 0 and *2 as well as the resulting R^2, Adj. R^2, and RMSE values.*

Subject	a	b	R^2	Adj. R^2	RMSE
0	0.053	1.882	0.803	0.793	0.033
2	0.033	1.707	0.670	0.656	0.016

Table 4.2 - The Second Order Polynomial Constants obtained from curve fitting the normalized isometric data obtained for Subjects 0 and 2 as well as the resulting R^2, Adj. R^2, and RMSE values.

Subject	a	b	c	R^2	Adj. R^2	RMSE
0	1.246	-0.484	0.211	0.919	0.917	0.090
2	1.149	-0.350	0.190	0.899	0.897	0.102

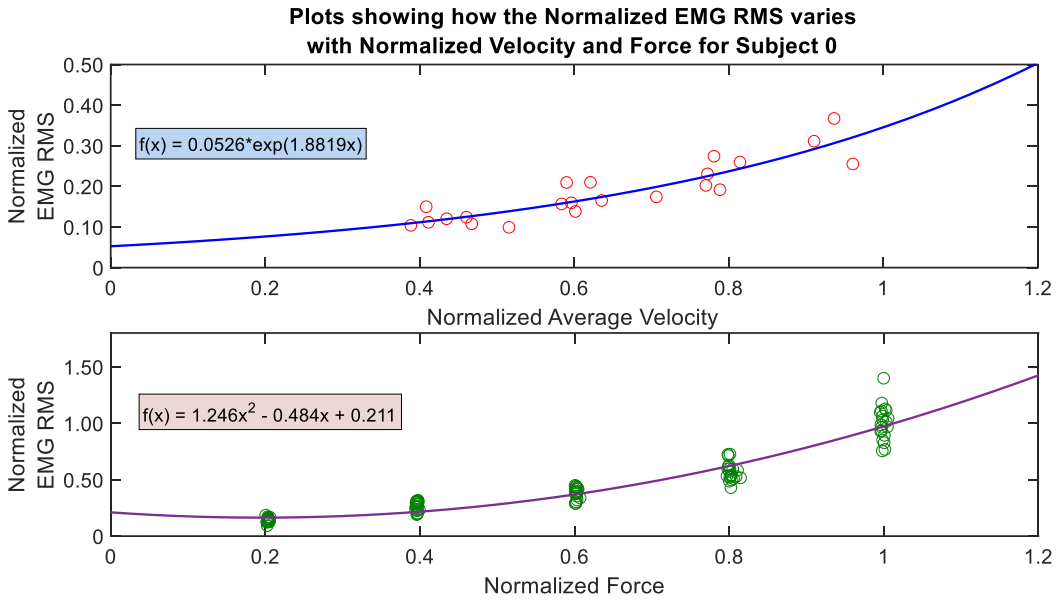

Figure 4.14 - Normalized EMG RMS vs Normalized Average Velocity and Normalized Force respectively, for Subject 0's Trial. The Plots also show the first order exponential relationship and second order polynomial relationship found between the Normalized EMG RMS and the Normalized Velocity and Force, respectively.

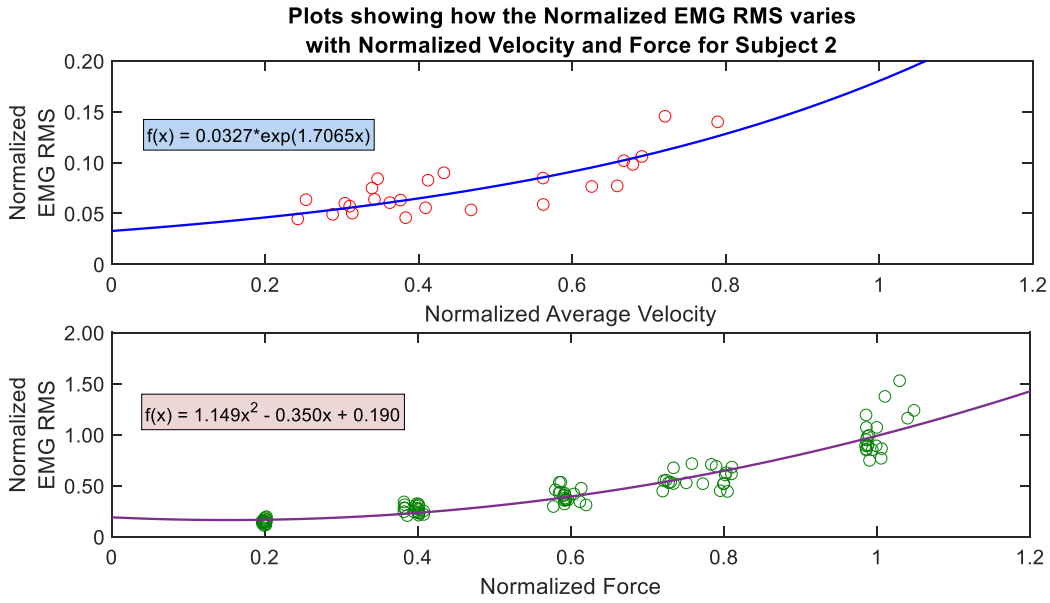

Figure 4.15 - Normalized EMG RMS vs Normalized Average Velocity and Normalized Force respectively, for Subject 2's Trial. The Plots also show the first order exponential relationship and second order polynomial relationship found between the Normalized EMG RMS and the Normalized Velocity and Force respectively.

One is to note how for *Subject 2*, exerting a constant force was found to be more challenging, resulting in more scattered points on the x-axis, when compared to the plots obtained for *Subject 0.* It is also clear that different subjects performed their flexion movements at different average velocities when compared to each other, even when provided with the same reference metronome beats whilst also given time to train. In fact, the average velocity range of the 25 movements performed by *Subject 0* was from 93.4 º/s up to 230.7 º/s whilst the range for *Subject 2* was from 58.3 º/s to 189.6 º/s. Thus, the flexions exerted by *Subject 2* were slower than those performed by *Subject 0.*

From the graphs obtained, it is also evident that the flexions instructed to be performed in line with the different metronome beats were not always performed in distinct velocity ranges from each other, with some points overlapping other metronome guided points. This was especially highlighted in *Subject 2*'s plots, where the flexions performed with the 120BPM reference were slower than those performed with the 50BPM reference. Nevertheless, it is also to be noted that *Subject 0* had longer training and better practise with this exercise than *Subject 2* which should have been the main contributor to the more defined ranges obtained by *Subject 0.* Mustard and Lee [73], in fact, have also commented how even when the instructions provided to the subjects are very specific, different subjects implement varying movement strategies when compared to each other. They have also discussed how it is easier for subjects to learn fast movements rather than slow movements, which is also visible in this study.

In the meantime, for easier comparison between the two subjects' relationships, an average fitted curve was computed for both relationships by averaging the parametric curves of both subjects. This averaging was done on the curves, rather than fitting a new curve to pass through all the points since there is less variability in the myoelectric signals obtained for one person when compared to a group of subjects [118]. These plots are provided in Figure 4.16. It is evident that while the relationships found for both subjects for the *isometric* experiments are very similar, the *anisometric* relationship obtained for *Subject 0* gives us more confidence than that obtained for *Subject* 2, since it shows the change in RMS value with increase in velocity more clearly.

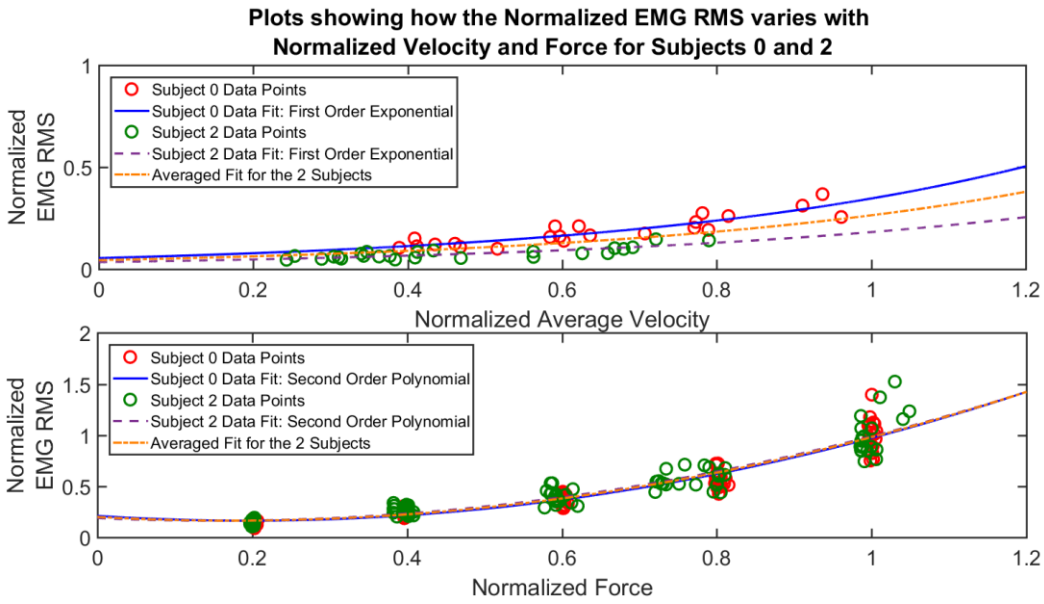

Figure 4.16 - Plots showing Subject 0's and Subject 2's Normalized EMG RMS Feature Values against Normalized Averaged Velocities and Force Values (red and green in both graphs), including the fitted first order exponential functions obtained from the anisometric experiments and the fitted second order polynomial functions obtained from the isometric experiments (solid blue and dashed purple for Subjects 0 and 2) respectively. The averaged fitted curves are also shown in dashed orange.

Nevertheless, all relationships obtained clearly indicate the increase in RMS with either feature. Despite the differences in the protocol and details of the experimental set-up from those reported in the literature, for the reasons elaborated in Sections 4.1.2 and 4.1.3 and the variations in the literature itself, the relationships obtained generally match those reported in the literature.

Although these results have provided useful insight, the specific relationships found in Section 4.5 relate to the elbow joint with biceps agonistic muscle recruitment. Therefore, these relationships cannot be directly applied to the hand and finger muscles which differ in many ways from the above. Lawrence and De Luca [118] specifically found that isometric relationships were found to be different for smaller muscles than those of larger muscles.

Nevertheless, the main scope of these experiments was to determine whether the same sEMG electrode can provide us with information in relation to their contraction type. Since positive relationships have been found for both contraction types, both signal states may be used for the prosthetic action intent system design, accordingly.

Furthermore, these results showed that the single EMG feature chosen, the RMS feature, could be used to discriminate between different levels of the same contractions which led us to propose to use this feature for both transient and steady-state signals

for information distinction. Thus, sEMG signal aspects which best characterise the two contraction types were to be identified.

4.6. Velocity and Force Characterisation

In the previous analysis, average RMS values were extracted to describe the energy within every flexion and static contraction. However, since raw EMG signals obtained from any muscle cannot be precisely reproduced on different occasions, digital smoothing algorithms are applied to the signals in order to create an envelope of the signal's development in time. This signal envelope also contains useful interpretation information and while there are several algorithms which may be used, enveloped RMS signals have been obtained in this work to determine motion and force contraction characterisations [10] [119]. The enveloped RMS signal that was obtained with time during elbow flexions and extensions, in relation to the elbow joint velocity, is shown in Figure 4.17.

This plot shows five continuous flexion and extension repetitions. Since the biceps muscle is the primary mover for flexion motions, as is clearly indicated in the plot, only the signal behaviours during flexions will be considered in this discussion.

From this relationship between the EMG RMS profile and the arm motion profile, it may be roughly concluded that the peak RMS values for every flexion correspond to the peak arm velocity. By only considering this peak point, which is also the point of the largest muscle recruitment, it is envisaged that the best characterisation of the movement may be obtained.

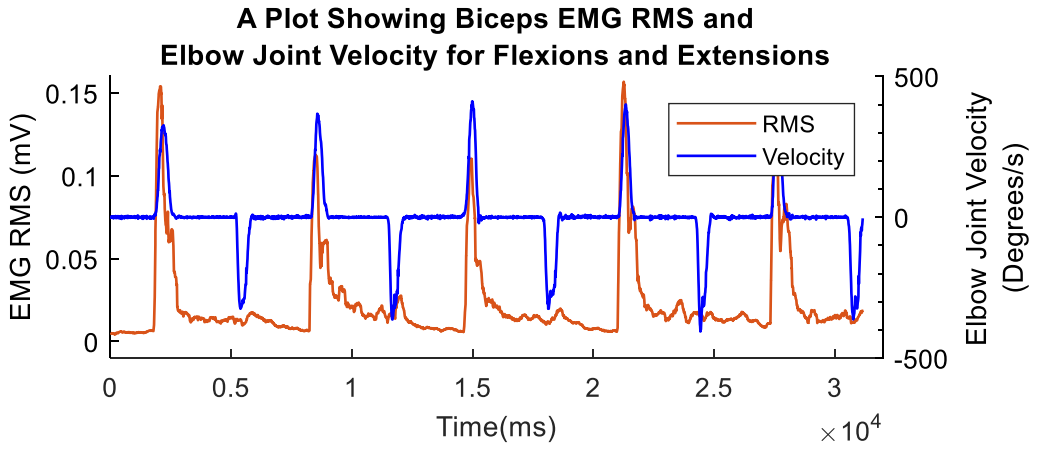

Figure 4.17 - The Biceps EMG RMS signal showing to vary with respect to the increase and decrease in elbow joint velocity during elbow flexions. The above zero velocities refer to elbow flexions while below zero velocities refer to elbow extensions. Since the biceps muscle is the primary mover for flexion motions, a high EMG response is only obtained during flexions.

Therefore, it may be concluded that the peak RMS value obtained during flexion generally represents the maximal kinetics of the arm movement. This peak RMS point may be described to be the maximum instance following the RMS transient stage of a dynamic movement.

For the best characterisation of static contractions, the behaviour of the EMG RMS envelope profile is to be related to changes in force levels, as shown in Figure 4.18. EMG signals during a static contraction are termed as steady-state. As shown in this plot, as soon as a static contraction level is reached, the EMG signal settles within a small range, ranging in amplitude levels with force level fluctuations. In contrary to the dynamic contractions discussed above, due to the nature of EMG signals during such static contractions, the best contraction characterisation is at any point in time.

The best characterisation points identified for both contractions relate to the way that an intuitive intent interpretation system may be designed. Whilst such characterisations have been obtained from a singular biceps sEMG channel, it is expected that finger movements as well as grasp contractions are similarly performed.

4.7. Conclusion

This chapter was aimed at identifying whether the EMG signals extracted during the two contraction types may contribute information in relation to the force and velocity parameters as well as identify which sEMG signal aspects best characterise these contraction types. The relationships obtained between the sEMG RMS feature and the force and velocity parameters confirmed that both transient and steady-state sEMG signals contain information in relation to the respective contraction exerted.

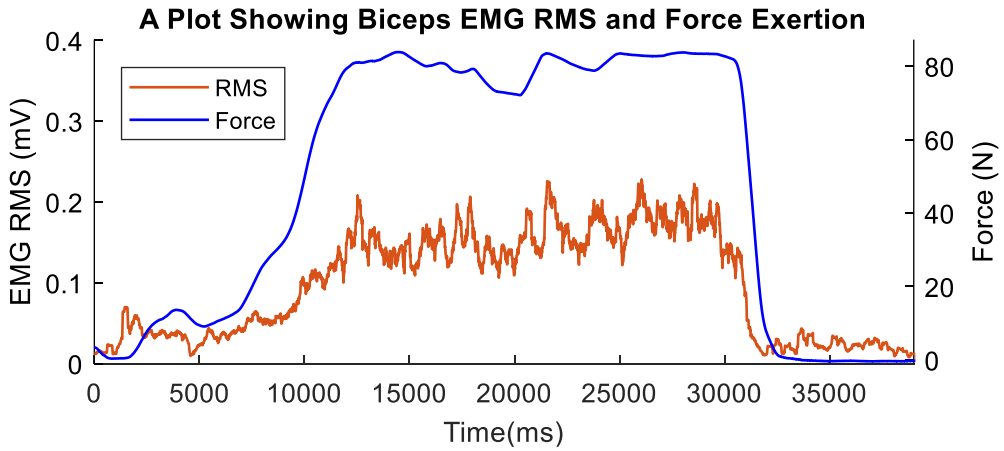

Figure 4.18 - The Biceps EMG RMS envelope signal increases with an increase in force exertion, which then settles within a narrow band during static force exertion of approximately 80N, and then decreases again with a decrease in force exertion.

This means that intuitive action intent could actually be achieved by separating motion contractions from force contractions, utilising the necessary information when required.

In order to identify motions from dynamic contractions, it has been concluded that the peak RMS point following the transient signal appears to be the best characterisation of the maximal kinetic of the motion. Meanwhile, there is no particular RMS point which best characterises static contractions, with the signal fluctuating with the contracted force level, in time. This singular EMG feature could therefore be used to discriminate between different hand motions as well as different grasping levels through intuitive hand use.

With appropriate use of this feature, a suitable prosthetic intent interpretation system could thus be implemented, with the aim of maximising the simplicity, dexterity and usability trade-off as identified in Chapter 1. This was to be done by keeping in mind the overall action intent system's efficiency, delay and reliability for intuitive control. Therefore, in this next chapter, the use of sEMG signals obtained from multiple skin surface locations on the forearm will be discussed in relation to the performance of different hand motions and grasps.

5. Intent Interpretation Framework Design

Following the specifications listed in the Introduction Chapter, as well as the information collected during the experiments reported in Chapter 4, one could devise the intent interpretation framework required to operate a prosthetic hand. For this framework to be in accordance with the required balanced trade-off, shown in Figure 5.1, various decisions had to be made throughout the different design and implementation stages, as will be explained in the upcoming sections.

5.1. Proto-Motions Characterisation

In order to provide the amputee with the capability of performing a large number of Activities of Daily Living (ADLs), the choice of grasping techniques which were to be made available had to be chosen carefully. The main aim was that the number of available commands was kept low for the sake of device simplicity and usability whilst still offering a fairly dexterous tool. In the literature, various grasps have been utilised, with the numbers and types varying between different research, as mentioned in Section 3.4. An analysis of the joint finger kinematics of various hand movements useful for ADL was carried out by a colleague within the context of the MAProHand project [120]. The conclusions from that analysis is reported in the next page and used in this study.

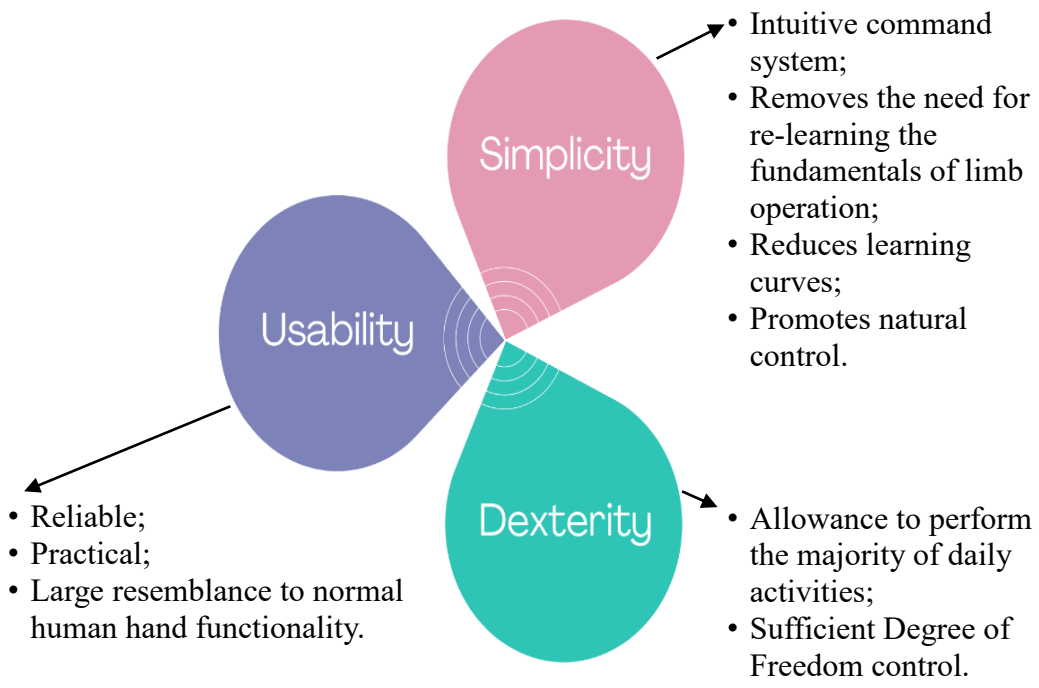

Figure 5.1 - The defined requirements for a balanced trade-off intent interpretation framework for hand prostheses.

Volunteers carried out ADLs with their constrained non-dominant hand while wearing a measurement glove to acquire finger joint kinematics. A principal component analysis of the joint kinematic data was carried out to obtain the Principal Components (PCs) which described most of the variance in the finger joint space. Since the obtained PCs could not be intuitively performed by the human hand, three human-like gestures, each transitioning between two grasps representing the extreme ends of the gestures, were chosen after careful analysis such that each gesture approximated one of the PCs, as shown in Figure 5.2. These gestures are here referred to as Proto-Gestures (PGs). The range of grasps within the first Proto-Gesture, PG1, is the most useful to a prosthetic user due to the highest joint angle variance, with the second and third Proto-Gestures, PG2 and PG3, respectively, contributing to less generally used grasps for ADLs. In this present work, it was sought to provide the user with acceptable dexterous capability of controlling a mechanical hand through the range of motions identified for these three PGs.

These PGs therefore allow the user to utilise any of the grasps which lie on the respective PG lines during the prosthetic arm's travelling, ultimately resulting in more grasping variations that may be exploited during task execution by the user. The grasps represented by the two extremes of each PG are listed in Table 5.1. Grasp 1+ and Grasp 1- are the grasps lying at the opposite extremes of PG 1. The same notation applies for the four other Grasps representing the other two PGs.

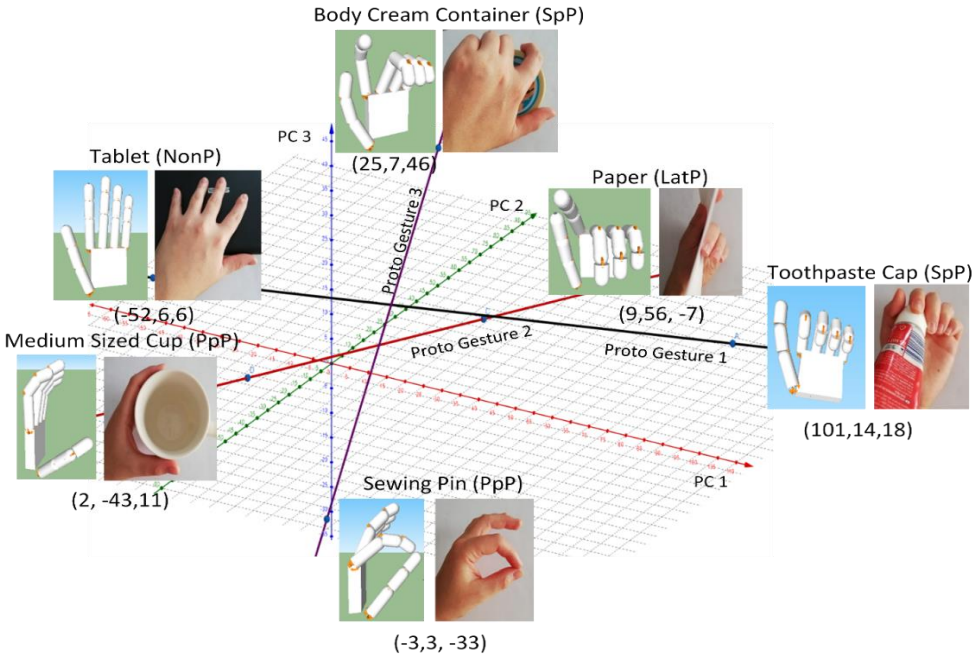

Figure 5.2 - The 3 resultant Proto-Gestures made up of 2 different grasp extremes each [120].

Table 5.1 - Defining the 3 grasp pairs representing the two extremes of the 3 Proto-Gestures.

Proto-Gesture	**PG 1**		**PG 2**		**PG 3**	
Grasp Number	**1+**	**1-**	**2+**	**2-**	**3+**	**3-**
Grasp Type	Toothpaste Cap Grasp a.k.a. Closed Fingers Grasp	Tablet Grasp a.k.a. Open Hand	Paper Grasp	Medium-Sized Cup Grasp	Body Cream Container Grasp	Sewing Pin Grasp

For this work, it was concluded that as a means of intuitive instruction, the subject should perform the movements in the same manner as the mechanical prosthetic hand would be required to perform. Thus, in order to make it easier for the subject to transition between the grasps without having to learn a lot of different grasping combinations, it was decided that only four movement sequences (relating to input control commands) should effectively be used. These motion sequences, referred to as Proto-Motions (PMs), consist of three different hand-closing PMs and one generic hand-opening PM. Proto-Motions involve movement performance from an initial hand grasp to an end grasp, in accordance to the PG end grasps listed in Table 5.1, with the difference that the relatively open hand Grasp 2- and Grasp 3+ are replaced by the open hand Grasp 1-. Therefore, these Proto-Motions allow the subject to navigate the mechanical prosthetic hand between the grasp extremes: Grasp 1- to/from Grasp 1+; Grasp 1- to/from Grasp 2+; and Grasp 1- to/from Grasp 3-. These yield the four Proto-Motions listed in Table 5.2.

Table 5.2 - The Initial and End Hand Postures which make up the four Proto-Motions.

Proto-Motion	PM 1	PM 2	PM 3	PM 4
Initial Hand Grasp	Closed Fingers Grasp/ Neutral Posture/ Paper Grasp/ Sewing Pin Grasp	Open Hand Grasp	Open Hand Grasp	Open Hand Grasp
End Hand Grasp	Open Hand Grasp	Closed Fingers Grasp	Paper Grasp	Sewing Pin Grasp

Proto-Motion PM 1 refers to the generic hand-opening motion, which may be activated by starting from any of the three closed hand grasps or the neutral hand state (the effortless posture which our hand naturally settles in with the least muscle tension). Meanwhile, Proto-Motions PM 2, PM 3 and PM 4 are the three hand-closing motions, which are activated by starting the movement from the 'Open Hand' grasp and ending in the 'Closed Fingers', 'Paper' or 'Sewing Pin' grasps, respectively.

In this manner, the subject would be able to choose the required Proto-Gesture and the direction of travel (opening or closing). It should be noted that this is different from the static posture methods used for posture classification in the literature described in Section 3.4. The subject would then be able to instruct the grasping levels of the prosthetic hand in accordance to the end grasp of the instructed motion as soon as contact with an object is made to achieve the intuitive flow discussed in Section 3.6.

5.2. sEMG Data Acquisition Equipment

In the literature review of Section 3.1.1, it was noted that six to eight symmetrically placed electrodes would be suitable for hand movement data collection. The *Myo* armband [121] is a widely-used device [122] [123] for hand EMG data acquisition. This armband consists of eight active EMG electrodes, referred to as pods, arranged in a band-like fashion in a manner which can be easily worn by subjects on their forearm. The in-built transmission module allows wireless data transmission through the Bluetooth Low Energy (BLE) protocol. Figure 5.3 shows a schematic of the *Myo* armband which operates at a sampling frequency rate of 200Hz, thus providing a frequency range from 0Hz to 100Hz. Despite this small range, it is known [123] [124] that this is still useful for hand movement classification. In view of the suitability of this portable and wireless EMG acquisition system, the *Myo* armband was chosen to acquire hand EMG data for the design of the EMG analysis algorithms.

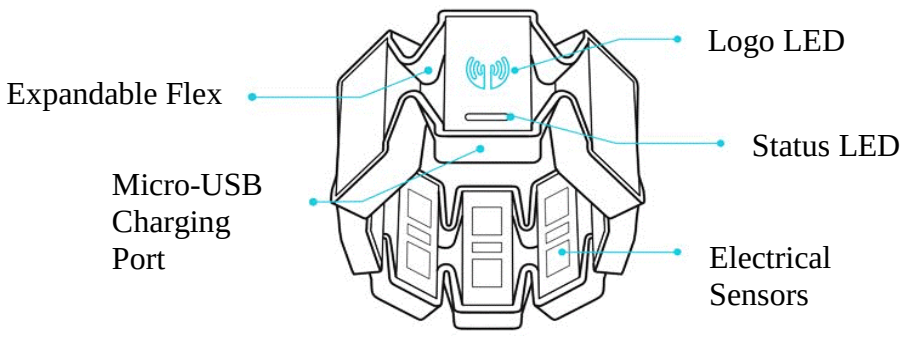

Figure 5.3 - The Myo Armband [125].

5.3. Signal Phases Identification

As has been confirmed in Chapter 4, sEMG signals are capable of providing us with information during both isometric and anisometric contractions. In order to exploit the two contraction types suitably, it was decided that the two kinds of contractions shown in Figure 5.4 were to be utilised during different parts of the intent interpretation framework. The sEMG features obtained during anisometric contractions were to be used to determine the user's commands with respect to the hand's desired movement direction according to the Proto-Motions defined in Table 5.2. The sEMG features obtained during isometric contractions were to be used to determine the prosthetic hand's grasping force. As can be seen in Figure 5.4, in order to determine the intended Proto-Motion, features need to be extracted from the brief time period of anisometric contraction, here referred to as the *Movement Phase*.

Conversely, features from the isometric contractions, here referred to as the *Force Phase*, are extracted from the period that comes after the Proto-Motion has been determined. These features are used to determine the level of force that the subject wishes to exert and which the user will ramp up to the required force level.

As was stated in Section 2.2.5, pattern recognition and proportional control techniques were thus implemented for intent interpretation of the *Movement Phases* and *Force Phases*, respectively.

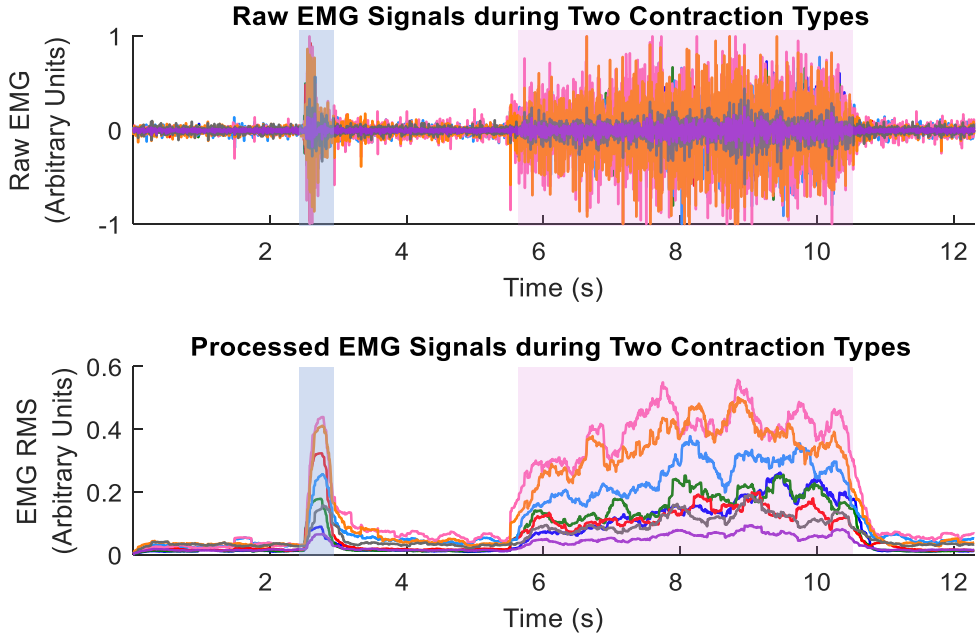

Figure 5.4 - Plots showing the behaviour of the eight EMG signals' during anisometric (shaded in blue) and isometric (shaded in pink) contractions, respectively. The top plot shows the raw EMG signals while the bottom plot shows the processed, EMG RMS signals using a 250 ms sliding window.

It may be noted that the sEMG plots have arbitrary units since the *Myo* armband converts the EMG analogue voltage signal sample to a digital number without any calibration information. This however does not pose any limitation on the use of the *Myo* armband since the EMG analysis algorithms only require relative EMG values.

For easier visual phase distinction, Figure 5.4 shows the two contraction types relating to the two phases, separately. However, for final prosthetic system use, the *Force Phase* is to be initiated as soon as the intended Proto-Motion is identified from the *Movement Phase*, lasting for as long as a pre-determined condition is met. This creates a loop such that the system always initiates in the *Rest Phase*, where the system is neither in the *Movement Phase*, nor the *Force Phase*. In this phase, the continuous extracted signal features could either indicate *Movement Phase* detection or no change in state. Once the *Movement Phase* is entered, sEMG features for motion command are extracted. Following Proto-Motion identification, the system then automatically enters the *Force Phase* where sEMG features are then extracted for force estimation commands until a pre- determined condition is reached, returning the system back to the *Rest Phase*. This flow is provided in Figure 5.5.

Nevertheless, for this work, the implementation of the two contraction type commands obtained from their respective phases were separately identified and analysed. Thus, the sub-systems within this flow were individually recognised.

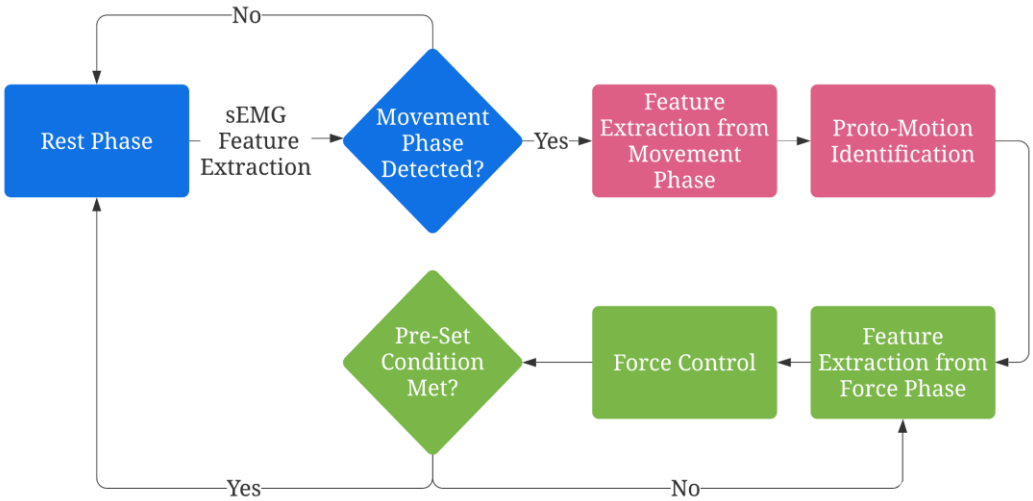

Figure 5.5 - The prosthetic framework flow, looping from the Rest Phase (blue blocks) to the Movement Phase (pink blocks) and the Force Phase (green blocks).

5.4. Movement Phase Intent Interpretation System

The *Movement Phase* intent interpretation system refers to the system developed to detect a *Movement Phase* from a *Rest Phase*, as well as identify the user's intended motion command. While a prosthetic action intent system is required to run online, or in real time, such that a decision can be made with regard to the prosthetic hand's state with every sample in time, an offline system is often used during the development stages to permit the study of different parameters. The main difference between the two is the ability of real-time feedback that may be provided to the user of an online system, which is not provided with offline systems.

The developed *Movement Phase* system can be divided into four stages as shown in Figure 5.6, namely: data collection, signal processing, movement detection and Proto-Motion identification. These four steps have been designed in a way as to ensure that the final system is balanced with respect to the three-attribute trade-off of simplicity, dexterity and usability, as will be explained throughout the text.

5.4.1. Data Collection

For sEMG data acquisition to take place through *Matlab*, the *Myo* band's Software Development Kit (SDK), which allows third party application interactions with the device, was used. For a successful interaction, a MEX file developed by Tomaszewski [126] was used such that EMG data could be enabled and streamed through the *Matlab* platform.

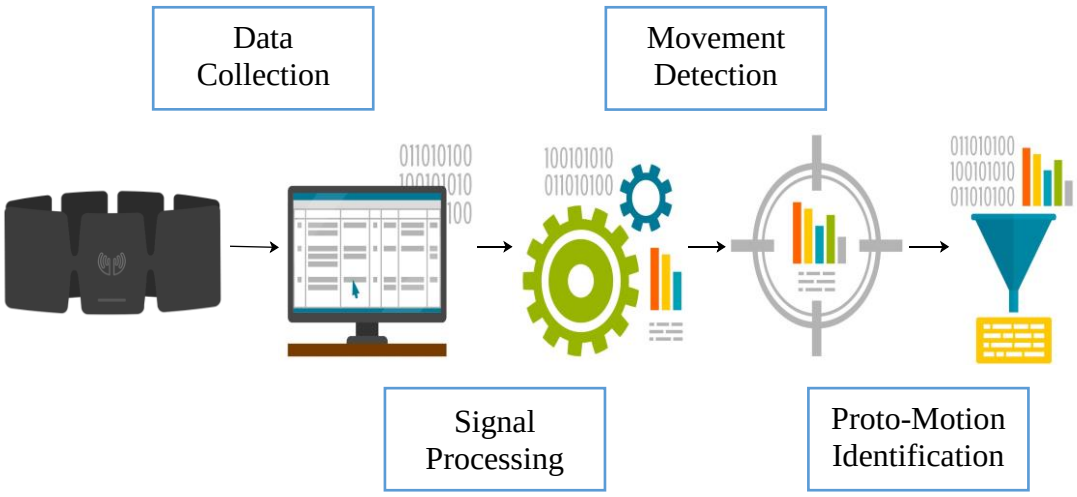

Figure 5.6 - The Movement Phase intent interpretation system flow made up of the data collection, signal processing, movement detection and Proto-Motion identification stages. [Some Resources for this design have been obtained from Freepik.com]

5.4.2. Signal Processing

The *Myo* armband does not provide developers with all the necessary specifications, in particular, it gives no information regarding the electronic low-pass filtering used. In order to obtain further understanding of the recorded sEMG signals, a frequency analysis was performed on some preliminary signals.

Figure 5.7 shows the magnitude spectrum of one sEMG signal corresponding to a hand movement. It may be noted that a 50Hz notch filter is being employed, however there is no clear indication of any other filtering being employed. A DC value was also noted and in an attempt to investigate whether signal detrending and high-pass filtering reduce the DC, preliminary tests were performed where signals were detrended and also high-pass filtered at a cut-off frequency of 10Hz. While this DC value was indeed reduced, no improvements were yielded on the Proto-Motion system, thus, it was decided that the signals were not to be digitally filtered or detrended.

Based on the discussions held in the literature review provided in Section 3.2.2 as well as that of Section 4.3.3, it was decided to extract solely the RMS feature from the EMG signals for the determination of the intended Proto-Motion, as well as for force estimation. Based on the discussion of Section 3.1.2, as well as from initial experimental analysis of the overall developed system as discussed in the next sections, the RMS feature was decided to be extracted from a sliding window of 250 ms with a single sample displacement of 5 ms. This window length was chosen as a balanced trade-off between keeping low feature variance and high sensitivity for action onset. Shorter window lengths, such as 100ms, increased the feature variance and negatively affected motion classification accuracy.

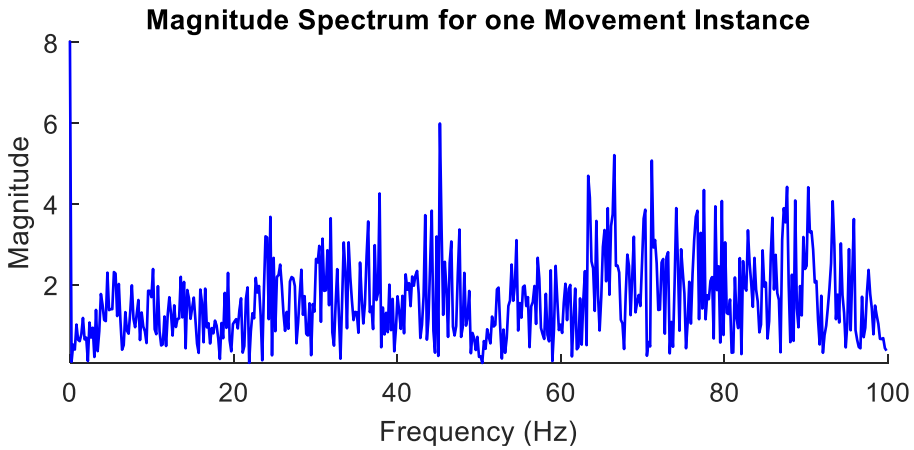

Figure 5.7 - Single-Sided Magnitude Spectrum of an sEMG signal from one electrode for one movement performance.

5.4.3. Movement Detection

In order to remove the need for a classifier to continuously predict the user's current state and thus reduce the number of misclassifications that may result from this classifier, a *Movement Detection Stage* was introduced.

This stage should be robust to random muscle twitching or contractions, therefore, it cannot be a simple sEMG onset algorithm [37] [38], ideally only detecting the intentional movement commands. Therefore, the implemented method was based on Binary Linear Discriminants.

The Binary Linear Discriminant Classifiers were designed to determine the class conditional posterior probability of an RMS feature belonging to a movement or a rest class. Section 3.2.1 showed that Linear Discriminant Classifiers have been successfully used for myoelectric systems, making the choice of this classifier a natural one. Since there are four Proto-Motion (PM) classes, four Binary Linear Discriminant Classifiers were used to pair-wise discriminate between each one of the four PM classes and the Resting class [127] [128] [129].

According to Bayes' Theorem, when only considering two classes, the posterior probability for class C_1, $p(C_1|\boldsymbol{x})$ with respect to class C_2 is given by Equation (5.1):

$$p(C_1|\boldsymbol{x}) = \frac{p(\boldsymbol{x}|C_1)p(C_1)}{p(\boldsymbol{x}|C_1)p(C_1) + p(\boldsymbol{x}|C_2)p(C_2)} = \frac{1}{1+exp(-a)} = \boldsymbol{\sigma}(a) \qquad (5.1)$$

where,

$$a = ln\frac{p(\boldsymbol{x}|C_1)p(C_1)}{p(\boldsymbol{x}|C_2)p(C_2)}\ ; \qquad (5.2)$$

$\boldsymbol{\sigma}(a)$ is the logistic sigmoid;

$p(\boldsymbol{x}|C_k)$ is the class conditional probability density function for C_k;

$p(C_k)$ is the class prior for C_k;

$\boldsymbol{x}$ is the feature vector.

The class prior, $p(C_k)$ specifies the probability that a feature vector $\boldsymbol{x}$, may belong to C_k. The class priors may be estimated by using Equation (5.3) [130].

$$p(C_k) = \frac{n_k}{N} \tag{5.3}$$

where,

n_k is the number of training instances belonging to C_k;

N is the total number of training instances.

Consider that the features of the classes are assumed to be Gaussian distributed. The multivariate Gaussian distribution density function for class C_1, $p(\boldsymbol{x}|C_1)$ is given by:

$$p(\boldsymbol{x}|C_1) = \frac{1}{(2\pi)^{\frac{D}{2}} |\boldsymbol{\Sigma_1}|^{\frac{1}{2}}} exp\left\{-\frac{1}{2}(\boldsymbol{x} - \boldsymbol{\mu_1})^T \boldsymbol{\Sigma_1}^{-1}(\boldsymbol{x} - \boldsymbol{\mu_1})\right\} \tag{5.4}$$

where,

D is the dimension of the feature vector;

$\boldsymbol{\Sigma_1}$ is the covariance matrix of the training feature vectors for class C_1;

$|\boldsymbol{\Sigma_1}|$ is the determinant of $\boldsymbol{\Sigma_1}$;

$\boldsymbol{\mu_1}$ is the mean of the training feature vectors for class C_1.

For Linear Discriminants, the classes are modelled with equal covariance matrices for both classes, C_1 and C_2, as shown in Equation (5.5). This is modelled by pooling-in the two class covariance matrices to obtain the common covariance matrix as shown in Equation (5.6). In order to eliminate issues of singularity and ill-conditioned matrices, a regularisation term is included for covariance matrix inversion, as shown in Equation (5.7) [131] [132].

$$\boldsymbol{\Sigma_1} = \boldsymbol{\Sigma_2} = \widehat{\boldsymbol{\Sigma}} \tag{5.5}$$

$$\widehat{\boldsymbol{\Sigma}} = \frac{\sum_{n=1}^{N}\sum_{k=1}^{K} M_{nk}(\boldsymbol{x_n} - \boldsymbol{\mu_k})(\boldsymbol{x_n} - \boldsymbol{\mu_k})^T}{N - K} \tag{5.6}$$

$$\widehat{\boldsymbol{\Sigma}}_{\boldsymbol{\gamma}} = (1 - \gamma)\,\widehat{\boldsymbol{\Sigma}} + \gamma \boldsymbol{I} \tag{5.7}$$

where,

M is an N by K class membership matrix such that M_{nk} = 1 if observation n is from

class k and M_{nk} = 0 if otherwise;

K is the total number of classes;

N is the total number of training feature vectors;

$\boldsymbol{\mu_k}$ is the mean of the training feature vectors for class k;

$\boldsymbol{x_n}$ is the feature vector at observation n;

$\boldsymbol{\Sigma_k}$ is the covariance matrix of class C_k;

$\widehat{\boldsymbol{\Sigma}}$ is the pooled-in covariance matrix;

$\widehat{\boldsymbol{\Sigma}}_{\boldsymbol{\gamma}}$ is the regularised covariance matrix;

γ is the regularisation term in the interval [0,1];

$\boldsymbol{I}$ is the Identity Matrix having the same dimensions as $\boldsymbol{\Sigma}$.

Hence, for a two-class problem, the posterior probability for C_1, representing the probability of the PM, can be obtained from Equation (5.8), as derived from Equations (5.1) and (5.2).

$$p(C_1|\boldsymbol{x}) = \boldsymbol{\sigma}\left(\left(\widehat{\boldsymbol{\Sigma}}^{-1}(\boldsymbol{\mu_1}-\boldsymbol{\mu_2})\right)^T \boldsymbol{x} - \frac{1}{2}\boldsymbol{\mu_1}^T\widehat{\boldsymbol{\Sigma}}^{-1}\boldsymbol{\mu_1} + \frac{1}{2}\boldsymbol{\mu_2}^T\widehat{\boldsymbol{\Sigma}}^{-1}\boldsymbol{\mu_2} + \ln\frac{p(C_1)}{p(C_2)}\right) \quad (5.8)$$

The four posterior probabilities obtained at every time sample during rest and motion instances have been empirically found to mainly result in a 0 or 1 value, as shown in Figure 5.8. In this figure, for different PM performances, all four posterior probabilities increase to a value of 1, albeit at slightly varying instances, clearly identifying the boundary within which a motion has been detected. It may also be noted that in those time instants where the subject is at rest in any of the grasp postures, all four discriminants detect that the subject is, in fact, at rest, with the class conditional probabilities resulting in a value of 0. Furthermore, while this figure shows very crisp probability changes, this is not the case for all subjects in all instances, with changes in the behaviour of these probabilities depending on the training data as well as the motion performance.

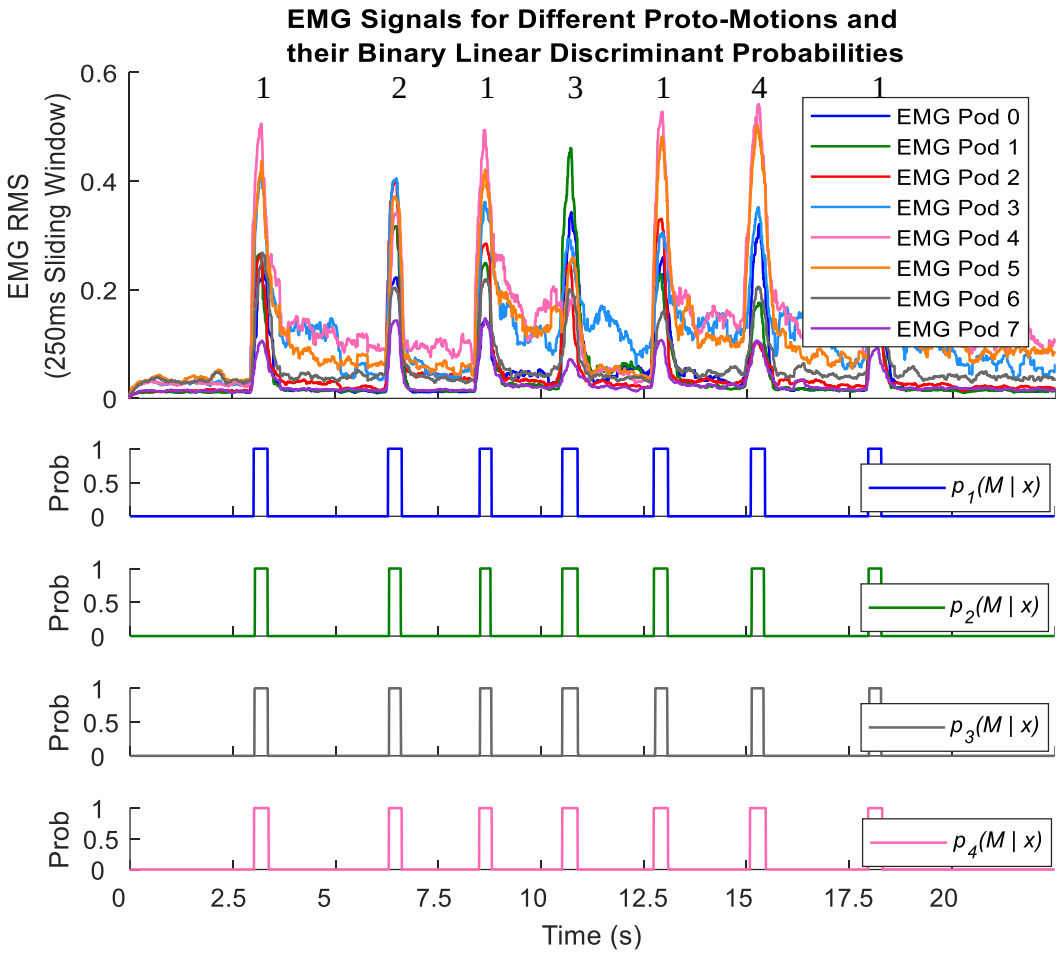

Figure 5.8 - The sEMG RMS signals obtained during different PM Performances and their respective Binary Linear Discriminant Probabilities. The numbers at the top of the first plot indicate the PM occurring in the EMG signal train. The PM numbers represent the PMs described in Table 5.2. The bottom plots in blue, green, grey and pink refer to the probability of a movement detection occurrence, M, obtained from the four PM – Rest pair-wise discriminants. $p_1(M|\boldsymbol{x})$ refers to the PM 1 – Rest binary Classifier such that the subscript number relates to the PM class. These probabilities are solely used for Movement Detection.

Movement detection is required to occur within the transient phase of the motion, prior to reaching the EMG RMS peaks. Therefore, the threshold for movement detection has been set to be the point where at least one of the four class conditional posterior probabilities have exceeded 0.5. Once this threshold is exceeded, a motion detection indicator flags this instance in variable $MD(\boldsymbol{x})$, as provided in (5.9).

$$MD(\boldsymbol{x}) = \begin{cases} 0, p(C_1|\boldsymbol{x}) < 0.5 \ \wedge \ p(C_2|\boldsymbol{x}) < 0.5 \ \wedge \ p(C_3|\boldsymbol{x}) < 0.5 \ \wedge \ p(C_4|\boldsymbol{x}) < 0.5 \\ 1, p(C_1|\boldsymbol{x}) > 0.5 \ \vee \ p(C_2|\boldsymbol{x}) > 0.5 \ \vee \ p(C_3|\boldsymbol{x}) > 0.5 \ \vee \ p(C_4|\boldsymbol{x}) > 0.5 \end{cases} \quad (5.9)$$

where,

$MD(\boldsymbol{x})$ is the movement detection flag for feature vector $\boldsymbol{x}$;

$p(C_k|\boldsymbol{x})$ is the class conditional posterior probability for PM k with respect to the Rest class.

It has been empirically determined that the same threshold value may be set for all four binary classifiers. This threshold value needs to be carefully set to obtain a trade-off such that false movement detection is minimised and true movement detection is maximised. For this work, a value of 0.5 has been found to be satisfactory.

In order to reduce the chances of false movement detection, a minimum period of samples is required for the class conditional posterior probability to continuously remain above the probability threshold to accept this as a valid movement detection. It was empirically found that 20 samples, corresponding to 100 ms, were sufficient for this purpose. This time window is denoted by W_T. Therefore, if W_T consecutive samples are above the probability threshold, it is considered that a motion has been detected and consequently, the system enters the *Proto-Motion Identification* stage to identify the specific motion intended by the subject.

W_T was carefully chosen to satisfy a trade-off between the maximisation of actual movement detections and minimisation of non-movement detections whilst also minimising detection delay. As shown in Figure 5.9, the three initial pink-shaded periods which occur during an instant where the subject should have been at rest indicate that the class conditional posterior probability for at least one Proto-Motion exceeded the threshold, however, these were short-lived at lengths of 18, 12 and 10 samples respectively, and were therefore ignored. Conversely, at around the 2750 ms instant, where the subject actually performed an intended hand movement, a class conditional posterior probability exceeded the threshold and remained above the threshold for 168 samples, satisfying W_T, hence leading on to the *Proto-Motion Identification* stage. This condition makes the movement detection more robust to false movement detections.

This figure also supports the chosen W_T since with a shorter W_T, the three initial instances may be falsely detected as movements. Meanwhile with a slightly longer W_T, the intended movement shown in this figure would still be detected. However, other performed movements resulting in signals which vary from the norm, may result in fewer samples where a class conditional posterior probability exceeds the threshold, risking them to be incorrectly ignored.

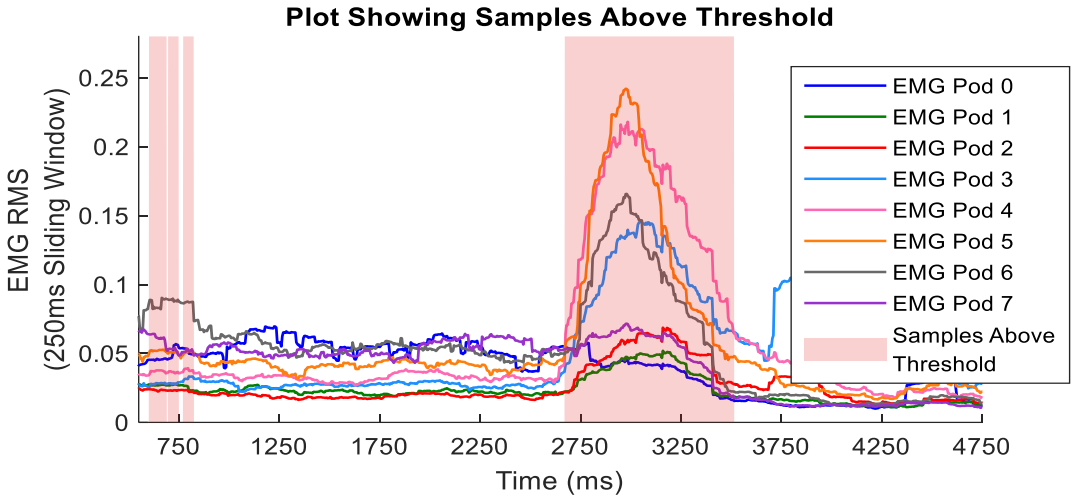

Figure 5.9 - A plot showing a period where the subject should have been at rest in the initial grasp, the performance of a Proto-Motion at around 2750 ms, and the return to rest in the final grasp. The pink shaded areas show the instances where the probability threshold was exceeded for at least one of the four discriminants. The first three areas were short-lived, indicating that these were not actual movements while the actual Proto-Motion was clearly detected, with the number of samples above threshold satisfying W_T.

5.4.4. Proto-Motion Identification

As indicated in Section 4.6, the peak EMG RMS values observed during elbow anisometric contractions closely corresponded to the peak movement velocity. This indicates that the peak RMS value is a suitable characterisation of movement kinetics. During Proto-Motion performances, similar EMG RMS profiles to those obtained during the arm movements were recorded. Therefore, by only considering the peak RMS values after motion onset, a general representation of the maximal kinetics of the Proto-Motion may be obtained. Thus, it was suggested that the eight RMS signal maxima values could be extracted and used as a feature to represent the Proto-Motion.

Since the RMS peaks of different channels have been generally found to occur within a few milliseconds from each other, the peak value from each channel may be extracted such that all the peak values are combined into one feature vector to characterise the Proto-Motion, as shown in Figure 5.10.

This can also be represented with a mathematical notation as follows:

Let the RMS of EMG Pod k be $x_k(t)$ and the total number of EMG Pods be K, where $k \in \{0, \dots, K-1\}$. Since the motion detection onset occurs at time T, the peak of $x_k(t)$, defined as x_k^*, occurs at $t > T$, resulting in the feature vector in (5.10).

$$\boldsymbol{x}^* = \begin{bmatrix} x_0^* \\ \vdots \\ x_{(K-1)}^* \end{bmatrix} \tag{5.10}$$

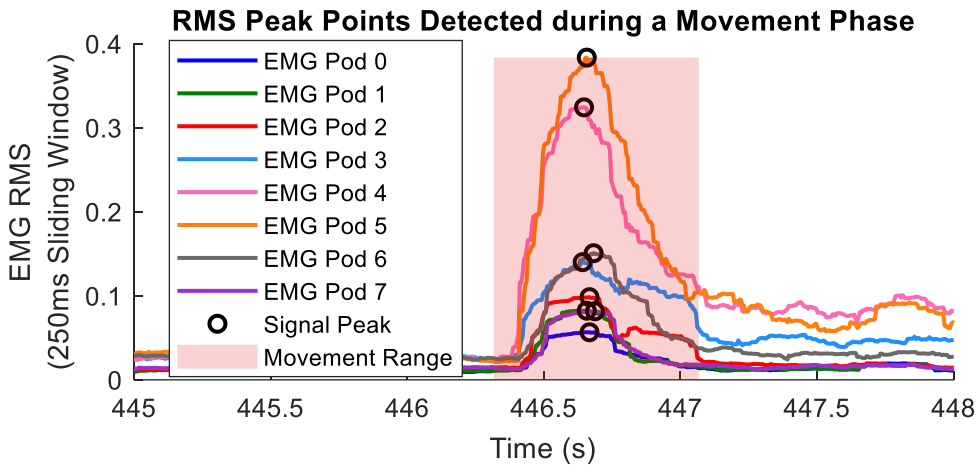

Figure 5.10 - A plot showing the 8 EMG RMS signals during a Proto-Motion performance, and their individually detected peaks. The areas which are not shaded in pink are the resting instances in the starting grasp and end grasp, respectively.

Thus, once a valid movement as discussed in Section 5.4.3 is detected, the RMS maxima occurring after the first valid above-threshold movement detected sample are sought for each EMG channel. For real-time systems, the prosthetic hand is to act on the user's movement intention within the electromechanical delay (EMD) range [70], to provide a sense of agency to the user [133] [134]. This delay is defined to occur between the time when the central nervous system (CNS) sends the motion instruction to the limb muscles and the actual contraction of these muscles and it is typically less than 300 ms [135] [136].

While it is important that any Proto-Motion performed by the subject is to be identified within this EMD range, one is to also ensure that the trade-off between the motion identification delay and the identification accuracy is maximised.

The search for the RMS maxima is done within a time-window WL_M, which is initiated from the first valid above-threshold movement detected sample. From preliminary testing, the WL_M values shown to detect all channel RMS maxima were identified to be between 200 ms and 300 ms. Figure 5.11 shows the discrepancies in the RMS maxima detected for $WL_M = 200$ ms and for $WL_M = 300$ ms for the same motion shown in Figure 5.9.

As can be noted, the WL_M window is completely dependent on the movement detection instance. Therefore, if the movement detection threshold is exceeded as soon as the motion is initiated, then a longer window is required to enable the identification of the signal maxima. However, a shorter WL_M window is sufficient if the threshold is exceeded halfway through the motion transient.

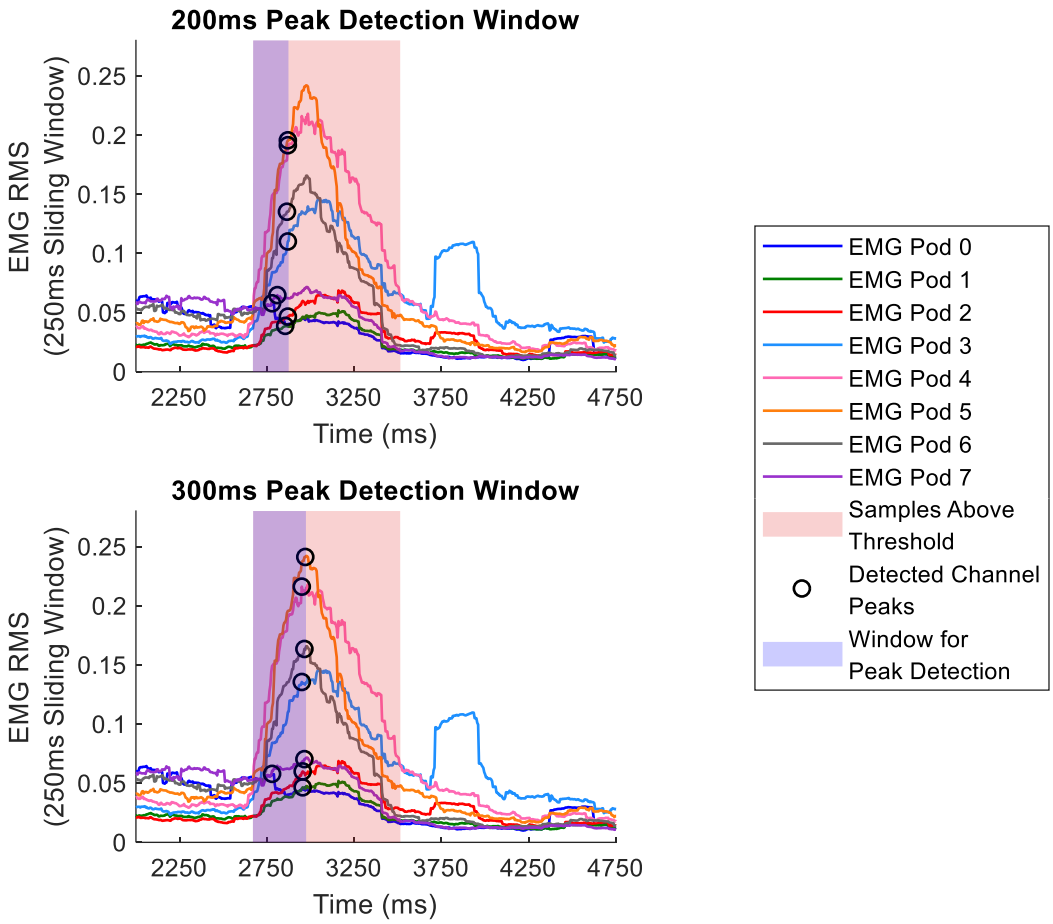

Figure 5.11 - Plots showing the Above Threshold Instances as well as the windows used for Proto-Motion RMS maxima detection. The top and bottom plots demonstrate the peaks detected with 200 ms and 300 ms WL_M values, respectively. The purple windows, indicating the RMS peak detection windows, start at the first Movement Detection Instance depicted by the underlying pink window.

The RMS maxima found in this window constitute the feature vector which is used to determine the Proto-Motion. As has been concluded in Section 3.7, a multi-class Gaussian LDA is used to classify the feature vector into one of the four Proto-Motions (PMs) and a Rest class. The inclusion of a Rest class at this stage makes it possible that any false movement detections may still be potentially identified as being none of the PMs.

Similar to the Gaussian LDA used for movement detection in Section 5.4.3, the assumption that the class distributions are normally distributed with equal covariance matrices is still retained [127] [128]. In this case, the class of any feature vector instance is found by using (5.11) [127].

$$C_k(\boldsymbol{x}) = \arg\max_k \delta_k(\boldsymbol{x}) \tag{5.11}$$

where,

$C_k(\boldsymbol{x})$ is the class determined by the classifier for feature vector $\boldsymbol{x}$;

$k \in \{1, \dots, 4\}$ is the class index each representing the Proto-Motion k, and $k = 5$ is the class index representing the Rest class;

$\delta_k(\boldsymbol{x})$ is the linear score function of class C_k for feature vector $\boldsymbol{x}$, shown in Equation (5.12) [127].

$$\delta_k(\boldsymbol{x}) = (\widehat{\boldsymbol{\Sigma}}^{-1}\boldsymbol{\mu}_k)^T\boldsymbol{x} - \frac{1}{2}\boldsymbol{\mu}_k^T\,\widehat{\boldsymbol{\Sigma}}^{-1}\boldsymbol{\mu}_k + \ln p(C_k) \qquad (5.12)$$

where,

$\boldsymbol{\mu}_k$ is the mean vector obtained from the training data of C_k;

$p(C_k)$ is the prior probability of class C_k as shown in Equation (5.3).

$\widehat{\boldsymbol{\Sigma}}$ is the common pooled covariance as provided in Equation (5.6);

Therefore, for any feature vector, $\boldsymbol{x}$, the linear score function $\delta_k(\boldsymbol{x})$ is estimated for the five different classes and $\boldsymbol{x}$ is assigned to the class with the largest linear score. From this score, separate class probabilities could also be found by using the sigmoid function as was done in Section 5.4.3. The linear decision boundaries created by such an LDA for three classes in a two-dimensional space is illustrated in Figure 5.12.

The LDA classifier for this work's system has been designed on *Matlab* by using the *fitcdiscr* function for the five classes, namely, PM 1, PM 2, PM 3, PM 4 and Rest. This function implements a regularised LDA, such that the covariance matrix used is regularised, as had been provided in Equation (5.7) [132].

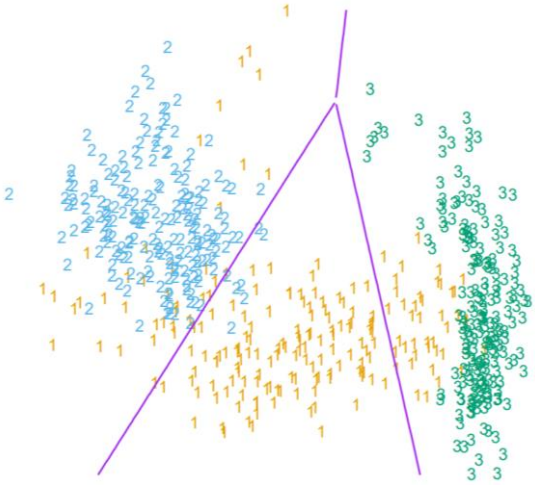

Figure 5.12 - Linear decision boundaries found by an LDA to classify three classes [137].

For motion detection, the amplitude of the channels is the most suitable deterministic factor to discriminate resting instances from movement instances and thus, no data standardization or normalization is performed. However, for motion identification, it was noted that the different EMG pattern sequences which are physiologically created by the muscle fibers in the different forearm areas are a more suitable discriminant than the signal amplitudes. Thus, for better separability between the feature vectors of the five different classes, feature vector normalization is carried out. This is done by firstly centering the data by removing the mean data vector, resulting in zero-mean data. The feature vector is then transformed into a unit norm vector such that it is effectively projected onto the unit sphere. This normalization is done with regard to the muscle recruitment pattern such that motion discrimination is based on the muscle synergistic pattern rather than the actual level of recruitment and this computation is provided in Equation (5.13).

$$\hat{x}_i = \frac{x_i - \mu_i}{\sqrt{\sum_{i=0}^{7}(x_i - \mu_i)^2}} \tag{5.13}$$

where,

$i \in \{0, \dots, 7\}$ is the EMG channel index;

$\hat{x}_i$ is the normalized feature value for channel i;

x_i is the EMG RMS feature value for channel i;

μ_i is the mean value over all classes for channel i.

By only targeting the RMS maxima of the motion for identification, the multi-class classifier is only required to make a class prediction once per detected movement. This removes the need for additional post-processing which has to be implemented with continuous classifiers. Such a step would otherwise be important, especially when considering the temporal changes in the transient signals. Due to this decision, training data is also drastically reduced, reducing the overall memory requirements of an onboard system to store such data in those cases where the classifiers would need to be re-trained.

The EMG signals recorded during Proto-Motion performances that were shown in Figure 5.8 are now shown in Figure 5.13, where these same motions are identified by the multi-class classifier. In the top plot, the samples which exceeded the binary class

threshold as described in Section 5.4.3 are shown in pink. Since the above-threshold period exceeds W_T for every individual motion, the *Proto-Motion Identification* stage is initiated every time such that a 200 ms WL_M window, depicted in purple, is used to find the channel maxima from which the feature vector for proto-motion classification is constructed.

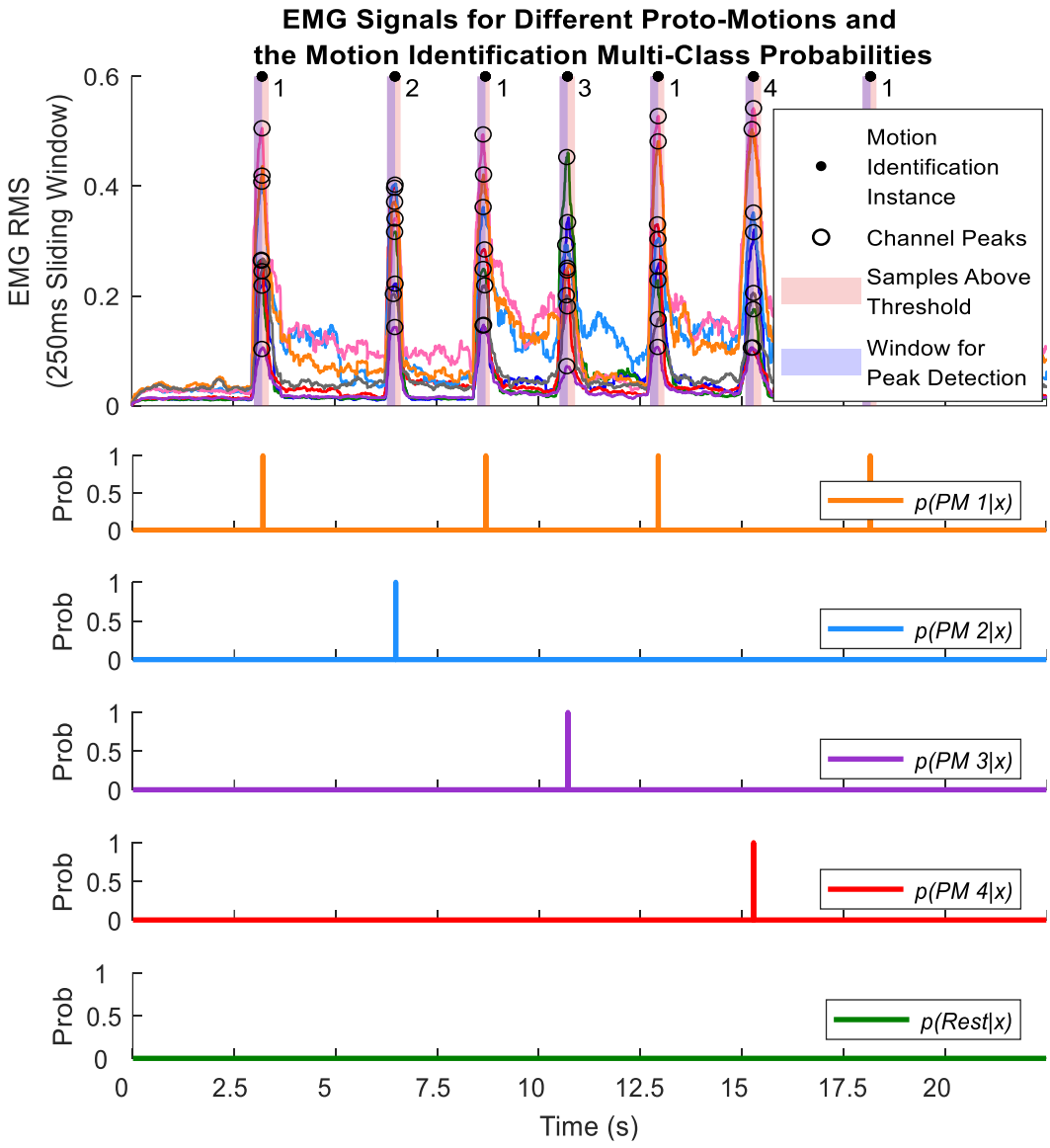

Figure 5.13 - The sEMG RMS signals recorded during seven PM performances and their respective multi-class posterior probabilities during Motion Identification Instances. The top plot shows those samples which were found to be above the movement detection threshold, the windows used to find the 8-channel peaks, the peaks detected, as well as the instance where a motion identification prediction was prompted. The numbers adjacent to every motion indicate the Proto-Motion performed. The PM numbers represent the PMs described in Table 5.2. The bottom plots show the posterior probabilities of the five classes within the multi-class classifier in time.

This WL_M window overlaps the pink, above-threshold window, such that it initiates at the first above-threshold sample. The motion identification decision is then made at the last WL_M sample, as shown in the figure with a black dot. At this instant, the recorded channel maxima from the WL_M window are utilised as the feature vector used to determine the posterior probabilities of the five classes within the multi-class classifier. The five bottom plots show the class-conditional posterior probabilities during these seven motion identification instances.

The numbers adjacent to every motion in the top plot indicate the Proto-Motion performed. Therefore, by comparing the resulting class posterior probabilities illustrated in the bottom plots, it can be concluded that the system correctly predicted all seven motions.

Since the system does not perform continuous multi-class classification, the probabilities for the five classes for all the non-motion identification samples are automatically set to 0.

5.4.5. Alternative to the LDA Classifiers

As has been mentioned above, LDA classifiers make two assumptions; that the data is normally distributed and the covariance matrices of the classes are equal. In order to test whether these conditions were met for different subjects, Mardia tests [138] and Bartlett tests [139] were implemented to determine multivariate normality and covariance matrix equality of Proto-Motion data collected from different subjects. A 5% level of significance was used for both tests.

Multivariate normality was also tested by using Quantile-Quantile (Q-Q) plots. Since the number of variables in this work was not singular, the squared distance from the centre of the data quantiles were plotted against a chi squared distribution. The choice of using squared distance values was since a specific positive or negative direction to the mean of the centre of the data cannot be defined when dealing with multiple dimensions [140].

Whilst the covariance matrices were not found to be equal for all subjects, multivariate normality varied between subjects and classes. Normality significance also varied for normalized and non-normalized data for different subjects. The Rest class was also found to not satisfy normality in all cases, for all subjects. This was expected since this

class was a combination of iterations recorded with the subject in different grasps, at resting levels.

Since the above suggests that linear discriminant conditions are violated to some extent by any subject, the LDA classifiers are not optimal. However, reduction in optimality may still be deemed as acceptable whenever simplicity is regarded as a large advantage. Due to their ease of computation, a less than optimal LDA classifier may still be regarded as a suitable choice, especially in work when the overall system would ultimately be required to operate on-board a microprocessor, as is the case with this work. The overall simplicity of these discriminants is also the reason why researchers opt for their implementation as the initial classifiers for any newly developed system [128].

While empirical classification results indicated that the boundaries found by LDAs were suitable for the implemented *Movement Phase* system, a natural step was to determine whether another classifier which does not make any assumptions regarding the data could give better results.

The Support Vector Machine (SVM) classifier is a non-probabilistic classifier [141] [142]. Whilst SVMs can be used as linear classifiers, the kernel trick makes it possible for the classifier to also have other decision boundaries if required [127]. However, for this work, the aim was to compare the performance of linear SVMs to LDAs, leaving higher dimensional space kernels unexplored.

A linearly separable two-class SVM classification problem makes use of the linear model in (5.14) which serves as the decision boundary hyperplane [127].

$$y(\boldsymbol{x}) = \boldsymbol{w}^T \boldsymbol{\phi}(\boldsymbol{x}) + b \qquad (5.14)$$

where,

$\boldsymbol{x}$ is the feature vector;

$\boldsymbol{\phi}(\boldsymbol{x})$ is a fixed feature space transformation;

b is a bias parameter;

$\boldsymbol{w}$ is a vector containing the coefficients which define an orthogonal vector to the hyperplane.

If t_n is the target class, where $t_n \in \{-1,1\}$, and n is the input feature vector number,

$\boldsymbol{w}$ and b should be chosen such that for all data points,

$$t_n y(\boldsymbol{x_n}) > 0 \tag{5.15}$$

While many solutions may exist for $\boldsymbol{w}$ and b, SVMs choose the values which lead to a maximised margin, where a margin is defined to be the perpendicular distance between the closest data point to the decision boundary and the boundary itself. The margin is maximised by utilising a subset of data points, termed as support vectors, rather than the closest data point, as provided in Figure 5.14.

For margin maximisation, all training data points need to satisfy (5.16) and (5.17), leading to a quadratic programming problem, where $n = 1, \dots, N$.

$$t_n(\boldsymbol{w}^T \boldsymbol{\phi}(\boldsymbol{x}_n) + b) \geq 1 \tag{5.16}$$

$$\arg\min_{\boldsymbol{w},b} \frac{1}{2}\|\boldsymbol{w}\|^2 \tag{5.17}$$

Through the use of Lagrange multiplier terms, $a_n \geq 0$, new feature vectors may be classified using the model in (5.18).

$$y(\boldsymbol{x}) = \sum_{n=1}^{N} a_n t_n k(\boldsymbol{x}, \boldsymbol{x}_n) + b \tag{5.18}$$

where,

$k(\boldsymbol{x}, \boldsymbol{x}_n)$ is the kernel function defined by:

$$k(\boldsymbol{x}, \boldsymbol{x}') = \boldsymbol{\phi}(\boldsymbol{x})^T \boldsymbol{\phi}(\boldsymbol{x}'). \tag{5.19}$$

b is found by:

$$b = \frac{1}{N_S} \sum_{n \in S} \left(t_n - \sum_{m \in S} a_m t_m k(\boldsymbol{x_n}, \boldsymbol{x_m}) \right). \tag{5.20}$$

where,

S is the set of indices of the support vectors;

N_S is the number of support vectors.

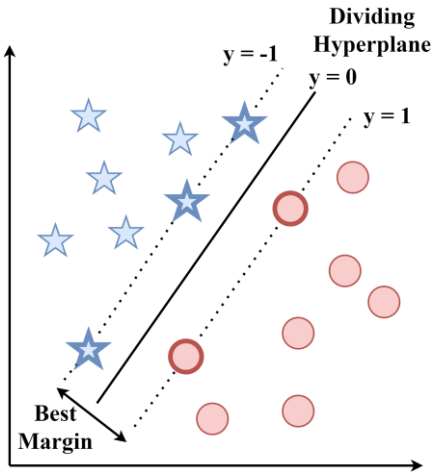

Figure 5.14 - Points from two classes (blue stars and red circles) are divided by a decision boundary hyperplane. This is chosen by the maximised margin, which is dominated by the support vectors (the points which lie on the margin hyperplanes, indicated by a bolder perimeter).

Slack variables, $\xi_n \geq 0$ may also be included for each training data point such that data points are allowed to cross their margin boundary, at a penalty, changing the classification constraints in (5.16) and (5.17) to (5.21) and (5.22). The introduction of $C > 0$ is responsible for controlling the trade-off between the margin and the slack variable penalty. (5.18) could then be updated accordingly.

$$t_n(\boldsymbol{w}^T\phi(\boldsymbol{x}_n) + b) \geq 1 - \xi_n \tag{5.21}$$

$$\arg\min_{\boldsymbol{w},b,\xi} C\sum_{n=1}^{N}\xi_n + \frac{1}{2}\|\boldsymbol{w}\|^2 \tag{5.22}$$

For this work, the four binary classifiers implemented as an alternative to the binary LDAs implemented in Section 5.4.3 were designed on *Matlab* by using the *fitcsvm* function [143]. The data, in this case, was standardised such that predictors were made insensitive to the measuring scales.

Essentially, SVMs are binary classifiers, thus, a multiclass classifier using SVMs may be obtained through approaches such as the One-Versus-One and One-Versus-All methods [127]. For this work, an Error-Correcting Output Codes (ECOC) approach [144] [145] was implemented with a One-Versus-One coding design for the *Proto-Motion Identification* stage. For this approach, the number of classifiers that were implemented using the *fitcecoc Matlab* function [146] were according to (5.23), where K is the number of classes.

$$Number\ of\ Classifiers = \frac{K(K-1)}{2} \tag{5.23}$$

For this work, 10 binary SVMs were therefore required to be implemented to exhaust all class pair combinations with a coding matrix, $\boldsymbol{M}$, as provided in Table 5.3.

A feature vector could then be assigned to one of the five classes which minimises the overall loss value for all binary learners by using (5.24).

$$\hat{k} = \arg\min_{k} \frac{\sum_{c=1}^{C} |m_{kc}| g(m_{kc}, s_c)}{\sum_{c=1}^{C} |m_{kc}|} \qquad (5.24)$$

where,

$\hat{k}$ is the classified class,

k is the class number $\in \{1, \ldots, 5\}$;

c is the classifier number $\in \{1, \ldots, 10\}$ such that $C = 10$;

m_{kc} are elements within the coding design matrix, $\boldsymbol{M}$;

s_c is the predicted classification score for the positive class of classifier c;

$g(m_{kc}, s_c)$ is the binary loss formula provided in (5.25).

$$g(m_{kc}, s_c) = \frac{\max(0, 1 - t_{kc} \cdot s_c)}{2} \qquad (5.25)$$

The results from the implementation of this alternative approach, in comparison to LDA classifiers are discussed in Section 7.1.6

Table 5.3 - The Coding Matrix used by the SVM ECOC where 10 classifiers are implemented such that for every one, only the two classes listed with a '1' or '-1' are considered as the binary classes to be classified.

		Classifier									
		1	**2**	**3**	**4**	**5**	**6**	**7**	**8**	**9**	**10**
Class	**PM 1**	1	1	1	1	0	0	0	0	0	0
	PM 2	-1	0	0	0	1	1	1	0	0	0
	PM 3	0	-1	0	0	-1	0	0	1	1	0
	PM 4	0	0	-1	0	0	-1	0	-1	0	1
	Rest	0	0	0	-1	0	0	-1	0	-1	-1

5.5. The Force Phase Intent Interpretation System

Based on the discussion in Section 2.2.3, force control helps to make the behaviour of the prosthetic hand resemble that of the human hand, leading to increased prosthetic usability.

As discussed in Section 4.6, EMG RMS values during a steady-state contraction represent the continuous contraction magnitude. For this prosthetic system, as discussed in Section 5.3, such contraction instances have been termed as *Force Phases*. Thus, when the system enters the *Force Phase*, each channel's instantaneous RMS value may be combined into a vector from which a continuous force value is estimated for every time sample.

This can also be represented with a mathematical notation as follows:

Let the RMS of EMG Pod k be $x_k(t)$ and the total number of EMG Pods be K, where $k \in \{0, \dots, K-1\}$. Since the *Force Phase* starts and ends at time T_{fs} and T_{fe}, respectively, a feature vector is obtained for every time sample where $T_{fs} \leq t < T_{fe}$, as provided in (5.26).

$$\boldsymbol{x}(t) = \begin{bmatrix} x_0(t) \\ \vdots \\ x_{K-1}(t) \end{bmatrix} \tag{5.26}$$

Since the robustness of such a force estimation system cannot be determined in an offline manner for the *Force Phase* signals, this system, unlike the *Movement Phase* system was only implemented with online conditions in mind. The data collection and signal processing steps discussed in Sections 5.4.1 and 5.4.2 for the *Movement Phase* system were also applied for this force estimation design.

The most common force estimation methods consist of simple averaging across all the different EMG channels [69] [147] [148], requiring manual adjustment of class specific gain values and thresholds. Scheme et al. [69] tested three different proportional control systems for amputee hand speed performance. The best performing method made use of the subjects' whole contraction dynamic range. In this method, instantaneous averages across all EMG channels are found for the different grasps which are then normalized between grasp specific maxima and minima. Training data for such a system requires contraction level ramping to maximum force levels. Due to its efficient usage of the whole dynamic contraction range and low

computational requirements, this method was chosen for force estimation interpretation in this work.

Whilst Scheme et al. utilised MAV signals, RMS values were used in this work, as follows [69]:

$$PC_i(\mathrm{t}) = \frac{\sum_{j=1}^{N} x_j(t) - TH_{min,i}}{TH_{max,i} - TH_{min,i}} \quad (5.27)$$

$$TH_{min,i} = \left(1 - \frac{P_{THmin}}{100}\right) x_{Min,i}^{Tr} + P_{THmin}\, x_{Max,i}^{Tr} \quad (5.28)$$

$$TH_{max,i} = \left(1 - \frac{P_{THmax}}{100}\right) x_{Min,i}^{Tr} + P_{THmax}\, x_{Max,i}^{Tr} \quad (5.29)$$

$$x_{Min,i}^{Tr} = \min_{k=1:k_i} \sum_{j=1}^{N} x_{i,j,k}^{Tr} \quad (5.30)$$

$$x_{Max,i}^{Tr} = \max_{k=1:k_i} \sum_{j=1}^{N} x_{i,j,k}^{Tr} \quad (5.31)$$

where,

$PC_i(t)$ is the proportional control force estimation interpretation signal for Grasp *i;*

N is the number of EMG Channels used;

$x_j(t)$ is the RMS value of EMG Channel *j* at time *t;*

P_{THmin} and P_{THmax} are the desired lower and upper boundaries expressed in terms of the maximum contraction;

$TH_{min,i}$ and $TH_{max,i}$ represent the lower and upper bounds of Grasp *i;*

$x_{i,j,k}^{Tr}$ is the RMS of the Training Data from Grasp *i*, *C*hannel *j* and Computation Window *k;*

$x_{Min,i}^{Tr}$ is the minimum computed RMS value from the Training Data for Grasp *i;*

$x_{Max,i}^{Tr}$ is the maximum computed RMS value from the Training Data for Grasp *i.*

These equations lead to normalized proportional control force values in the range of 0 to 1, in accordance to the desired lower and upper boundaries set. The minimum and maximum force control thresholds could then be defined according to subject preference. For this work, force estimation was quantised to four force levels, namely: Resting Level, Low Level, Medium Level and High Level.

In order to mitigate noisy signals, the proportional control force signal was averaged over a 100 ms sliding window and then assigned to one of the four quantised force levels. Furthermore, in order to further prevent frequent switching between levels, a hysteresis concept as shown in Figure 5.15 was used such that the force level was incremented if the force estimation signal exceeded some upper threshold, and decremented if it decreased below a lower threshold. For this work, these upper and lower thresholds were empirically defined, noting which force levels required higher/lower thresholds for the subject's setup. The final mitigation procedure ensured changes between force estimation levels to only occur once a 200 ms continuous decision stream was at the same force level. Admittedly, such measures may cause force control lag, however, a balance is to be found between user perceivable delay and reliability of the output force levels. This algorithm resulted in an estimated force signal which consisted of the estimated force level output per sample in time.

5.6. The Three-Attribute Trade-Off

Both implemented *Movement Phase* and *Force Phase* systems have been designed in such a way as to provide amputees with an intent interpretation framework which has a balanced trade-off between the three attributes of simplicity, usability and dexterity. The attributes have been satisfied as provided in Figure 5.16, relating to the requirements that have been listed in Figure 5.1.

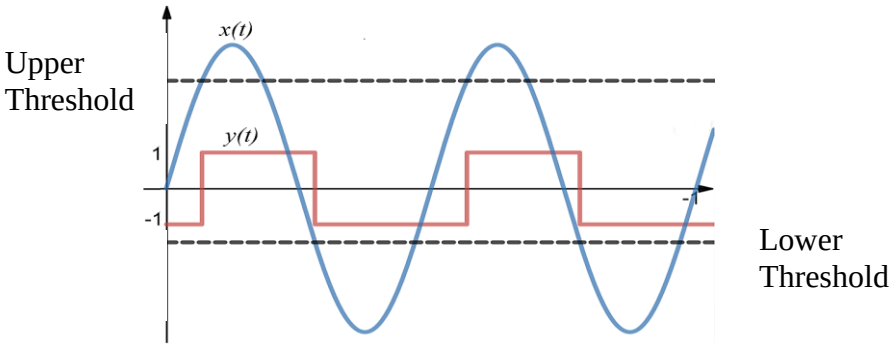

Figure 5.15 - Example of a Hysteresis Output, y(t), for a given Input Signal, x(t) [149].

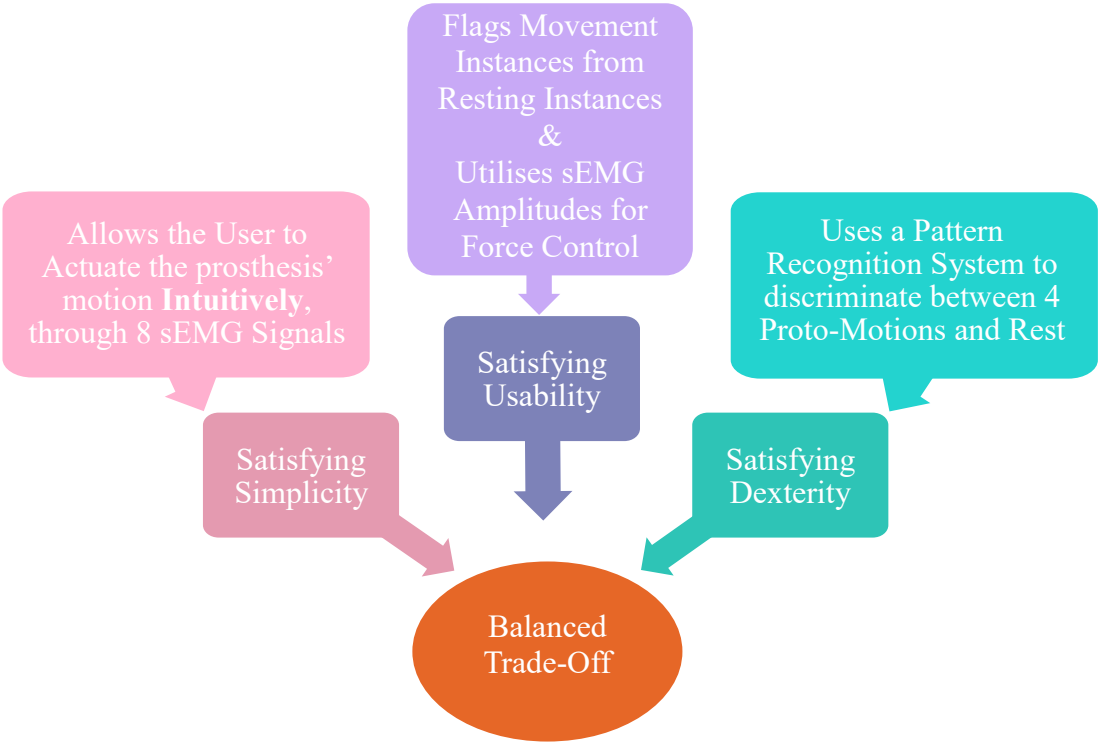

Figure 5.16 - A Diagram showing how the three attributes are being balanced in the developed intent interpretation framework.

Through the use of the sEMG phenomenon, human intuition is being exploited, allowing the prosthetic user to actuate the prosthesis through intuitive motions, providing natural control. This phenomenon removes the need for the user to re-learn the fundamentals of limb operation, thus reducing the steep learning curve that is introduced with non-intuitive intent interpretation systems. Through such a choice, simplicity is satisfied.

System reliability, and in turn, usability, are increased by the elimination of continuous motion predictions by introducing a movement detection algorithm. Additionally, the implementation of an intuitive sEMG grasping force estimation algorithm contributes towards making the behaviour of the prosthesis resemble human hand grasping functionality. These functionalities contribute towards a more practical and useful system.

Meanwhile, through pattern recognition motion discrimination between the four Proto-Motions and the Rest state, system simplicity and usability are retained whilst providing a good level of dexterity due to the sufficient degrees of freedom provided by the specifically chosen Proto-Motions.

5.7. Intent Interpretation Framework Design Conclusion

This chapter has described in detail a system that may be trained using EMG data to detect intentional hand actuation, identify the intended Proto-Motion and estimate a grasp force level to drive a mechanical prosthetic hand. The design decisions taken were in accordance to the aim of balancing the initially identified three-attribute trade-off. Several testing protocols were thus devised in order to obtain quantitative, as well as qualitative, performance results of the systems, as will be discussed in Chapter 6. Since the prosthetic hand is still under development in a separate task of the MAProHand project and it is out of scope of this project, the performance of this system could only be virtually tested, where required. The results of offline and real-time tests are presented in the next chapter.

6. Testing Methodology

For the different testing protocols that were devised to obtain quantitative and qualitative results of the offline system's performance, five normal limbed subjects (*S0*-*S4*) and two transradial amputees (*A1*, *A2*) were recruited in accordance to the University of Malta's research ethics guidelines. The five normal limbed subjects were two males and three females within the age group of 22 to 25 years old. All normal limbed subjects, except for subject *S4*, were right-hand dominant. In the meantime, subjects *A1* and *A2* were both right-hand dominant males and left-hand amputees. Subject *A1* was a congenital amputee while subject *A2* had to undergo amputation due to trauma. Both amputees had no previous experience with myoelectric prosthetics, having only utilised cosmetic prostheses which provide no useful functionality features. The participation of the amputee subjects was intended to provide invaluable insight into the differences in training and usability from that of normal limbed subjects as well as assess the suitability of the framework for the amputee target group.

6.1. sEMG Data Acquisition Protocols

For the sake of consistency, a protocol was determined for the donning of the *Myo* armband on the dominant forearm for the normal limbed subjects and on the amputated limb for the amputees. Pod 0 was always placed on the forearm flexor bundle which can be felt with the aid of palpation during subject finger clenching and wrist flexion. This quasi-specific site is found on the forearm's ventral aspect, as shown in Figure 6.1. The logo on Pod 3 of the band was always placed facing the fingers whilst having it positioned on the forearm's bulge, four fingers (approximately 5 cm) distal from the elbow. Clip add-ons were inserted between the pods, when necessary, to ensure a snug fit and direct contact with the skin.

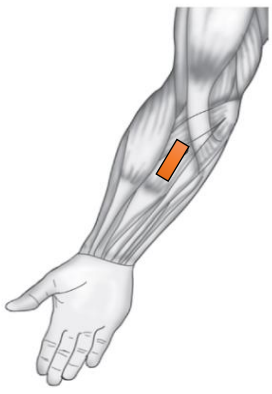

Figure 6.1 - The Forearm Flexor Bundle.

As shown in Figure 6.2, the overall setup consisted of a chair, two towels secured on the chair's arm rest, a laptop and monitor. The subjects were always seated on the chair with their forearm placed on these towels and they were asked to keep their wrist in a semi-supinated position, being extra cautious that no wrist movements were performed during motions. The towels allowed arm elevation whilst ensuring that the sEMG sensors were not in contact with any materials that could have shifted their position.

6.2. Offline Movement Phase Testing Sessions

In order to obtain performance measures for the offline *Movement Phase* system without real-time feedback as designed in Section 5.4, several controlled motion repetitions had to be recorded. To enable proper cross-validation of the data, four data runs were collected consisting of nine repetitions per Proto-Motion (PM), resulting in 36 repetitions per PM. Since PM 1 consists of four variations as explained in Section 5.1, only one of these variations was to be performed per run, with a different variation performed on every run. The data collected from a session was termed as *Episodic Data* from an *Episodic Session*.

During these experiments, the subjects were seated with the same arm posture throughout the whole experiment whilst eight seconds of data per repetition were acquired. During these eight seconds, sufficient EMG data was collected, covering the initial resting grasp, the performance of the instructed Proto-Motion and the final resting grasp.

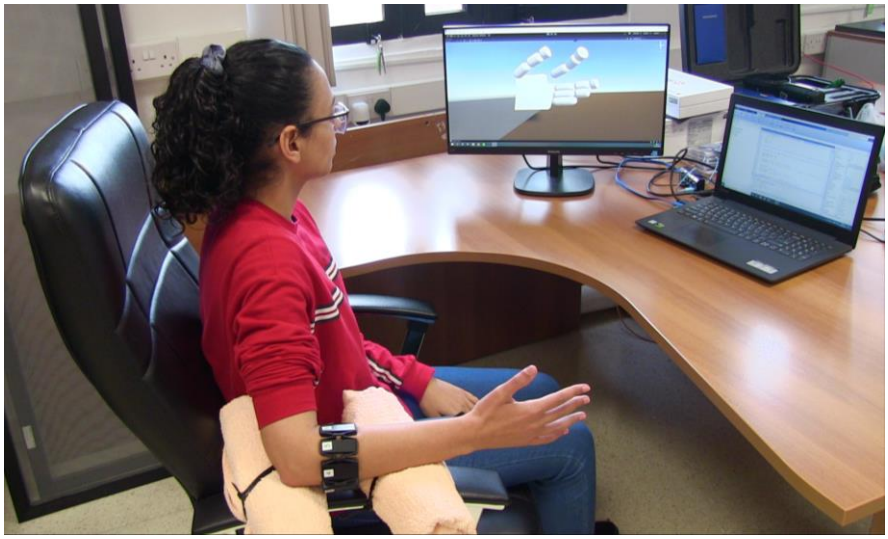

Figure 6.2 - The Testing Setup which included the seated subject with the forearm placed on the towels, with the wrist in a semi-supinated position. The Myo band was placed on the forearm bulge of the subject's dominant hand whilst not being in contact with any materials. The laptop and monitor were placed in a comfortable position for the subject to follow the experiment.

Prior to data collection, all subjects were provided with a brief training session where motion reproducibility at the required speeds and in the correct posture was promoted. Subjects were also allowed to rest whenever necessary to prevent muscle fatigue.

In order to assess inter-session performance, in particular whether system training on one day could be used to operate the system on a different day without training afresh, subject *S0* performed this episodic session on two different days, referred to as *Day 1 Episodic Session* and *Day 2 Episodic Session*, approximately three months apart. Due to the challenges brought about by the COVID-19 pandemic, such an inter-session analysis could only be done for a single subject.

6.2.1. Amputees Testing Sessions

The amputee subjects do not provide the same visual feedback to the experimenter as the normal limbed subjects due to their absent hand. Thus, in order to ensure that the amputees were in fact performing distinct Proto-Motions (PMs) prior to data collection, EMG signals from a small number of motion repetitions were initially recorded and processed using two methods.

The first method calculated the cosine angle between the feature vectors of each PM pair by using Equation (6.1), providing an indication of PM vector similarities. The closer the cosine angle was to 1, the higher the similarity was concluded to be.

$$\cos\theta = \frac{\boldsymbol{u} \,.\, \mathbf{v}}{|\boldsymbol{u}| \,.\, |\boldsymbol{v}|} \qquad (6.1)$$

where,

$\boldsymbol{u}$ and $\boldsymbol{v}$ are the mean RMS motion maxima feature vectors of the PM pair.

The second method plotted the PM RMS maxima feature vectors as radar charts for visual assessment, as shown in Figure 6.3. In this case, the plot clearly shows that the different PMs have different sEMG RMS feature vector patterns, except for PM 1 and PM 4. Nevertheless, PM 1 shows slightly higher amplitudes when compared to PM 4. These similarities were mostly attributed to the similarities between the extension of the middle, ring and little fingers during PM 4 performances to the extension of all five fingers during PM 1 performances. Thus, such a Radar Plot allowed the experimenter to qualitatively assess whether the PMs being executed by the amputee were sufficiently distinct as represented in the RMS feature vector space.

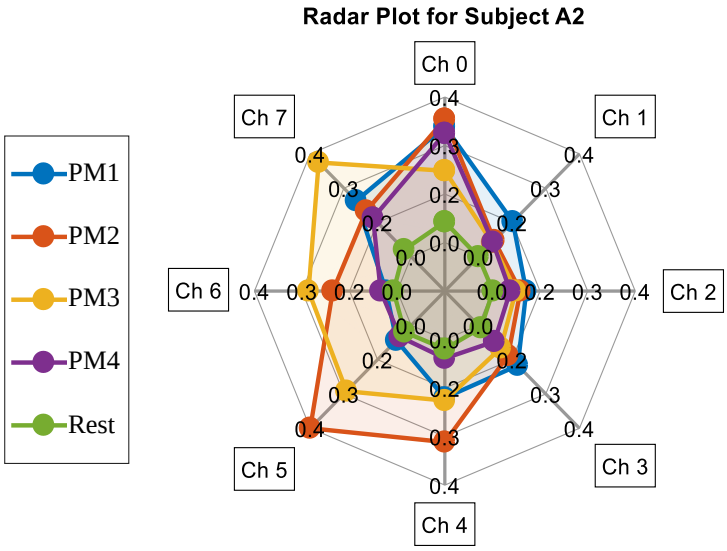

Figure 6.3 - A radar chart showing the mean RMS values obtained from the four PM and Resting Instances, for the 8 different sEMG Channels.

While this plot shows the non-normalized feature vectors, additional radar charts showing the normalized feature vectors as well as standard deviations of these vectors were also plotted, providing the experimenter with the most information possible.

6.2.2. Offline Results Methodology

From the episodic data collected, four runs of nine, 8 s repetitions added up to 36 repetitions per Proto-Motion (PM). In order to effectively obtain reliable and generalised performance results for the offline system, cross-validation [150] was implemented, such that these 36 repetitions per PM were split into 6 sets, each having 6 repetitions per PM.

The system's performance relies on the correct detection of movement instances as well as correct prediction of the motion classes. Thus, one of the data sets was used to train the movement detection binary classifiers, and the remaining five sets were used in 5-fold cross-validation for Proto-Motion identification multi-class LDA training and overall testing. This was repeated by training the movement detection binary classifiers each time with a different set, as illustrated in Figure 6.4. The 'Movement Detection Training Set', 'Proto-Motion Identification Multi-Class LDA Training Set' and 'Testing Set' refer to the sets used for movement detection binary classifiers training, multi-class LDA training, and Movement Detection and Proto-Motion Identification testing, respectively.

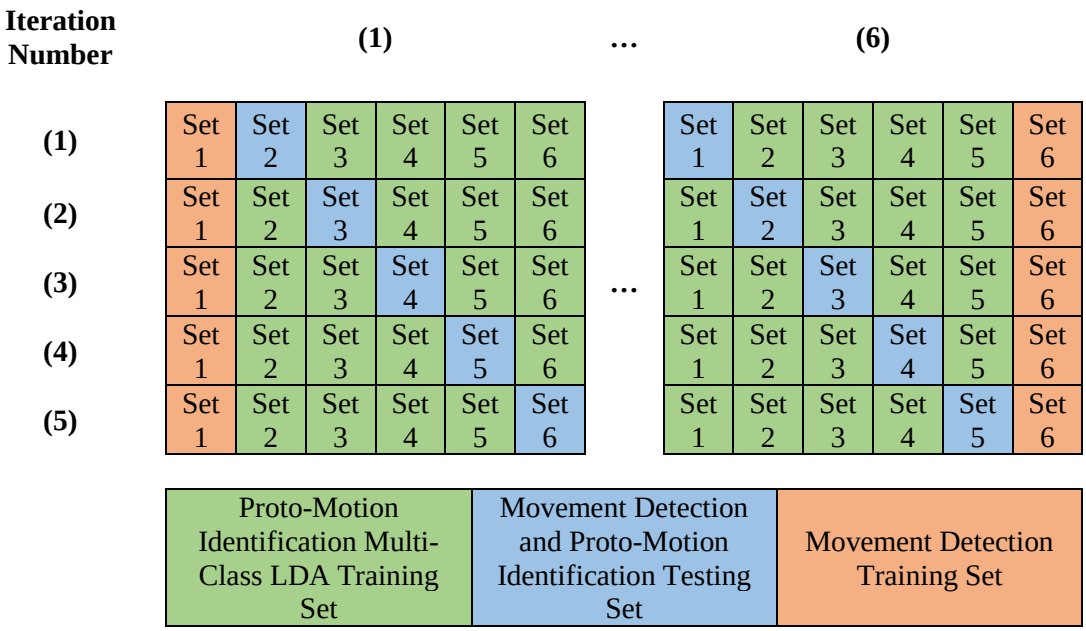

Figure 6.4 - Full cross-validation technique where six, 5-fold cross-validations are performed, ensuring that with every set that acts as the Movement Detection Training set, the other sets are 5-fold cross-validated.

Thus, when a set acted as the 'Movement Detection Training Set' or as the 'Proto-Motion Identification Multi-Class LDA Training Set', the extracted motion feature vector per repetition within the set, consisting of the EMG RMS maxima, was used for training the movement detection binary classifiers and the Proto-Motion identification classifier, respectively.

Feature vectors for the Rest class were extracted from before and after the movement phases of the four PM repetitions within these sets to represent the rest states at the different grasps. Since the resting instances exceeded the motion instances, only a random sample of these was kept to keep the classes balanced.

When a data set was used as a 'Proto-Motion Identification Multi-Class LDA Testing Set', the full 8 seconds of recorded data per repetition within that set was used to determine the number of detected movements, as well as their respective class predictions. These 8 seconds per repetition consisted of the initial resting grasp phase, the performance of the instructed Proto-Motion and the end resting grasp phase.

6.2.2.1. Movement Detection Testing

For every 5-fold cross-validation iteration, 6 repetitions x 4 PMs x 5 folds amount to 120 expected PM detections and identifications, i.e. 6 repetitions/PM x 5 folds amount to 30 expected detections and identifications per PM. The full cross-validation

technique consists of six, 5-fold cross-validations. Thus, with each fold having 30 instances of each PM, in total, there are 6 x 30 = 180 instances per PM to be detected and identified, and 180/PM x 4 PMs = 720 Proto-Motion instances in total to be detected and identified.

However, since the full 8-second trials were used for testing, these did not only consist of the movement phase, but also included the grasp resting phases prior and post movement, as illustrated in Figure 6.5 (a). This led to additional movement detections in the *Movement Detection Stage* due to the sufficient number of samples having exceeded the thresholds set for the movement detection binary classifiers, accumulating the number of rest class instances. Since such instances were not the cued Proto-Motions, these were considered as False Positives (FPs) for the movement detection. Five kinds of movement detection FPs have been identified from the different subjects' results, resulting from: uncued random hand or arm movements, uncued Proto-Motion performances, multiple movement detections of the cued Proto-Motions, involuntary twitching, and erroneous classification decisions. The first three causes are illustrated in Figure 6.5 (b-d). Such false movement detections were subsequently processed by the *Proto-Motion Identification Stage*.

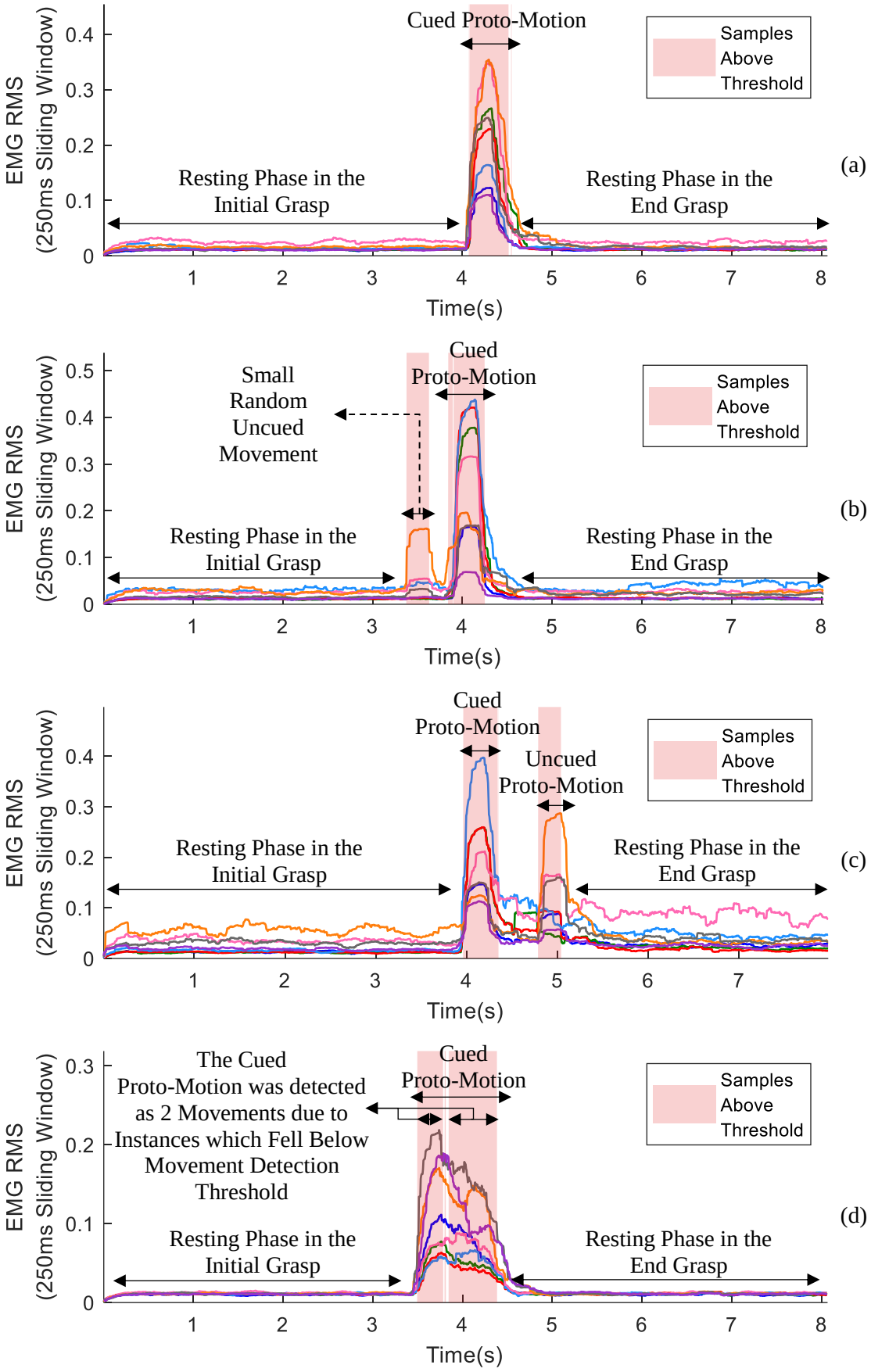

Figure 6.5 - (a) Full 8 s trials showing: the resting phase in the initial grasp prior to performing the Proto-Motion, the detected Proto-Motion, and the resting phase post the Proto-Motion in the end grasp; (b) an uncued small random hand or arm movement detected prior to the Proto-Motion; (c) a Proto-Motion performed on cue and another uncued Proto-Motion; (d) multiple movement detections of the cued Proto-Motion performance.

Movement detection testing can be analysed from a confusion matrix as illustrated in Figure 6.6, such that the sum of True Positives (TPs) and False Negatives (FNs) labelled within a red box should always be 720, relating to the 720 cued PM instances. The number of False Positives (FPs) is dependent on the EMG signals, muscle recruitment and subject behaviour, as well as the sensitivity of the binary classifiers, as discussed above. In this work, the number of True Negatives (TNs) cannot be defined since this relates to all the samples in time at which a movement was not cued and a movement was not detected.

The most general measure of classifier performance is the accuracy measure as provided in (6.2), however, this does not entail a detailed analysis of the performance of the separate classes. Two widely used measures for class specific analysis are the sensitivity and specificity. Sensitivity quantifies the identification rate of TPs, as in (6.3). Specificity quantifies the identification rate of TNs, as in (6.4) [151].

$$Accuracy = \frac{TP + TN}{TP + FP + FN + TN} \tag{6.2}$$

$$Sensitivity = \frac{TP}{TP + FN} \tag{6.3}$$

$$Specificity = \frac{TN}{FP + TN} \tag{6.4}$$

For movement detection testing, since the TNs cannot be quantified, only the separate TP, FP and FN counts as well as the sensitivity measure may be presented, and are thus provided as analysis measures for the separate subjects in Section 7.1.1.

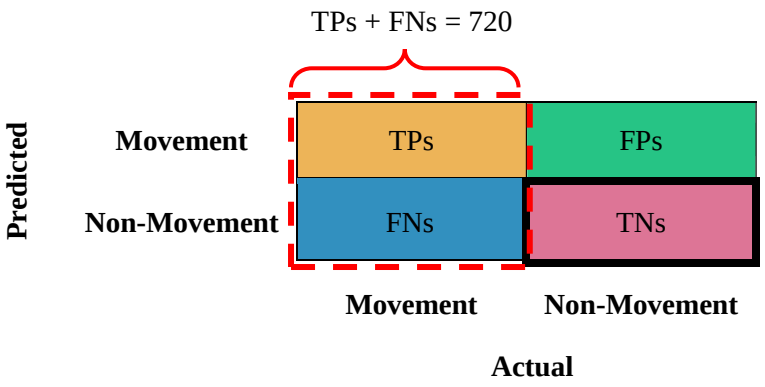

Figure 6.6 - A confusion matrix for Movement Detection testing, showing the TPs, FPs, FNs and TNs.

6.2.2.2. Proto-Motion Identification Testing

Proto-Motion identification testing involves testing of the movement detection TPs and FPs, as illustrated in the confusion matrix of Figure 6.7. Due to the nature of the false positive movement detections discussed in Section 6.2.2.1, these are not accounted for in the testing of the *Proto-Motion Identification Stage* with the other four PMs, and are separately analysed in Section 7.1.4. This is since it was not always possible to determine whether these detected uncued instances were in fact performances of any one of the PMs or not, making it impossible to determine whether these were then correctly identified in the *Proto-Motion Identification Stage* or not. Meanwhile, the performance of the separate PM classes for the multi-class LDA classifier was assessed on the basis of the intended Proto-Motion in each trial, excluding FNs of the *Movement Detection Stage*. The accuracy, sensitivity and specificity of each class are analysed in Section 7.1.2 using (6.2), (6.3) and (6.4). For a complete analysis, the specificity of the Rest class is also determined and presented alongside all the measures for the PM classes, depicting the number of PM performances which were misclassified as not being any of the four PMs.

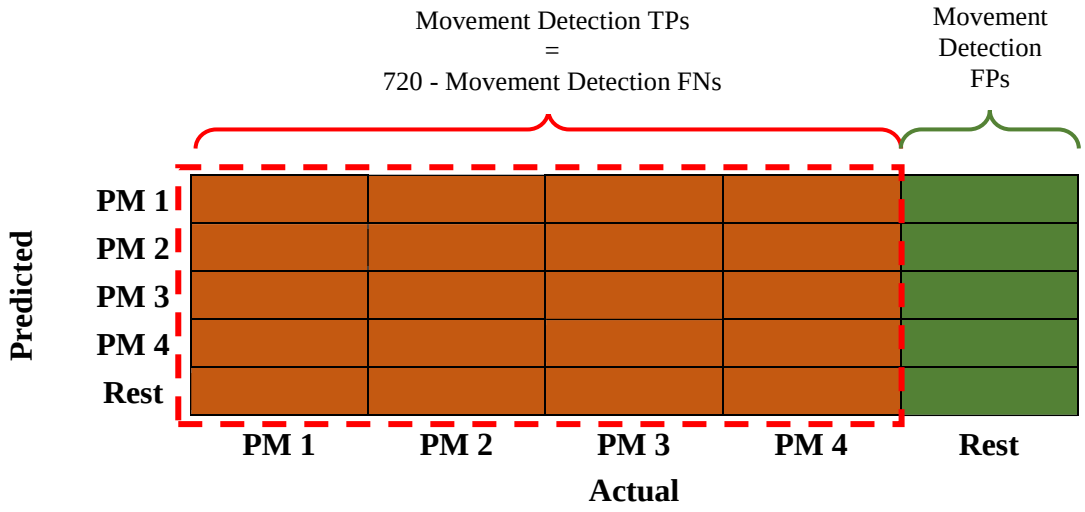

Figure 6.7 - A confusion matrix for Proto-Motion testing where the green cells represent the number of movement detection FPs, as well as how they were then classified in the Proto-Motion Identification Stage. The cells in orange indicate the movement detection TPs for the four PM classes and their classification in the Proto-Motion Identification Stage. The analytical measures were separately and independently obtained for the two groups.

6.2.2.3. Overall System Testing

A confusion matrix layout for the whole *Movement Phase* intent interpretation system, consisting of both stages listed above is as illustrated in Figure 6.8, where the cells in green indicate the number of movement detection FPs, as well as how they were then classified in the *Proto-Motion Identification Stage*. The cells in blue indicate the movement detection FNs (i.e. missed movements), as well as Proto-Motion identification FPs for the Rest class (i.e. those PM instances which were misclassified as Rest instances in the *Proto-Motion Identification Stage*).

Finally, the cells in orange indicate the movement detection TPs and Proto-Motion identification TPs, FNs and FPs for the four PM classes. All the cells within the red border should always total to the 720 cued Proto-Motions, as discussed above.

For a more generalised measure between subjects and classifiers, an overall accuracy measure was obtained using (6.5) such that the accuracy of the *Movement Phase* system could be described as the sum of correctly detected and identified motions from the 720 cued Proto-Motions. This measure therefore takes into consideration the performance of both the movement detection testing as well as the Proto-Motion identification testing. These accuracy results are provided in Section 7.1.3.

$$Overall\ Accuracy = \frac{TP_{PM\,1} + TP_{PM\,2} + TP_{PM\,3} + TP_{PM\,4}}{720} \qquad (6.5)$$

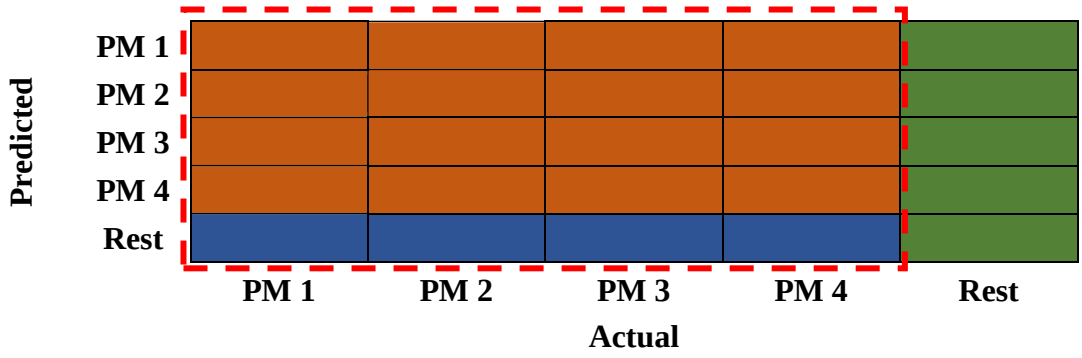

Figure 6.8 - A confusion matrix for the whole tested system where the green cells represent the number of movement detection FPs, as well as how they were then classified in the Proto-Motion Identification Stage. The cells in blue indicate the movement detection FNs, as well as Proto-Motion identification FPs for the Rest class. The cells in orange indicate the movement detection TPs for the four PM classes as well as how they were then classified in the Proto-Motion Identification Stage. The cells within the red border should always total to the 720 Proto-Motion tested instances.

6.2.3. Episodic Inter-Session Results Methodology

As mentioned in Section 6.2, only subject *S0* performed the episodic test on two days for inter-session assessment. Apart from obtaining the cross-validated measures discussed above for the separate day tests, further analysis was then done by using *Day 1* episodic data as the training group and *Day 2* data as the testing group, and vice-versa. In this case, the data was not cross-validated. This resulted in 144 PM instances in total (36 per PM) to be detected and identified per test. These results are discussed in Section 7.3.1.

6.3. Online Movement Phase Testing Session

Besides the offline episodic testing sessions, an online continuous testing protocol was designed for *Movement Phase* testing where the subject performed a continuous trail of Proto-Motions for an extended period of time at the subject's own pace, and where the system was carrying out movement detection and Proto-Motion classification in real-time.

It was deemed that a sequence of around 100 different PM movements was appropriate, therefore a systematic flow was chosen such that all the different PMs could be equally performed. Since the motions used for this work allow the subject to transition from all the closed grasps to the single open grasp and vice-versa, the subject was instructed to loop between one grasp and the next by following the PM sequence shown in Figure 6.9. The sequence was repeated 17 times, such that the 'Neutral to Open' motion was only performed once, resulting in 103 motions. Due to this sequence, PMs 2, 3 and 4 were performed 17 times each, while PM 1 was performed 52 times. In the case where the subject misplaced one of these motions by another, this was corrected at a later stage in the flow.

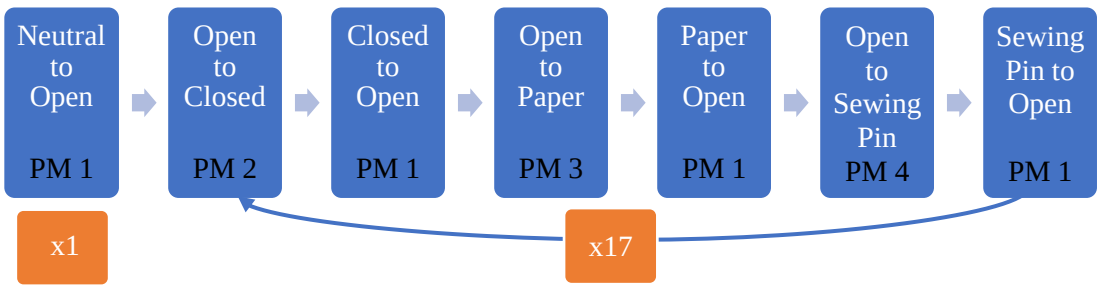

Figure 6.9 - Continuous Testing Sequence, adding up to 103 Movements.

The subject was provided with visual feedback of the motion predictions made by the intent interpretation system in real-time through a *Unity* project interface. This interface included a visual representation of a hand, developed mainly by another member of the research team [120], which behaved according to the identified motions.

For the same reasons mentioned in Section 6.2, only subject *S0* performed this session from the normal limbed subjects, which was carried out on the same day as that of the *Day 2 Episodic Session*. The data obtained from this episodic session was used as training data for the continuous session. These results are discussed in Section 7.2. This testing session was used to identify how well the system can detect and identify motions in a continuous scenario, as well as for inter-session analysis.

Inter-session results were obtained by using the system trained with *Day 1 Episodic Session* data. Note that the continuous online session was only performed once with the same day training data and then re-analysed offline, with different day training data. These results are presented in Section 7.3.2.

Subject *A2* was also a participant for one continuous session, which was held on a different day from the episodic testing session. In this case, this subject was not asked to participate in a *Day 2 Episodic Session*, thus, inter-session results could be obtained from this subject's data by using the continuous system trained with *Day 1 Episodic Session* data. These results are also presented in Section 7.3.2.

6.4. Force Phase Intent Interpretation System Testing Session

For force estimation system analysis in real-time, a testing protocol was devised to test subject *S0*'s performance when instructed to alter the step-wise contraction levels in specified time frames for the three grasps. The *Matlab* to *Unity* interface mentioned above was utilised to provide force level feedback through the use of four different hand colours (white, grey, blue, red) as shown in Figure 6.10. The force feedback colours remained the same, irrespective of the grasp being tested. Thus, the figure shows a combination of the grasps and force level feedback colours, accordingly.

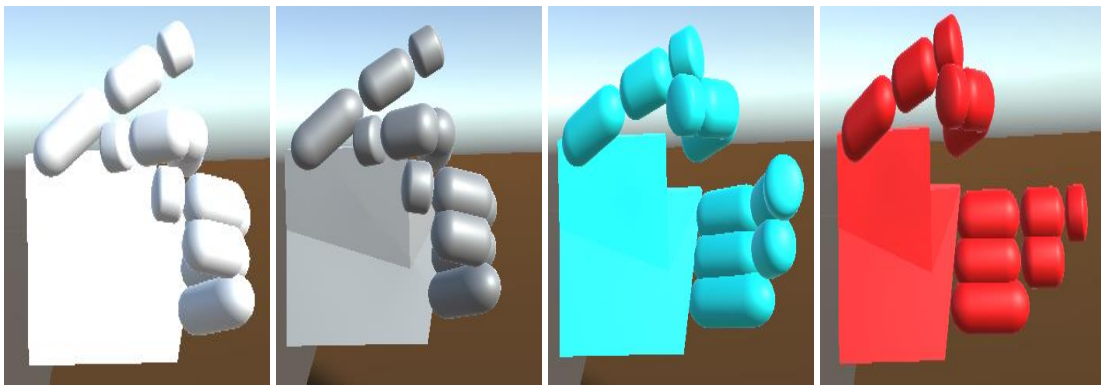

(a) (b) (c) (d)

Figure 6.10 - The Unity Interface during (a) a Rest Force Level, depicted by a white colour, (b) Low Force Level, depicted by a grey colour, (c) Medium Force Level, depicted by a blue colour and (d) High Force Level, depicted by a red colour. These force level colours occurred for all grasps, with these figures illustrating the Closed Fingers Grasp in (a) and (b), the Paper Grasp in (c), and the Sewing Pin Grasp in (d).

The devised protocol instructed the subject to settle in the first grasp, the Closed Fingers grasp, at a Resting Force Level. On the first sound cue, the subject was then instructed to increase the grasp contraction to generate a Low Force Level for a 5 second frame. After these 5 seconds, the subject was then instructed to increase the force to Medium Level, and then to High, accordingly. After these steps, the required force levels descended back in sequence, with 5 seconds between each level, as shown in Figure 6.11. This whole process was repeated five times per grasp, with each repetition referred to as a cycle. This protocol was repeated for the Paper grasp and Sewing Pin grasp, respectively.

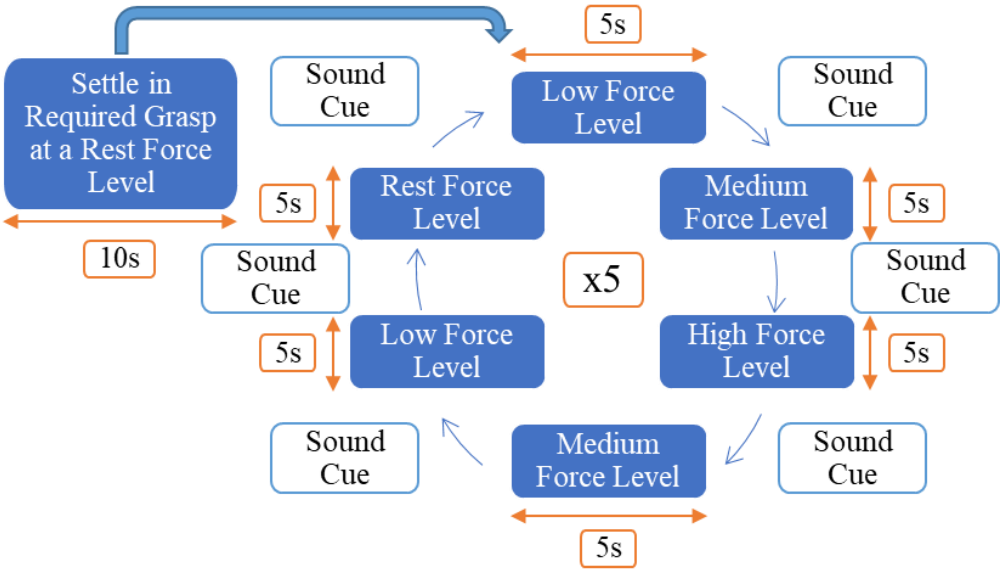

Figure 6.11 - Force Estimation Testing Sequence.

6.4.1. Force Estimation Training Session

Prior to this online force estimation testing session, training data was collected such that the TH_{min} and TH_{max} values required for normalized proportional control value computations, PC_i, used to eventually determine the quantised estimated force level output described in Section 5.5, could be determined. This brief testing session consisted of ten force contraction runs of five seconds each, for the three closed grasps. During each run, the force level of a closed grasp posture was ramped up from the resting condition up to the highest capable force. This training session included ten EMG contraction ramping instances, amounting to 50 s of EMG contraction data, per grasp. Since this experiment was only performed by one subject, these boundary values were only required to be found once.

The top plot in Figure 6.12 shows the EMG RMS signals recorded during the ten ramping instances for the Closed Fingers grasp, and is also representative of the other two grasps. The instantaneous EMG RMS values from the eight channels were summed according to the method described in Section 5.5, providing a single force signal shown in the middle plot of Figure 6.12. By setting P_{THmin} and P_{THmax} to the desired values, the lower and upper bounds for that grasp, $TH_{min,i}$ and $TH_{max,i}$, could be determined. Through the use of these boundary values, the normalized proportional control values, PC_i, could then be obtained in real time, as shown in the bottom plot of Figure 6.12. Due to this normalization step, based on the set lower and upper bounds, any EMG instances that fell below the normalized 0 and 1 force values were capped to these minimum and maximum values, accordingly. Therefore, the objective was to set this to work in a range within a comfortable subset of contraction levels for the subject.

P_{THmin} and P_{THmax} were found to be optimal at 0.05 and 0.25, respectively, and were set for all three grasps. These values were empirically chosen, based on a few online trial runs prior to actual data collection. The training ramped forces reached maximum contraction levels in this work, however, the higher levels were not as easily reached during the actual experiments, leading to choosing much lower boundaries. In real-life settings, it is not ideal for users to exert maximum possible contractions to set the prosthetic's force level, especially since this causes discomfort and pain, with the sense of unease increasing with time. Boundary discrepancies are dependent on subject comfort as well as the force range of the training data.

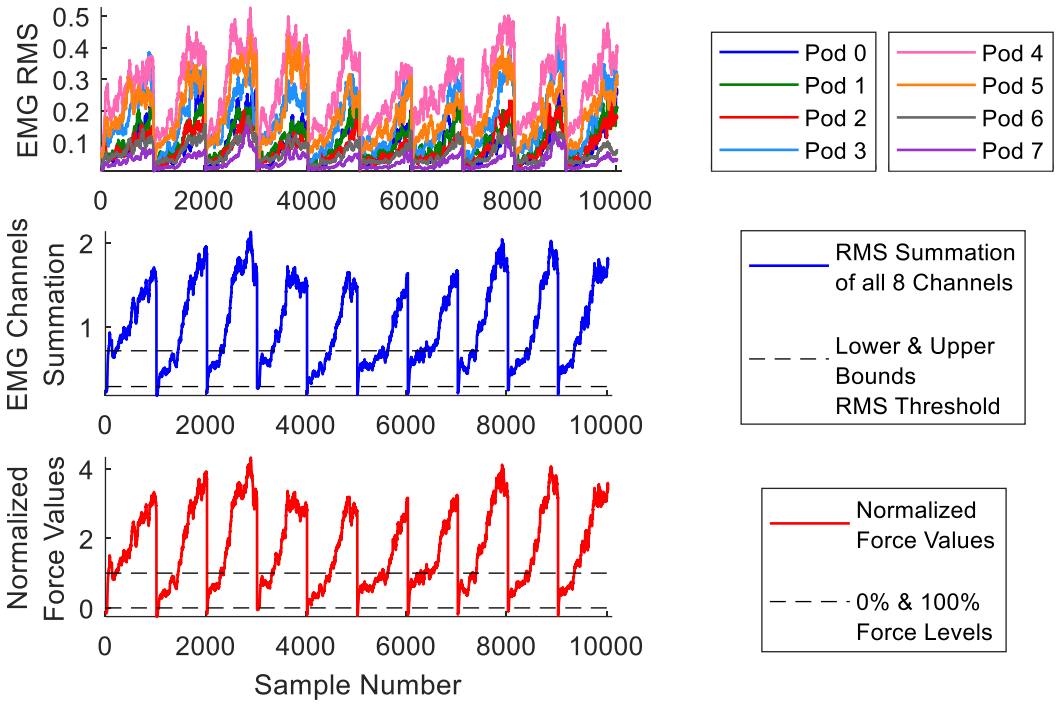

Figure 6.12 - The top plot shows all EMG RMS signals during the ten ramping contractions performed in the Closed Fingers grasp. The middle plot shows the signal obtained following the eight channel EMG RMS summation, as well as the lower and upper bounds, $TH_{min,i}$ and $TH_{max,i}$ obtained. The bottom plot shows the normalized Proportional Control output value for this grasp, specifically outlining the lower and upper bounds that would need to be considered in real time at 0% and 100%.

6.4.2. Force Estimation Results Methodology

For quantitative performance analysis of the force level estimation during the three different grasp contractions, system accuracy was defined on the basis of the number of correctly output force level samples, in comparison to the instructed force levels, termed as the ideal signal. Since the output force levels, termed as the estimated signal, included an obvious delay at the start of every cycle for every grasp type, the accuracy between the ground truth force signal and the estimated force signal was estimated by shifting the ideal signal so as to align with the first Rest to Low force level rising edge of the estimated signal. This was done per cycle as shown in Equations (6.6) and (6.7), ensuring that the accuracy measure was not penalised due to system and human reflex delays whilst obtaining measures that most faithfully represent the graphics. Average accuracy and delay values were obtained for the separate grasps, in accordance to (6.8) and (6.9).

$$Accuracy_{i,m} = \frac{1}{S_{i,m}} \sum_{s=0}^{S_{i,m}-1} C_{i,m}(s) \tag{6.6}$$

$$C_{i,m}(s) = \begin{cases} 0, & x_{i,m}(s - d_{i,m}) \neq y_{i,m}(s) \\ 1, & x_{i,m}(s - d_{i,m}) = y_{i,m}(s) \end{cases} \quad (6.7)$$

$$\overline{Accuracy_i} = \frac{1}{5} \sum_{m=1}^{m=5} Accuracy_{i,m} \quad (6.8)$$

$$\overline{d_i} = \frac{1}{5} \sum_{m=1}^{m=5} d_{i,m} \quad (6.9)$$

where,

$i \in \{1, \dots, 3\}$ is the grasp index representing the Closed Fingers, Paper and Sewing Pin grasps, respectively;

$m \in \{1, \dots, 5\}$ is the cycle number;

$S_{i,m}$ is the total number of samples for grasp i, cycle m force testing;

$s \in \{0, \dots, S_{i,m} - 1\}$ is the sample number;

$d_{i,m}$ is the number of samples that represents the delay between the first rising edge of the ideal and the estimated signals for grasp i, cycle m;

$y_{i,m}(s) \in \{0, \dots, 3\}$ is the estimated force level signal for grasp i, cycle m, at sample s where the range reflects the Rest to High force levels in ascending order;

$x_{i,m}(s - d_{i,m})$ is the ideal force level signal for grasp i, cycle m, at sample $(s - d_{i,m})$, such that:

$$x_{i,m}(s - d_{i,m}) \in \begin{cases} \{0, \dots, 3\}, & (s - d_{i,m}) \geq 0 \\ 0, & (s - d_{i,m}) < 0. \end{cases}$$

The actual signals as well as quantitative accuracy, sensitivity and specificity measures for the three grasps are provided and discussed in Section 7.4.

6.5. Testing Methodology Conclusion

All the above-mentioned tests were carefully devised such that a suitable analysis could be made on the capability of the designed systems from an offline and online point of view for the eventual movement and force action intents of a prosthetic hand. The results obtained are presented and discussed in the following chapter.

7. Results and Discussion

As has been explained in Chapter 6, in order to analyse the performance of the designed systems, numerous tests were devised and performed by different subjects. The results obtained following data processing, their analysis, as well as a discussion on these measures are all provided in the sections below.

7.1. Offline Movement Phase Testing Results and Discussion

This section presents the results obtained following the *Movement Phase* testing methodologies described in Section 6.2.2 for offline episodic experiments performed by the five normal limbed subjects and the two amputees. Unless stated otherwise, these results relate to the LDA classifiers.

7.1.1. Movement Detection Classification

As discussed in Section 6.2.2.1, the success of the *Movement Detection Stage* could be quantitatively defined from the True Positive (TP) counts, False Negative (FN) counts, False Positive (FP) counts and the sensitivity measure. The results obtained for the seven subject tests are shown in Figure 7.1, Figure 7.2, Figure 7.3 and Figure 7.4. As discussed earlier, the TP and FN counts for every subject add up to the 720 cued PM instances whilst the FP counts may vary depending on the several factors discussed in Section 6.2.2.1.

From these plots, it is clear that the sensitivity of this part of the system is high, exceeding 95% for all subjects. Whilst the system only managed to detect all the cued PMs for one subject, *S4*, subject *A2* had the least successful movement detection rate. It can also be noted how for the two amputees, higher FN rates, leading to lower TP and sensitivity rates were obtained, when compared to the normal limbed subjects. If the two subject groups are treated separately, the normal limbed subjects obtained a movement detection mean sensitivity rate of 99.19% ± 0.94% whilst the amputees obtained a mean rate of 96.81% ± 1.18%. Inconsistencies in PM performances have been noted to be a great contributor to missed movement detections, especially when the sample training data consists of specific amplitudes for which the testing data lies out of the norm.

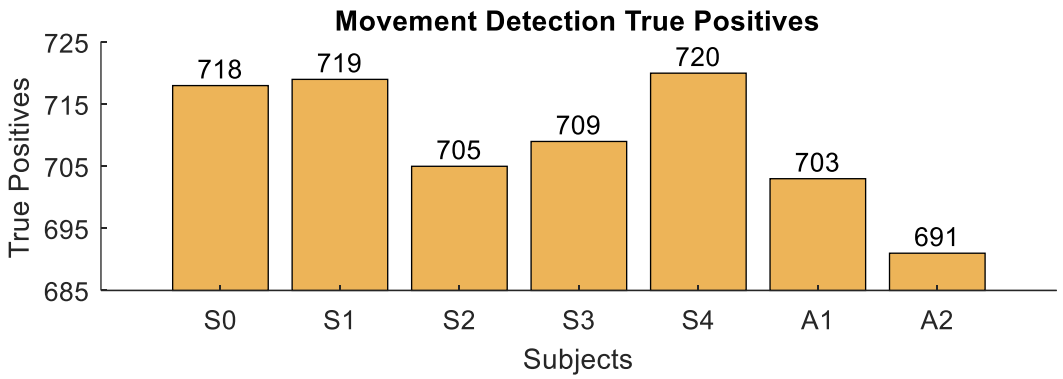

Figure 7.1 - Movement detection true positive counts for the seven subjects, out of a maximum of 720.

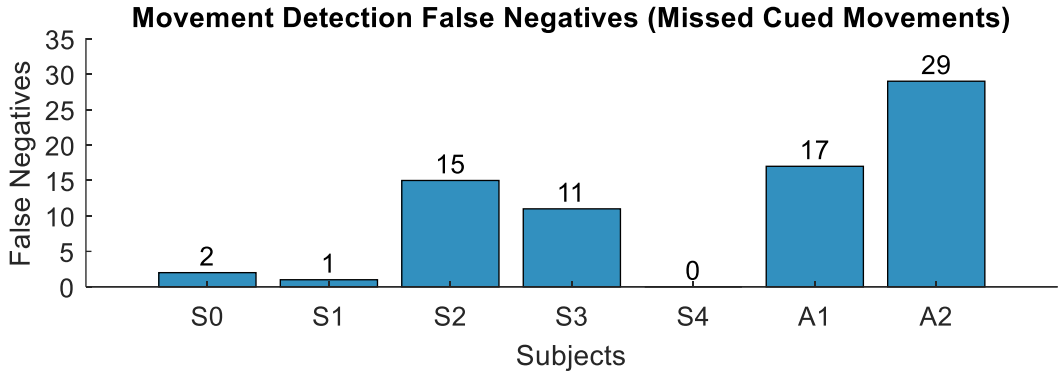

Figure 7.2 - Movement detection false negative (missed cued movement) counts for the seven subjects.

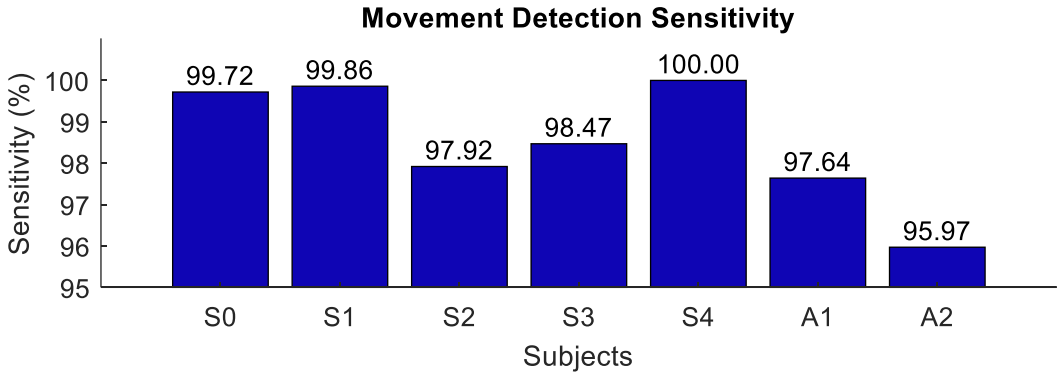

Figure 7.3 - Movement detection Sensitivity measure for the seven subjects.

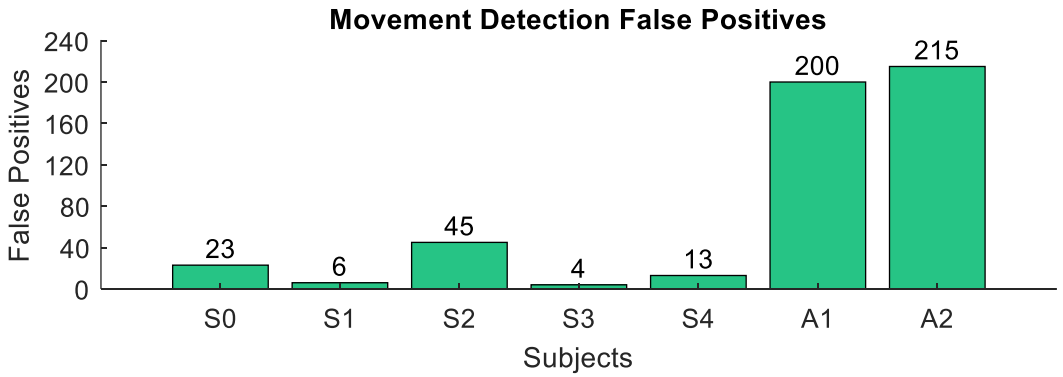

Figure 7.4 - Movement detection false positive counts for the seven subjects.

The discrepancy between the subject groups is also evident in the number of detected movement FPs, with the highest normal limb subject count being 45 and the lowest amputee subject count being 200. As discussed in Section 6.2.2.1, five types of causes have been identified for these instances being labelled as movement FPs. The evident amputee movement inconsistencies leading to signal inconsistencies also played a large part in the larger number of detected FPs since in those cases where the training data consisted of lower amplitudes, the classifiers became prone to happy triggering. Multiple false positive movement detections, however, were obvious muscle recruitment detections, which occurred when the subjects should have been at rest. The experimenter had limited control over this behaviour, especially when there was no visual feedback of the subject's limb activity. It was also noted that amputees showed a greater difficulty with resting while holding a grasp posture. This led to more fluctuating muscular activations, reflecting the subjects' high efforts to remain in posture resulting in higher contribution to movement detection FPs.

Nevertheless, normal limbed subjects were also prone to performing uncued movements. This was especially true for subject *S2* who was very fidgety and was not as cooperative, even after being corrected. In fact, this subject resulted in the highest FP value from the normal limbed subjects. Due to there being multiple causes for movement detection FPs, with most proving to be difficult to determine their root cause, it was decided that their classification analysis in the *Proto-Motion Identification Stage* was to be separated from the other four PM classes. These results are provided in Section 7.1.4.

7.1.2. Proto-Motion Identification Classification

As discussed in Section 5.4.4, the time-window WL_M used to detect RMS maxima as soon as a movement detection is confirmed was found to empirically cover the signal maxima when set between 200 ms and 300 ms. For an appropriate classification performance analysis, episodic testing of the *Proto-Motion Identification Stage* was done according to Section 6.2.2.2 for three different WL_M values; 100, 200 and 300 ms. Figure 7.5, Figure 7.6 and Figure 7.7 provide a graphical illustration of the class sensitivity, specificity and accuracy measures for all subjects combined for systems implementing the 100, 200 and 300 ms WL_M values, respectively. For each plotted box, the mark in the middle indicates the median TPR value (50^{th} percentile), with the top and bottom edges indicating the 75^{th} and 25^{th} percentiles for that class.

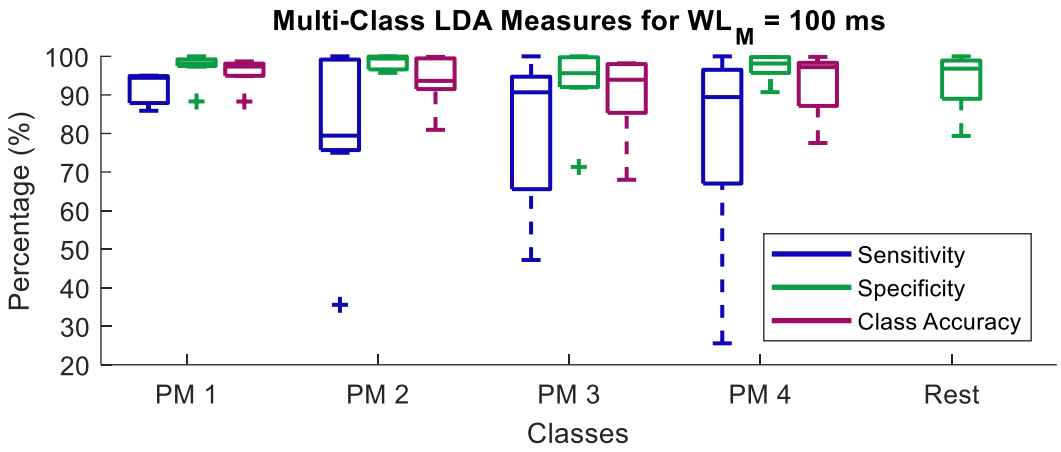

Figure 7.5 - Sensitivity, Specificity and Class Accuracy measures for the four PM classes and the Specificity measure for the Rest class for Proto-Motion identification testing at WL_M = 100 ms. These box plots contain measures from all seven subjects.

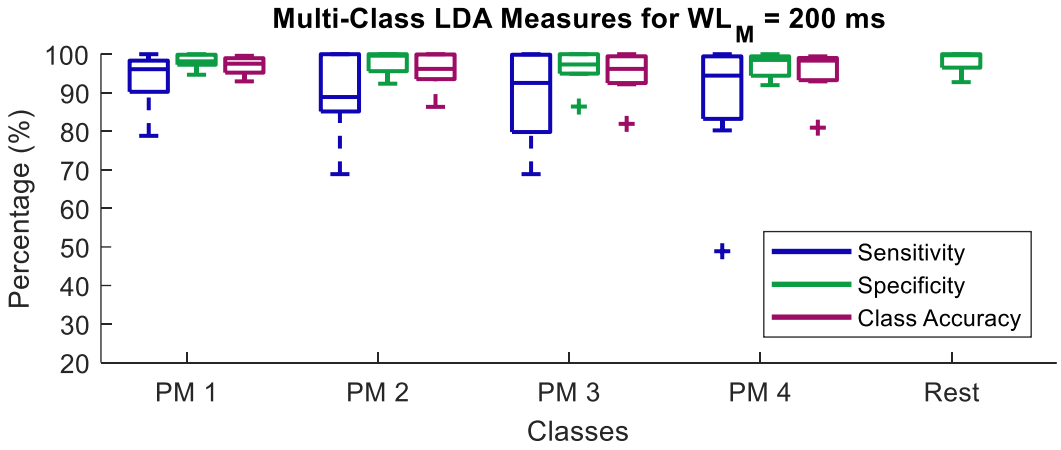

Figure 7.6 - Sensitivity, Specificity and Class Accuracy measures for the four PM classes and the Specificity measure for the Rest class for Proto-Motion identification testing at WL_M = 200 ms. These box plots contain measures from all seven subjects.

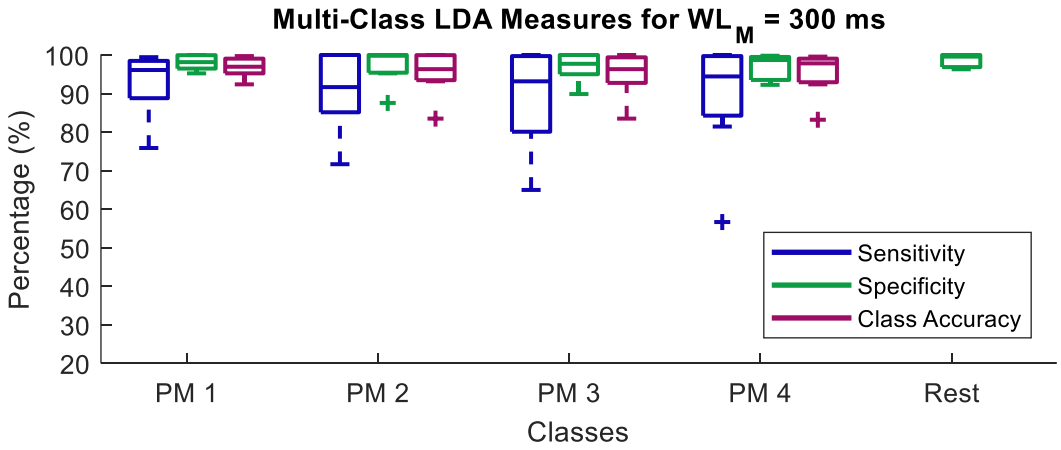

Figure 7.7 - Sensitivity, Specificity and Class Accuracy measures for the four PM classes and the Specificity measure for the Rest class for Proto-Motion identification testing at WL_M = 300 ms. These box plots contain measures from all seven subjects.

Outliers and extreme data points are shown as plus signs and whiskers, respectively. The indicated outliers, in this case, have a value of more than 1.5 times the interquartile range, defined by the subtraction of the 25th percentile from the 75th percentile [152]. The median indicators provide information with regard to sample skewness.

It is clearly noticeable that the three WL_M values contributed towards sensitivity, specificity and accuracy improvements for some classes and reductions in others. Sensitivity measures at a WL_M value of 100 ms resulted in lower medians when compared to the other two, whilst also experiencing very low sensitivity instances for individual subjects for the PM 2, PM 3 and PM 4 class. The specificity measure compares well to the others, however, lower extremities in the PM 3 and Rest classes are a further disadvantage. The larger range of Rest class specificities in the 100 ms WL_M case also suggests that for this value, more motion instances were incorrectly classified as falling in the Rest class. These discrepancies are also reflected in lower class accuracy ranges. As was also visually noted, such a performance decrease was expected due to the window being too short to capture the RMS maxima required for classification.

Meanwhile, the differences between the 200 ms and 300 ms tests are less obvious, showing that the two values resulted in very similar outcomes, leading to the conclusion that a 200 ms window was only unsuitable to capture the RMS maxima for a very limited number of instances. Whilst these similarities are clear from the two plots, the final conclusion with regard to which window would provide the best quantitative results is discussed in Section 7.1.3.

Nevertheless, since decision delay plays an important factor in the success of prosthesis acceptance, the preferance of the 200 ms window over the 300 ms window is natural. For more in-depth, subject specific analysis, the sensitivity, specificity and class accuracy measures of the four PM classes and the specificity of the Rest class are shown for the seven individual subjects in Figure 7.8 to Figure 7.14, respectively, for a WL_M value of 200 ms.

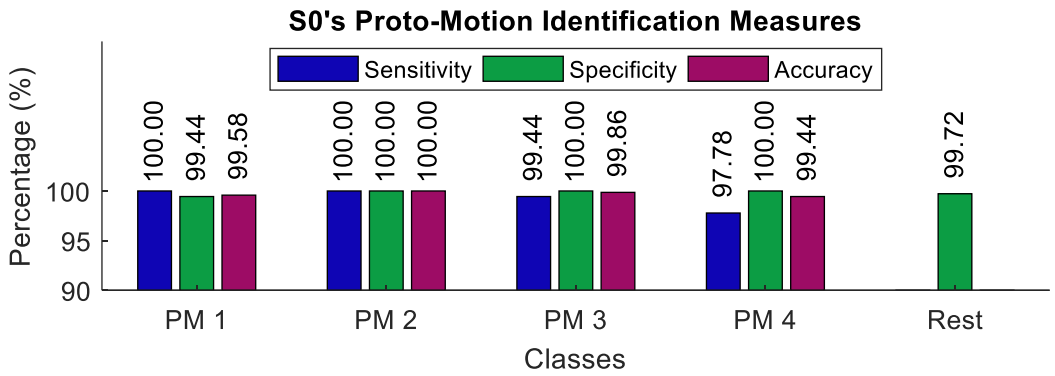

Figure 7.8 - Subject S0's Proto-Motion identification Class Sensitivity, Specificity and Accuracy measures for the four PM classes and the Specificity for the Rest class.

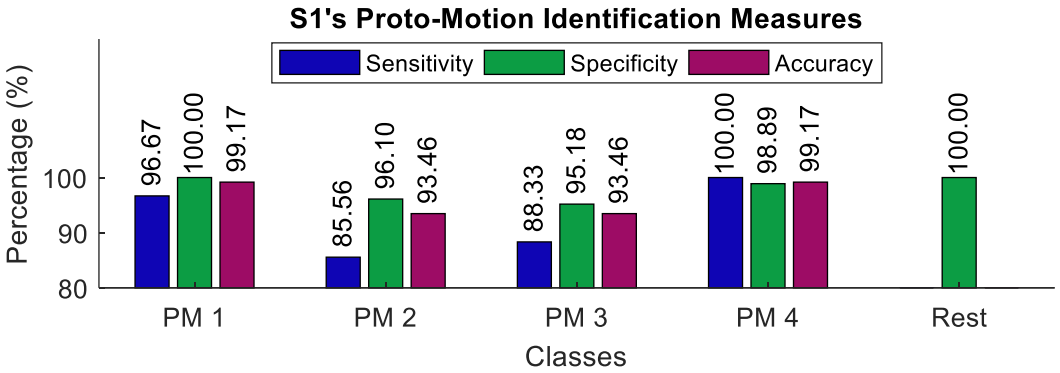

Figure 7.9 - Subject S1's Proto-Motion identification Class Sensitivity, Specificity and Accuracy measures for the four PM classes and the Specificity for the Rest class.

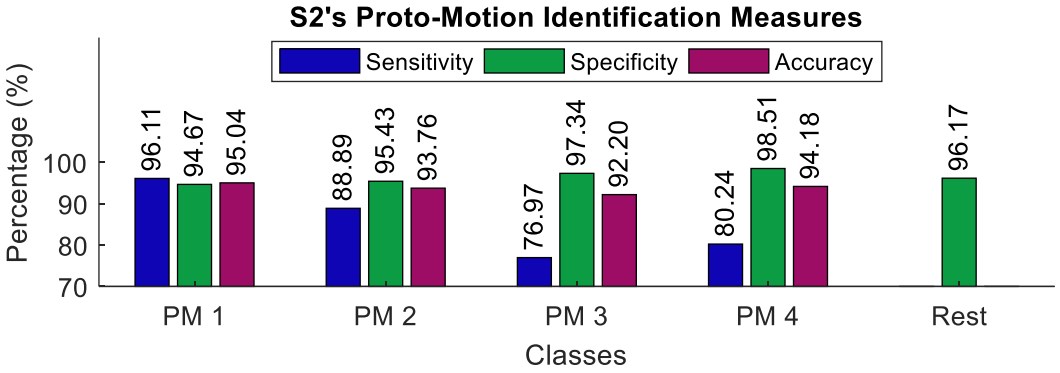

Figure 7.10 - Subject S2's Proto-Motion identification Class Sensitivity, Specificity and Class Accuracy measures for the four PM classes and the Specificity for the Rest class.

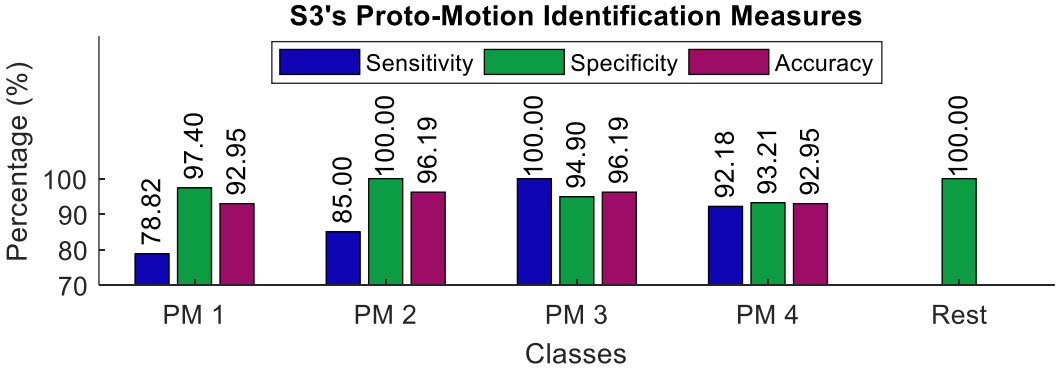

Figure 7.11 - Subject S3's Proto-Motion identification Class Sensitivity, Specificity and Class Accuracy measures for the four PM classes and the Specificity for the Rest class.

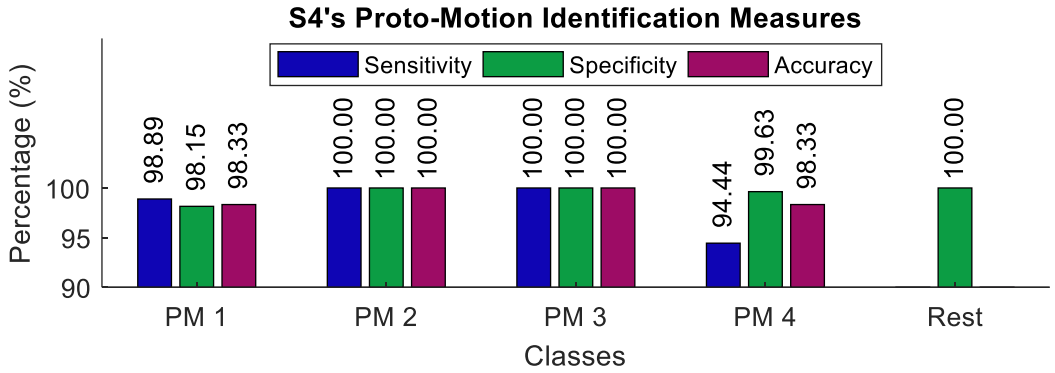

Figure 7.12 - Subject S4's Proto-Motion identification Class Sensitivity, Specificity and Class Accuracy measures for the four PM classes and the Specificity for the Rest class.

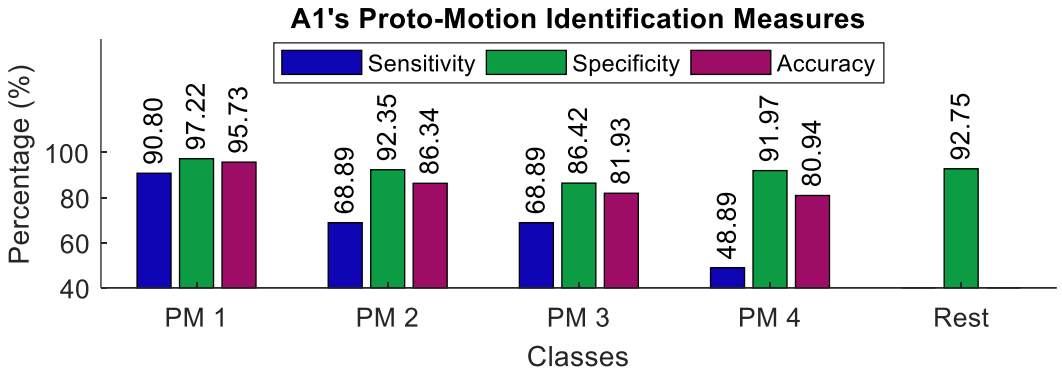

Figure 7.13 - Subject A1's Proto-Motion identification Class Sensitivity, Specificity and Class Accuracy measures for the four PM classes and the Specificity for the Rest class.

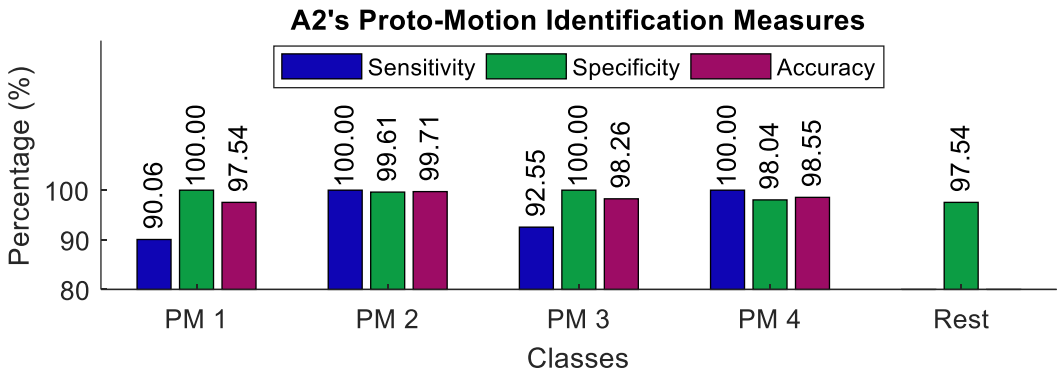

Figure 7.14 - Subject A2's Proto-Motion identification Class Sensitivity, Specificity and Class Accuracy measures for the four PM classes and the Specificity for the Rest class.

From all seven subjects, the highest performing multi-class classifier was for subject *S0*, achieving perfect sensitivity, specificity and accuracy for PM 2; and subject *S4*, achieving perfect sensitivity, specificity and accuracy for PM 2 and PM 3; apart from all the other class measures, well exceeding the 94% mark. Subject *A2*'s results also show the high success of the classifier, exceeding 90% for all measures across all classes. In fact, PM 2 and PM 4 class instances were all correctly identified whilst there were no motions which were incorrectly identified as PM 1 or PM 3. The results for this subject also suggest higher success in comparison to the other three normal-

limbed subjects *S1, S2* and *S3*. Meanwhile, subject *A1*'s results suggest that this was the least successful classifier, obtaining the least sensitivity value of 48.89% for the PM 4 class. Another two classes resulted in sensitivities less than 70%, which are also low in comparison to those obtained by other subjects.

When considering the results from all subjects, there is no noticeable pattern of which class is superior or inferior to the others. In general, the multi-class LDA has been successful, achieving individual class accuracies higher than 92% for all subjects except for subject *A1*, who achieved a minimum class accuracy of approximately 80% for PM 4. Meanwhile, the high Rest class specificities for all subjects also suggest that the number of motion instances misclassified as not being one of the four motions was very limited.

7.1.3. Overall Movement Phase System Accuracy

The measure that encapsulates the performance of the whole *Movement Phase* system, including the *Movement Detection Stage* and *Proto-Motion Identification Stage*, is the overall accuracy, as described in Section 6.2.2.3. As a continuation of the discussion of Section 7.1.2, the overall accuracies of the system considering the three WL_M values are shown in Figure 7.15. This figure confirms the previous conclusion that while the smaller window of 100 ms presents the advantage of shorter decision delays, the overall system accuracy is much lower when compared to longer windows. Whilst this is not always the case, the majority of subject results suggest so. The similar 200 and 300 ms window length accuracies confirm that an increase in window length does not automatically warrant higher system accuracies. Therefore, the rest of the discussion shall only consider the 200 ms WL_M results.

Through comparison of the 200 ms results, it may be concluded that subject *S0* obtained the highest accuracy from both normal limbed and amputee subject groups. This was expected since this subject had additional training opportunities, in comparison to all others. All normal limbed subjects exceeded the 80% overall accuracy mark with the lowest overall accuracy obtained by subject *S2*. This was also expected since this subject was very fidgety whilst being highly inconsistent with the performed movements.

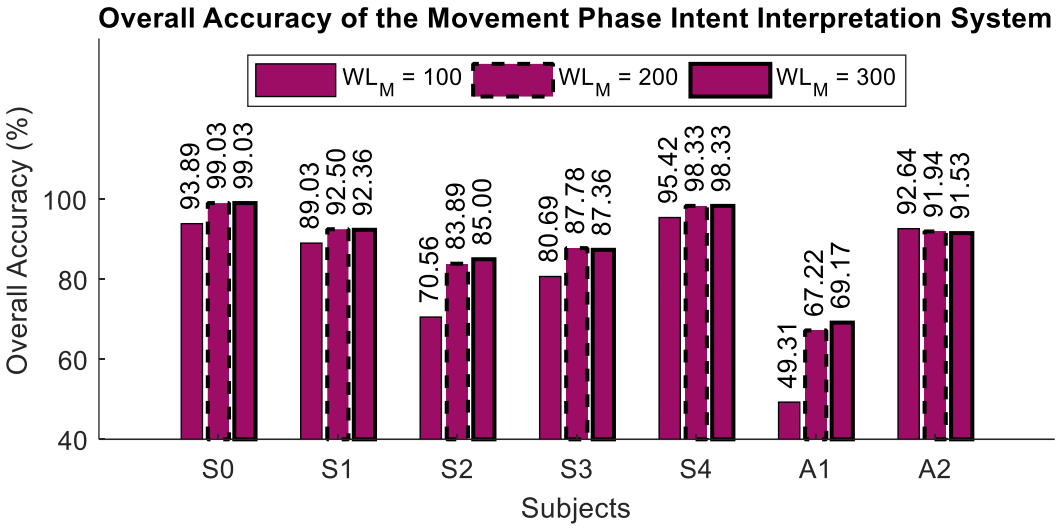

Figure 7.15 - The Overall Accuracy of the Movement Phase Intent Interpretation System for all seven individual subjects, considering the three different Proto-Motion identification WL_M tests. These accuracies represent the number of correctly detected and identified PMs, from the total 720 cued motions.

The high overall accuracy obtained by subject *S4* is very promising, especially when considering that this subject had no previous training. This indicates that this subject has very good control over the hand muscles during the exertion of different movements, irrespective of the lack of training experience. This subject was also the only left-handed participant, however, it cannot be concluded that this high accuracy was a direct cause of the difference in hand dominance.

Meanwhile, the two amputees obtained large overall accuracy discrepancies, with subject *A1* achieving the lowest overall accuracy rate of 67.22% and subject *A2* achieving a fairly high overall accuracy of 91.94%. The overall accuracy of subject *A2* exceeded the overall accuracy of normal limbed subjects *S2* and *S3*, whilst faring very closely to the overall accuracy of subject *S1*.

The lowest accuracy result by the first amputee subject *A1* was expected. Subject *A1* was a congenital subject, who had no life experience with exerting such finger movements. Thus, his brain is not used to sending such signals to his missing limb, requiring more effort from the subject to try to differentiate between the movement contractions. Nevertheless, the subject's experience was improved when the experimenter suggested looking at the intact limb performing the same motion at the same time. The subject indicated that he had no singular finger sensations from the missing limb and the only control that he had was on flexor and extensor groups. The lack of experience with using this hand in a natural way also contributed to muscle recruitment inconsistencies, resulting in less movement detections and correct

identifications. These inconsistencies may have also been caused due to subject adaptation in a bid to achieve better signals. Other variables such as the lack of visual feedback from the experimenter's end to guide the subject as required, when compared to normal limbed subject sessions, are also envisaged to have affected the end results. As is usually the case with prosthetic fittings, the subject would need to undergo further rigorous training in order to determine whether such a system would ultimately be well-suited.

In comparison, the other amputee, subject *A2,* had the arm amputated due to a work-related accident. This means that this subject had learnt to move the fingers of his own hand before amputation. This was evident from the control shown over the voluntary contraction of the different phantom fingers. Nevertheless, while the subject was comfortable with the closing motions, this subject struggled with PM 1 where finger extension was required. The exercise of looking at the intact limb performing the motions also aided this subject with recruiting the appropriate muscles representing the motion performances of the amputated limb. However, the subject commented that this reduced the mental concentration that could be afforded to contract the amputated limb's muscles. Whilst this subject had such limitations, the overall accuracy results proved that the subject managed to be mostly consistent in the performed motions, except for those instances which were missed in the *Movement Detection Stage*.

The results obtained by the amputee subjects suggest that congenital subjects may achieve lower *Movement Phase* intent interpretation system accuracies when compared to non-congenital subjects. However, since the pool of local amputee subjects eligible to participate in this experiment was small, and this aggravated further by the COVID-19 restrictions, it is not possible to verify this observation at this stage. Nevertheless, it is to be considered that every amputee will have different capabilities, different movement restrictions as well as different muscular atrophies. The latter mostly depends on amputation surgical outcomes, with no amputation procedure being identical to the other. Thus, while these results show extremely satisfactory results with very limited training, one may be hopeful that higher accuracies may eventually be obtained with more rigorous and regular training, especially with direct feedback from a mechanical prosthetic hand. In future work, a longitudinal study may be done with congenital and non-congenital amputees to determine whether improvement is possible from both groups. Nevertheless, the results obtained from both amputees confirm that the designed system may in fact be used by the transradial focus group.

From the above discussed results, it can be concluded that the system accuracy rates obtained for all these subjects are satisfactory, also providing us with the insight that different subjects would require different training, for performance improvement. Subjects who showed PM pairs signal similarities (typically between PMs 1 and 4, and PMs 2 and 3), would require further muscle isolation training, aiding with contraction isolations for different motions. In the meantime, for subjects who showed specific difficulties such as subject *A2*, a lot more training is required for PM 1 performance improvements, with subject *A1* requiring overall training on the control and performance of all PMs.

Whilst the analysis above has been done on the individual subjects' results, the box plot in Figure 7.16 provides a graphical insight on the overall accuracies when the subjects are split into the two groups, namely the normal limbed and amputee subject groups. The lowest extreme data point for the normal limbed subjects exceeds the amputees' median whilst the normal limbed median exceeds the amputees' highest extreme data point. The mean overall accuracies of the two subject groups are provided in Table 7.1.

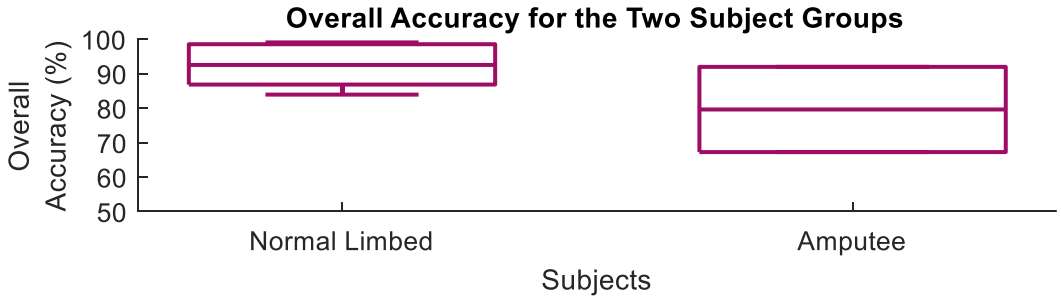

Figure 7.16 - Box plots containing the overall accuracies for a WL_M value of 200ms for the five normal limbed and two amputee subjects, separately.

Table 7.1 - The Overall Accuracy Mean for the two subject groups.

	Normal Limbed Subjects Group	**Amputee Subjects Group**
Overall Accuracy Mean	92.31% ± 6.57%	79.58% ± 17.48%

7.1.4. Identification of Movement Detection False Positives

The movement detection FPs for the individual subjects have been illustrated in Section 7.1.1 and their respective Proto-Motion identification TP measure is shown in Figure 7.17. This TP measure relates to how many of these movement detection FPs were then identified to not be any of the four PM classes. It is evident from the plot that these false movement detections were never fully corrected to fall within the Rest class. As has been discussed in Section 6.2.2.1, there were multiple causes for these false detections, which in reality, may have not been false detections at all. Since it was out of the scope of this project to identify whether every movement detection FP was in fact a movement or simply a binary classification error, a more detailed analysis on this concept needs to be carried out in future work. In such offline analysis, this is not possible, especially when there was no visual feedback of the hand movements performed by the amputee subjects. A more practical analysis of this concept may be done in an online setting, where movement detections are traced in real-time, giving the experimenter more flexibility over determining which false movement detections were legitimate and which ones were not, as discussed in Sections 7.2 and 7.3.2.

Furthermore, whilst the aim of the *Movement Detection Stage* was to reduce the detection of unnecessary motion, the detection of these instances was dependent on the training data set used for the four, binary class LDAs, changing their sensitivity accordingly. Thus, a more in-depth analysis could also be carried out in order to identify which training sets resulted in specific false detections, and which did not.

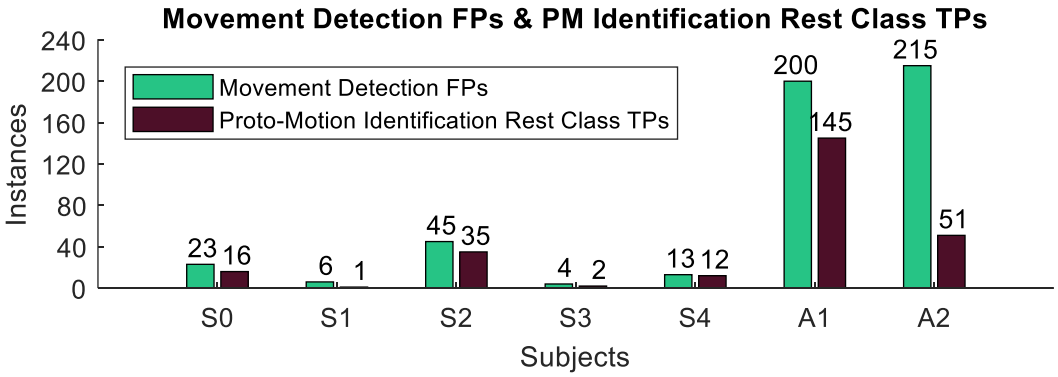

Figure 7.17 - The seven subject movement detection FPs and their respective PM identification measure, represented as the Rest class TP measure.

7.1.5. Results Comparison with Literature

To analyse the performance of the offline *Movement Phase* intent interpretation system, the obtained results will be compared to three chosen results reported in the literature who have all implemented different intent interpretation systems.

The study by Li et al. [54] provides an insight as to how data extracted from intact and amputated limbs differ. The five participants within the study were all non-congenital transradial amputees, the majority of which having experience with myoelectric prosthetics. This experience may be regarded as advantageous due to muscular control experience. For 12 sEMG channels and 11 motion classes (including both hand and wrist motions), and by using a continuous LDA classification method, the results showed that the amputated arm accuracy results were significantly lower than intact limbed results. The average accuracies were of 94% ± 3% and 79% ± 11% for the intact and amputated hand experiments, respectively. The latter accuracy was reduced to 69% ± 18% when only the five hand-grasp patterns were considered. The normal limbed subject results are very similar to what has been achieved in our study, for the four hand motion classes. For the amputee subjects, the accuracy obtained in this work relates closer to the combined hand and wrist motions accuracy presented by Li et al, showing an increase in accuracy percentage for hand movement classes in this work. It is also evident from both studies that with amputated limbs, the deviation in accuracies is typically increased.

Hudgins et al. [32] used both transient and steady-state data as training data for four contraction types (forearm supination, elbow extension, wrist flexion and forearm pronation), which were correctly classified at an average of 91.2% ± 5.6% for normal limbed subjects and 85.5% ± 9.8% for amputees. The contractions studied by Hudgins et al. should have been more easily detectable due to the larger muscles responsible for their actions, which may explain the better performance obtained for the amputees when compared to our work.

In the study by Kanitz et al. [37], which used hand movements similar to those in our study, only a segment of the transient EMG signals was used to make a prediction, resulting in average true positive rates of 96% and 95% for normal limbed subjects and myoelectric experienced amputees, respectively. The performance of the experienced amputees is comparable to that of the normal limbed subjects, which leaves open the question on whether experience helps amputees to perform better.

7.1.6. Classifier Types Comparison

As discussed in Section 5.4.5, linear SVM classifiers were also implemented to compare the degree of performance of such model free classifiers to the performance of the less than optimal classifiers, the LDAs, as provided above.

7.1.6.1. Movement Detection Classification Comparison

For ease of comparison, movement detection TP and FN counts as well as sensitivity measures obtained for all subjects with the separate implementation of LDA and SVM classifiers are shown in Figure 7.18, Figure 7.19 and Figure 7.20, respectively. From the TP and FN counts as well as the resultant sensitivity measures, it can be noted that whilst the detection of the cued Proto-Motions increased for the normal limbed subjects with the SVM classifiers implementation, this decreased for both amputees.

In order to determine whether the difference in movement detection sensitivity between the use of LDA and SVM classifiers was statistically significant, a paired, one-tailed t-test [153] was performed on the normal limbed subjects' sensitivity results using a statistical significance value of 0.05 [154]. As mentioned in Section 7.1.3, the amputee subject pool was not homogenous and thus, statistical conclusions could not be drawn on them. The null hypothesis of this test claimed that the movement detection sensitivity mean for binary LDA classifiers was equal to the movement detection sensitivity mean for binary SVM classifiers. The alternative hypothesis claimed that the movement detection sensitivity mean for binary SVM classifiers was greater than the movement detection sensitivity mean for binary LDA classifiers. The resultant p-value of 0.07 concluded that the null hypothesis could not be rejected and there was no evidence to support the claim that the SVM classifiers provided better movement detection results.

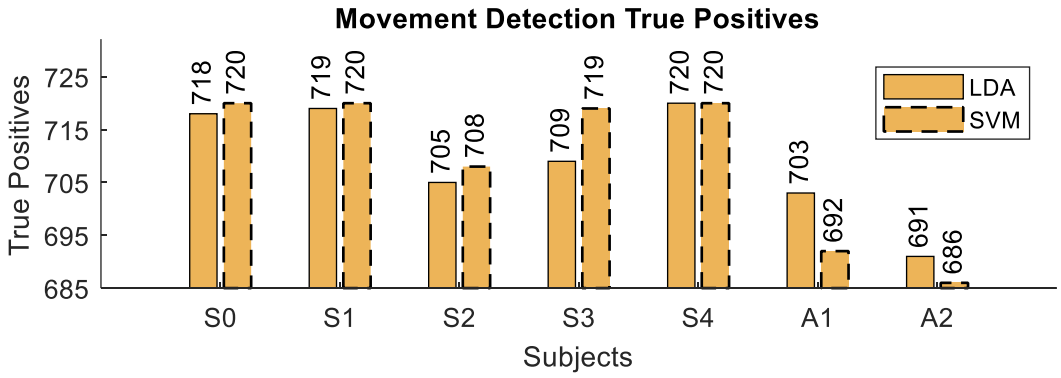

Figure 7.18 - Movement detection true positive counts out of a maximum of 720, for the seven subjects for the LDA and SVM binary classifier systems.

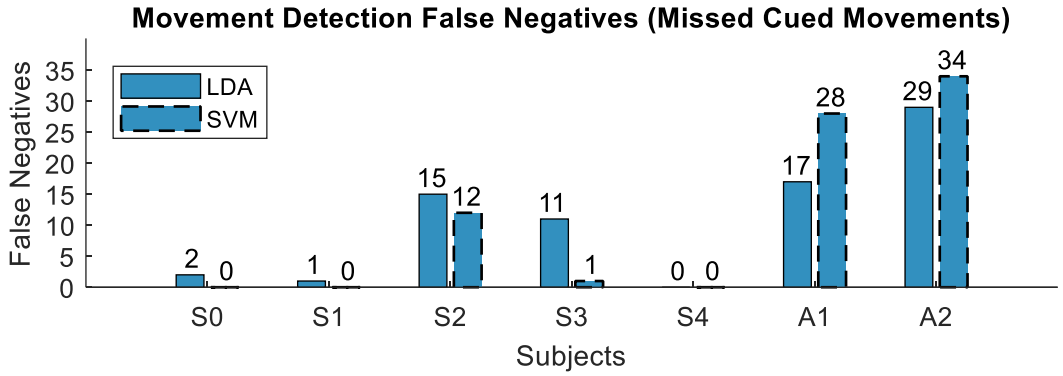

Figure 7.19 - Movement detection false negative counts for the seven subjects for the LDA and SVM binary classifier systems.

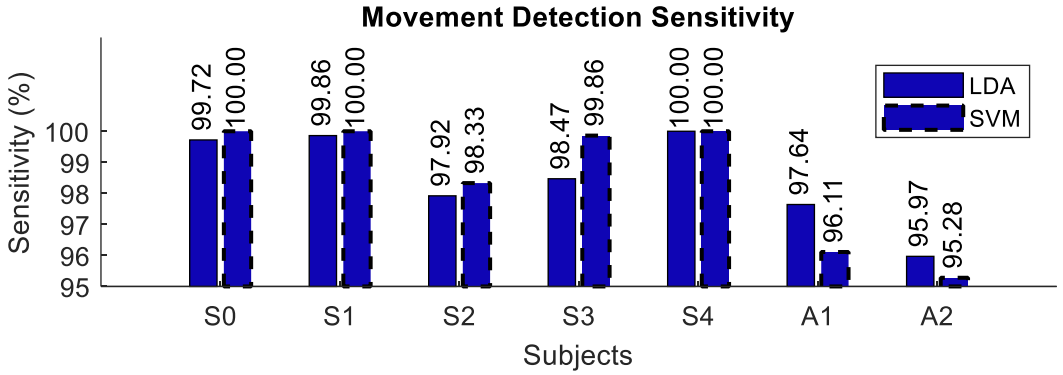

Figure 7.20 - Movement detection Sensitivity measure for the seven subjects for the LDA and SVM binary classifier systems.

Movement detection FPs for both LDA and SVM classifiers are shown in Figure 7.21 and it may be clearly noted that this count decreased with the latter classifier for all subject testing. This decrease was analysed to be primarily due to the SVMs being less sensitive to amplitude fluctuations caused by changes in muscle recruitments in the middle of Proto-Motion performances as well as being less sensitive to small muscle recruitments caused by unintended small movements, which were otherwise captured by the LDAs. The scope of the *Movement Detection Stage* was to only prompt for a multi-class PM decision whenever required, thus reducing the risks of misclassifications. Thus, this decrease in FPs may warrant a conclusion that binary SVMs are a more suitable option for this stage within the system. One, however, needs to keep in mind whether LDA systems which detected more movement detection FPs would still be capable of correcting these instances in the *Proto-Motion Identification Stage*.

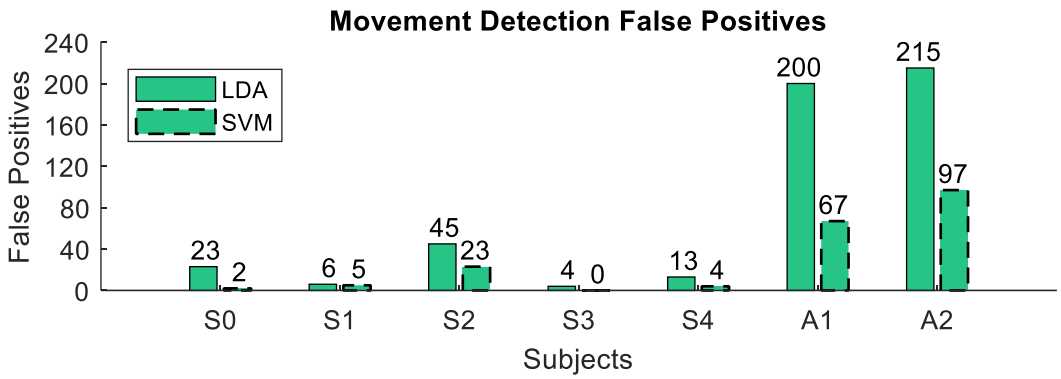

Figure 7.21 - Movement detection false positive counts for the seven subjects for the LDA and SVM binary classifiers.

Figure 7.22 shows how only a small number of movement detection FPs for SVM systems were then corrected during PM identification testing. Since it was out of the scope of this project to identify whether every movement detection FP was in fact a movement or simply a classification error, it cannot be concluded whether the SVM binary classifiers in fact prove to be superior to the LDAs for the movement detection stage. A more detailed analysis on this concept needs to be carried out in future work.

7.1.6.2. Proto-Motion Classification Comparison

As was concluded in Sections 7.1.2 and 7.1.3, the best value found for WL_M for Proto-Motion identification was of 200 ms. Thus, the Proto-Motion identification SVM tests were only implemented with this feature value, for all seven subjects. For performance comparison of the two multi-class classifiers, a graphical depiction of the sensitivity, specificity and class accuracies for each class are shown in Figure 7.23 and Figure 7.24, for LDA and SVM classifiers, respectively. These box plots include the collective data of the seven participating subjects, regardless of their subject group.

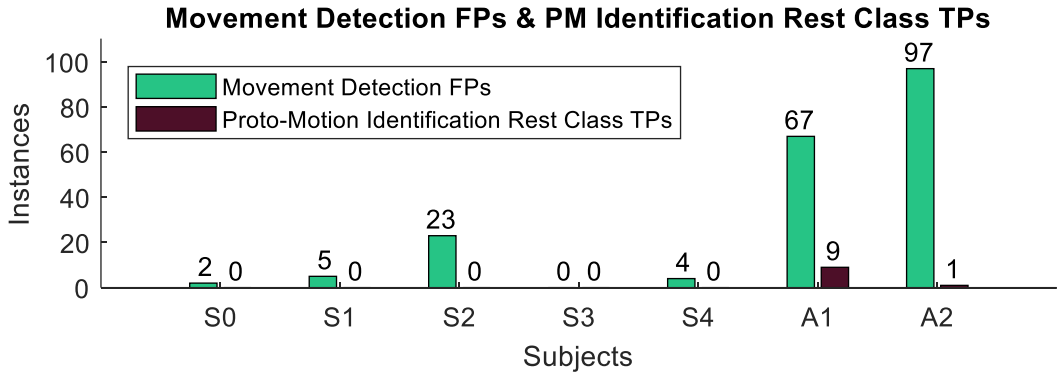

Figure 7.22 - Movement detection false positive counts for all subjects for SVM binary classifiers and their respective Proto-Motion identification Rest class true positive counts.

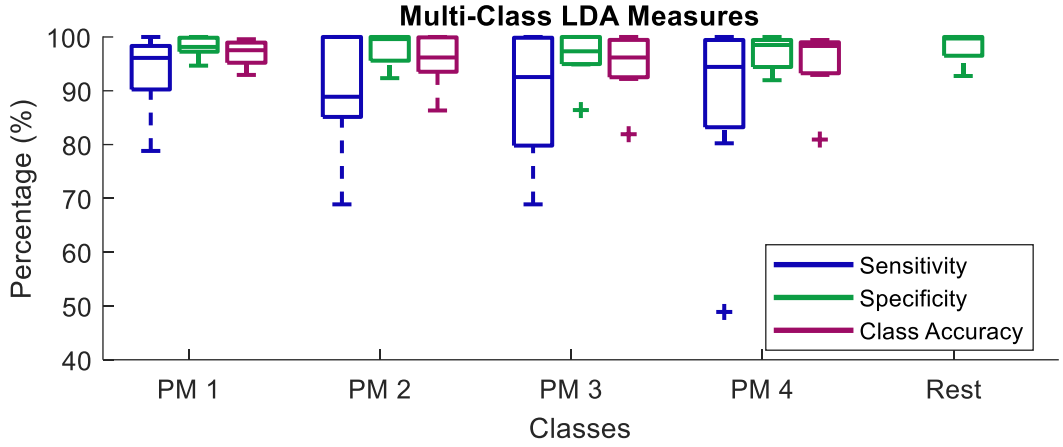

Figure 7.23 - Sensitivity, Specificity and Class Accuracy measures for the four PM classes and the Specificity measure for the Rest class within the multi-class LDA. These box plots contain measures from all seven subjects.

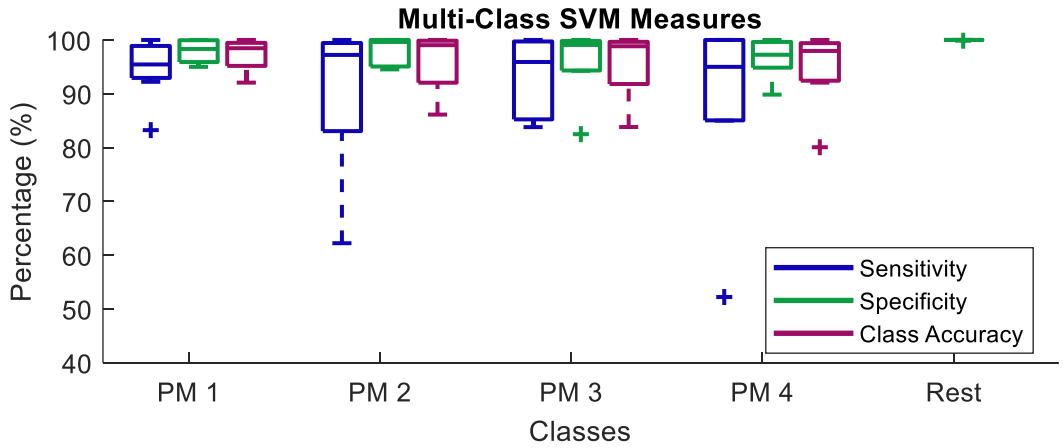

Figure 7.24 - Sensitivity, Specificity and Class Accuracy measures for the four PM classes and the Specificity measure for the Rest class within the multi-class SVM. These box plots contain measures from all seven subjects.

From these figures, it can be noted that in general, higher specificity measures for both classifiers was obtained. The largest differences noted between the classifier measures were the sensitivity and accuracy measures, with all SVM sensitivity median measures exceeding the 90% mark and all SVM class accuracy median measures closely approaching the 100% mark. An interesting point is the Rest class specificity measure. For the SVM classifier, this measure resulted in 100% for six subjects out of all seven, suggesting that this classifier was well suited for discriminating the PM classes from the Rest class. Whilst the LDA classifier resulted in high Rest class specificity values, these were lower than the SVM, confirming that the model free classifier is more capable of discriminating the motion classes from the singular non-motion class.

The remaining measures showed very similar ranges for both classifiers. Thus, paired one-tailed t-tests were performed using the normal limbed subjects' class accuracy values using a statistical significance value of 0.05. The null hypothesis of these tests claimed equal class accuracies for both classifiers while the alternative hypothesis claimed that class accuracies obtained with the SVM classifiers system were greater than those using the multi-class LDA classifier. The resultant p-values of 0.58, 0.49, 0.42 and 0.57 for classes PM 1 to PM 4, respectively, concluded that the null hypothesis could not be rejected for all classes and there was no evidence to support the claim that the SVM classifiers resulted in better Proto-Motion identification.

7.1.6.3. Overall System Accuracy Comparison

For comparison of both stages within the system, the performance of the LDA and SVM systems may essentially be compared through the overall system accuracy obtained for every subject. This subject-specific comparison is shown in Figure 7.25, where it is evident that the SVM system achieved higher overall accuracies than the LDA system for all subjects, except two.

The accuracy difference between the two is provided in Table 7.2 and a paired, one-tailed t-test was also performed on the normal limbed subjects' results in order to determine statistical significance, as was done for the separate movement detection and identification stages above. The test used a statistical significance value of 0.05 where the null hypothesis claimed an equal mean overall accuracy for both classification systems while the alternative hypothesis claimed that the mean overall accuracy obtained with the SVM system was greater than that using LDA classifiers. The resultant p-value of 0.14 concluded that the null hypothesis could not be rejected and there was no evidence to support the claim that the use of SVM classifiers in both movement detection and Proto-Motion identification stages resulted in better overall accuracies in comparison to LDA classifiers.

This also suggests that unless data is projected to a higher dimensional space by using SVM kernels or other non-linear classifiers, more accurate results using a linear system will not be obtained. Such analysis with non-linear classifiers, however, would need to be done in future work.

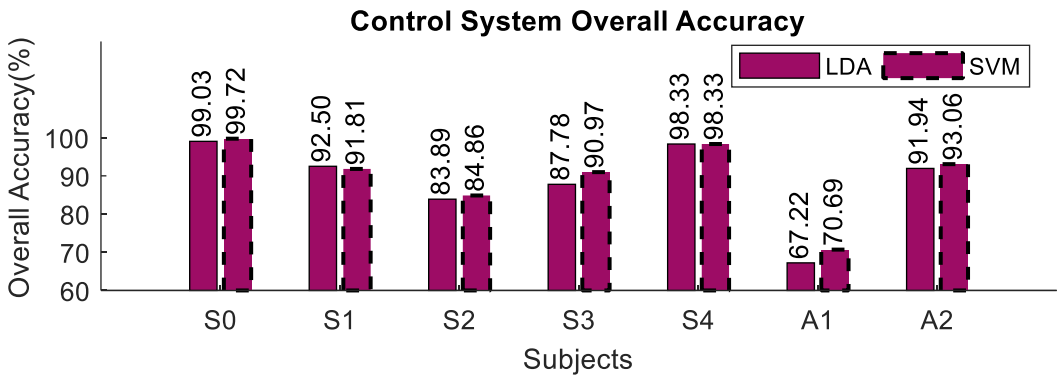

Figure 7.25 - Overall system accuracy only considering the 720 cued Proto-Motions.

Table 7.2 - The overall accuracy difference between SVM and LDA systems.

	S0	***S1***	***S2***	***S3***	***S4***	***A1***	**A2**
SVM - LDA Overall Accuracy (%)	0.69	-0.69	0.97	3.19	0.00	3.47	1.12

7.2. Continuous Detection and Classification

As was explained in Section 6.3, an online continuous session was also performed by subject *S0* on *Day 2*. This continuous testing session was performed by using *Day 2* episodic data to train all the LDA classifiers within the system stages. The subject took a total of approximately four and a half minutes to perform all the requested continuous motions, with a subset of them shown in Figure 7.26. The WL_M value set for real time peak detection was that of 200 ms. Due to the conclusions reached in Section 7.1.6, only a system using LDA classifiers was implemented.

With regard to movement detection, all 103 performed movements were detected, reaching a sensitivity of 100%, whilst no false positive movements were recorded. From the plot, it may be noted that from a total of nine movements, whilst all were correctly detected, only seven were correctly identified. As shown from the sensitivity, specificity and class accuracy measures in Figure 7.27, only PM 2 had perfect sensitivity, specificity and accuracy rates. The most common misclassifications were of PM 1 being identified as PM 4 whilst there were two instances where PM 3 instances were incorrectly identified as the Rest class.

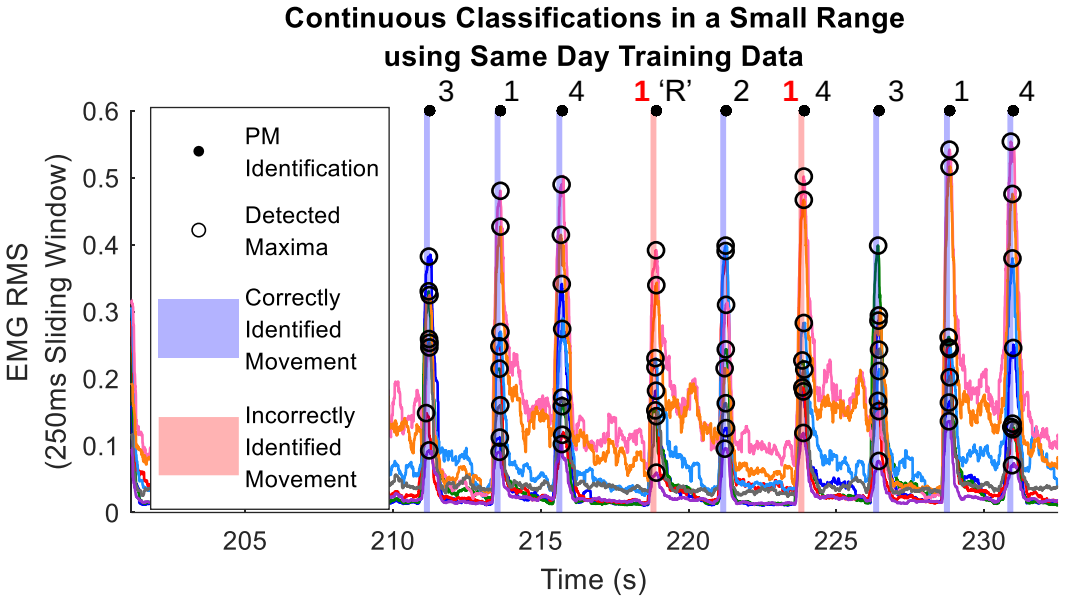

Figure 7.26 - A small range of the performed continuous session motions, showing detected movements, and classifier Proto-Motion identifications with same day training data. The shaded areas in purple are the 200 ms WL_M windows used to detect the RMS movement peaks, following movement detection, which the multi-class LDA then correctly identified. The shaded red areas are the same as the purple areas, however, which the multi-class LDA incorrectly identified. The black dots at the top show identification instances and the black numbers indicate the predicted PM number. The numbers in red indicate the actual PM class, whenever the prediction was incorrectly made. The PM numbers relate to the Proto-Motions listed in Table 5.2 whilst 'R' refers to a predicted Resting class.

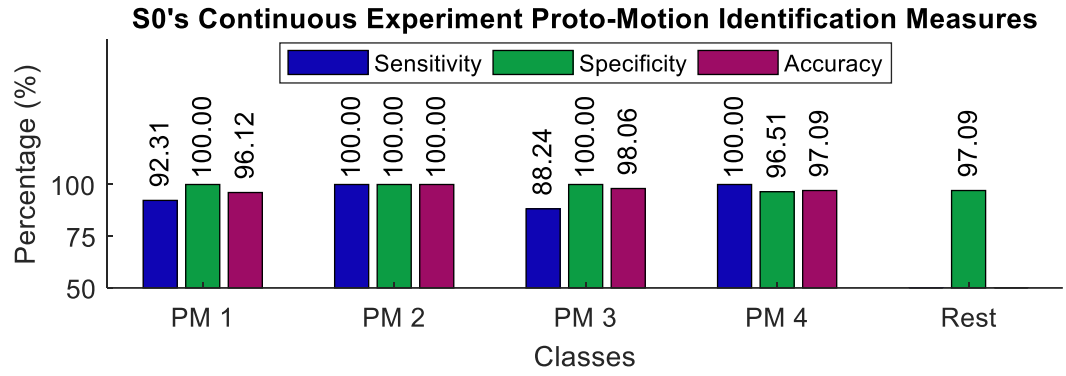

Figure 7.27 - Subject S0's Proto-Motion identification Sensitivity, Specificity and Class Accuracy measures for the four PM classes and the Specificity for the Rest class for the same day continuous experiment. These results were obtained by using an LDA classifier and WL_M of 200 ms.

The overall accuracy of this continuous test resulted in 94.17%, which is less than the 99.03% overall accuracy rate obtained from the *Day 1* episodic test, but still comparable to the mean overall accuracy obtained from the normal limbed subject episodic tests. Thus, it may be concluded that the system is capable of high performance even in less controlled, continuous detection settings.

In comparison to a popular online study, Hargrove et al.'s [39] virtual clothes pin test obtained classification accuracies higher than 90% for seven contraction types. Since these motions included elbow flexion/extension, wrist flexion/extension, hand

open/close and no motion, the fact that the muscles responsible for wrist and elbow movements differ from the intricate hand motion muscles, it may be concluded that the results obtained from the continuous classifier of this work compare very well to the results of Hargrove et al.

In future work, online system analysis would also need to include other real-time control performance metrics, such as motion selection time, motion completion time and motion completion rate [54]. These metrics, however, may only be obtained from specific tests, requiring larger design and implementation efforts, which was not within the scope of this work.

7.3. Inter-Session Reliability Results

The results that have been discussed until now have only treated same day training and testing, for both episodic as well as continuous testing. Ideally, prosthetics do not have to be trained every time they are donned, thus, inter-session reliability is critical. Due to the conclusions reached in the above sections, all results presented have been obtained from systems which implemented LDA classifiers for all stages and used a WL_M value of 200 ms.

7.3.1. Episodic Inter-Session Testing

In Section 7.1, a detailed analysis of the movement detection, Proto-Motion identification and overall accuracy measures for subject *S0*'s *Day 1 Episodic Data* was provided. For this data set, an overall accuracy of 99.03% was obtained. The same analysis was done for subject *S0*'s *Day 2 Episodic Data*, resulting in an overall system accuracy of 98.19%. This result shows that if the classifiers are trained for each session, high accuracies may be obtained. However, it is desirable to explore whether the classifiers trained for one session may be re-used in a subsequent session without re-training.

For the inter-session tests described in Section 6.2.3, movement detection, Proto-Motion identification and overall accuracy measures were also obtained. Whilst both testing data resulted in no movement detection FPs, only the *Day 2* test resulted in a 100% movement detection sensitivity. For *Day 1*'s test, this reduced to 70.83%, as shown in Table 7.3. The identification measures for those Proto-Motions that were in fact detected are shown in Figure 7.28 and Figure 7.29 for *Day 1* and *Day 2*, respectively, whilst the overall accuracies of the system are provided in Table 7.4.

Table 7.3 - The number of movement detection FPs and the movement detection Sensitivity obtained for the two inter-session episodic tests.

	Day 1 Testing Data	Day 2 Testing Data
Movement Detection FPs	0	0
Movement Detection Sensitivity	70.83%	100%

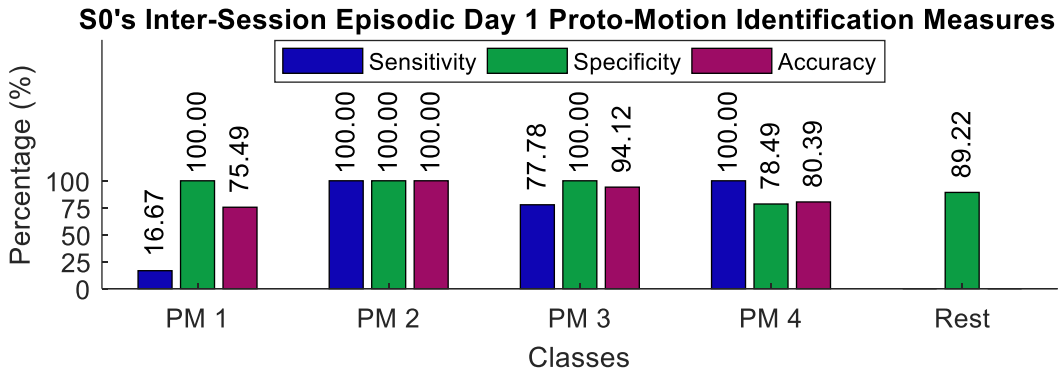

Figure 7.28 - Subject S0's Proto-Motion identification Sensitivity, Specificity and Class Accuracy measures for the four PM classes and the Specificity for the Rest class for the inter-session, episodic test where Day 1 data was used for testing, with the system trained with Day 2 data.

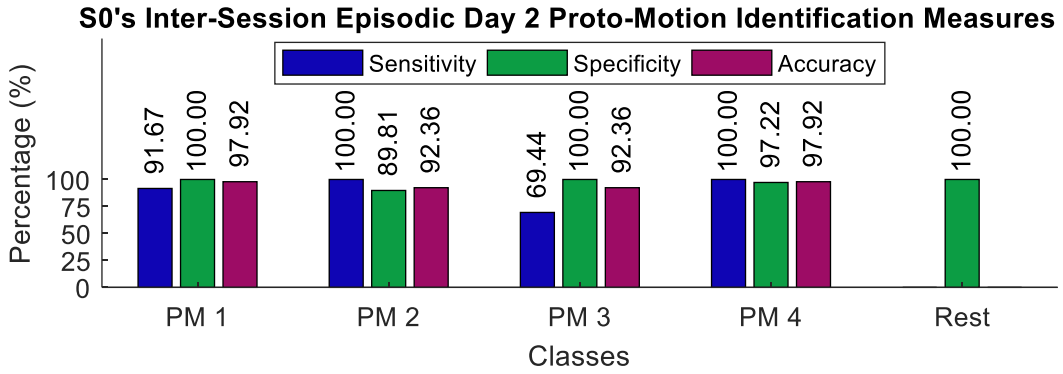

Figure 7.29 - Subject S0's Proto-Motion identification Sensitivity, Specificity and Class Accuracy measures for the four PM classes and the Specificity for the Rest class for the inter-session, episodic test where Day 2 data was used for testing, with the system trained with Day 1 data.

Table 7.4 - The Overall Accuracy obtained for the two inter-session episodic tests.

	Day 1 Testing Data	Day 2 Testing Data
Overall Accuracy	49.31%	90.28%

From these results, it is highly evident that *Day 1 Training Data* was more successful with detecting and identifying *Day 2*'s data, than vice versa, with a substantial difference between the final accuracies obtained.

A quick comparison between the mean and variance values obtained from Proto-Motion EMG signals on different days concluded that higher EMG RMS maxima magnitudes were recorded on *Day 2*. This change in training data directly affected the performance of the *Movement Detection Stage*, with a drastic sensitivity reduction of this stage for *Day 1*, in comparison to *Day 2*. For *Day 1* testing, the largest majority of undetected movement were PM 4 movements, amounting to 27 out of the total 36 PM 4 movements.

From the Proto-Motion identification results, it is also evident that the change in training and testing sets also affected the sensitivity, specificity and class accuracy measures recorded for the two day sessions as shown above. The decrease in Proto-Motion identification specificity of *Day 1*'s Rest class shows how a number of PM movements were incorrectly identified to fall within the Rest class. The majority of these were found to be PM 1 and PM 3 movements. The lowest sensitivity measure for *Day 1* testing has been concluded to be due to a large number of PM 1 movements having been misclassified as PM 4 movements.

The artefacts causing such signal changes are ideally identified and mitigated, aiming towards a final system which is robust enough to detect and adapt to changes. Further discussion on the causes of such signal changes will be held in Section 7.3.3.

7.3.2. Continuous Inter-Session Testing

From subject *S0*'s continuous inter-session test, movement detection sensitivity remained at 100%, successfully detecting all 103 movements, as was also noted for the same day continuous test in Section 7.2. However, in this test, one movement detection false positive was also detected towards the end of one PM 1 movement. This was then incorrectly identified by the PM identification stage as a PM 4 instance.

The sensitivity, specificity and class accuracy measures for all PM classes and the specificity for the Rest class for this test are shown in Figure 7.30. Whilst the sensitivities for the PM 2 and PM 4 classes remained at 100%, in comparison to the same day continuous test results, the sensitivities of PM 1 and PM 3 were reduced, with the lowest reaching 58.82%. The specificity measures also show that no movements were falsely identified to belong to the PM 1, PM 3 and Rest classes.

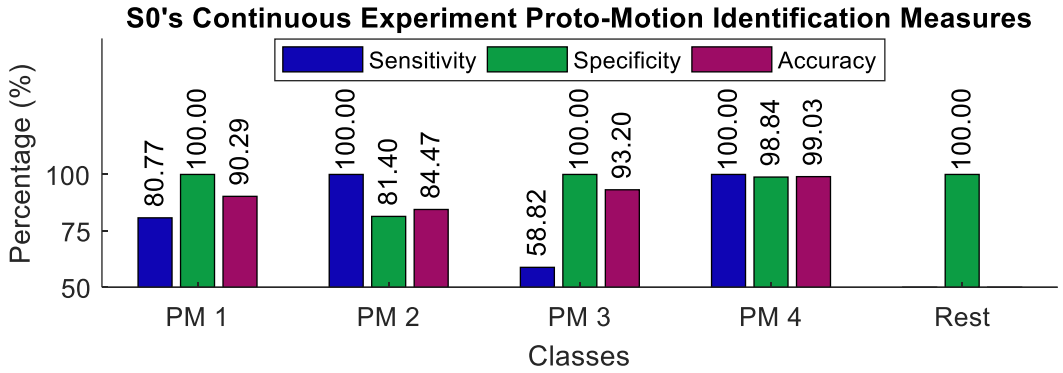

Figure 7.30 - Subject S0's Proto-Motion identification Sensitivity, Specificity and Class Accuracy measures for the four PM classes and the Specificity for the Rest class for the inter-session continuous experiment.

The class accuracies obtained for this test were also lower than those obtained for the same day continuous test, leading to an overall accuracy of 83.50%, compared to 94.17% for the same day continuous test. This suggests that the overall accuracy of the system is expected to decrease when trained with data acquired on a different day.

Meanwhile, the same nine motions presented in Section 7.2, Figure 7.26, are shown in Figure 7.31. This plot shows how these same nine motions were identified. In comparison to Figure 7.26, the majority of these motions were correctly predicted in both experiments. Nevertheless, whilst one PM 1 instance was misclassified by both systems, albeit predicting it to belong to different classes, both figures show a movement which was incorrectly predicted in one experiment and correctly predicted in the other. This concludes that system capability of different motion instance identification differs in accordance to the training data used.

It is also to be noted that instant motion identification feedback was provided to the subject during the same day continuous test, but not for the inter-session continuous test. With feedback, the subject had the advantage of identifying the causes of incorrect identifications, serving as an adaptation opportunity, which may have contributed to the better results.

Meanwhile, in order to obtain an inter-session result from one of the amputees, since subject *A2* was the best performing among the two amputee subjects, this subject was chosen to perform a continuous test on *Day 2* using an online system trained using the episodic data collected from this subject on *Day 1*. Note that for this subject, the continuous test using same day training data was not performed due to the much longer session time required.

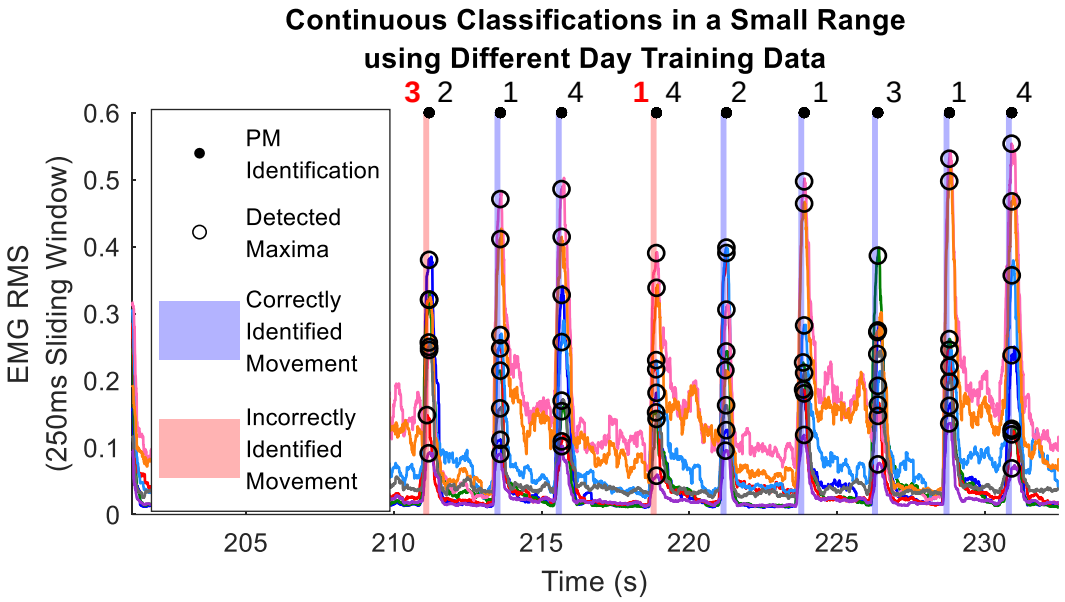

Figure 7.31 - A small range of the performed continuous session motions, showing detected movements, and classifier Proto-Motion identifications with different day training data. The shaded areas in purple are the 200 ms WL_M windows used to detect the RMS movement peaks, following movement detection, which the multi-class LDA then correctly identified. The shaded red areas are the same as the purple areas, however, which the LDA incorrectly identified. The black dots at the top show identification instances and the black numbers indicate the predicted PM number. The numbers in red indicate the actual PM class, whenever the prediction was incorrectly made. The PM numbers relate to the Proto-Motions listed in Table 5.2.

Movement detection for this session also achieved 100% sensitivity. However, the number of movement detection false positives amounted to 44 and only eight out these 44 were then corrected and identified as Rest class instances, with the remaining 36 detected Rest instances classified as one of the four PM classes. From visual analysis of the sEMG data, it was concluded that this high FP detection occurred because the subject was struggling to maintain a relaxed force level in the Open Hand position, leading to unnecessarily high amplitudes. This suggests that it may be more intuitive for amputees to simply relax their muscles as soon as a motion is performed, rather than remain in the final grasp posture with minimal muscle recruitment.

The sensitivity, specificity, and class accuracy measures for the *Proto-Motion Identification Stage* are shown in Figure 7.32. Whilst all PM 3 and PM 4 movement instances were correctly identified, PM 2 showed the least sensitivity at 47.06%. In this case, none of the movements were incorrectly identified to fall in the Rest class. The overall accuracy for this system was 90.29% which is higher than subject *S0*'s inter-session continuous test accuracy of 83.50%, also faring very closely to the overall accuracy of the same subject's episodic test of 91.94%.

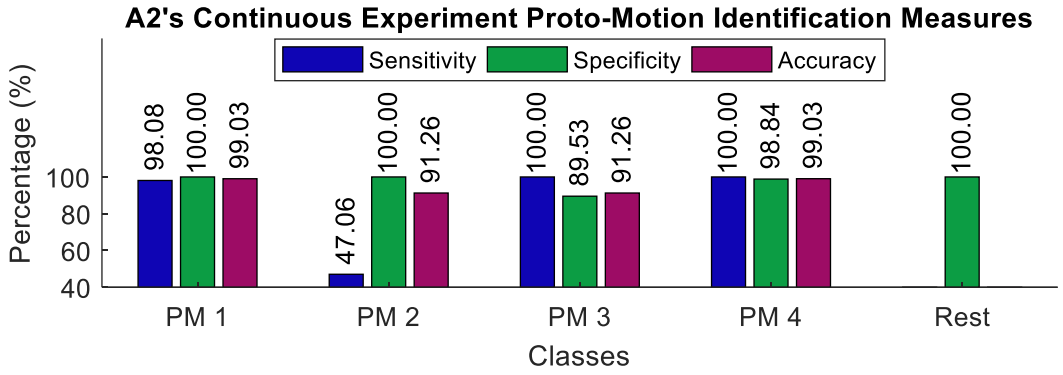

Figure 7.32 - Subject A2's Proto-Motion identification Sensitivity, Specificity and Class Accuracy measures for the four PM classes and the Specificity for the Rest class for the inter-session continuous experiment.

If these measures are compared to the episodic testing measures of this subject, shown in Figure 7.14, it can be noted that the PM 1 sensitivity increased whilst the PM 2 sensitivity decreased between sessions. The increase in PM 1 accuracy is attributed to better motion performances, resulting in better discrimination of this class. Furthermore, while episodic data for this class were only recorded with a starting Closed Fingers grasp, the continuous session was performed as intended, with PM 1 instances rotating between starting gestures. This indicates that by the second session, the subject gathered enough experience to confidently perform these motions. The decrease in accuracy for PM 2 has been linked to inaccurate positioning of the *Myo* band. Whilst such positioning did not affect the classifier's ability to distinguish between the other classes, analysis of the misclassification types concluded that the classifier became more prone to identifying PM 2 as PM 3. This concludes that the classifier may be more sensitive to electrode positionings for some classes than for others.

The results obtained from this subject have also shown that subjects are also capable of improving and adapting to the system when provided with the necessary feedback.

7.3.3. Inter-Session Results Discussion

Electrode positioning discrepancies and lack of motion performance homogeneity, including wrist movements, could have been the external factors responsible for signal inconsistencies in the episodic and continuous sessions performed by subjects *S0* and *A2*.

With regard to sEMG electrode positioning, the ultimate care was taken to ensure similar lateral and distal *Myo* band positioning for all sessions. In fact, prior to *Day 2*

data capture, a small testing session utilising *Day 1* training data was held in order to determine whether the *Myo* band could be more optimally placed so as to maximise the performance of the system using the already trained classifiers. This explains why subject *S0*'s inter-session *Day 2* results showed higher accuracies than *Day 1* results.

However, as has also been visually analysed from separate brief experiments, even the most minor electrode positioning discrepancies could contribute to large signal changes. From a prosthetic point of view, it is envisaged that electrodes would ultimately be fixed in place to the mechanical prosthetic device. Therefore, repetitive electrode positioning may be mechanically solved, by ensuring that the prosthetic arm always fits the amputated limb in the same manner. This also solves between-electrode spacing irregularities. Nevertheless, further insights on electrode displacements effects on this intent interpretation system may be obtained through specified testing.

Meanwhile, for these tests, both correct subject posture as well as motion consistency were imposed. Nevertheless, humans are inconsistent by nature and slight differences in major muscle exertion, such as wrist muscles, may impact recorded data. Whilst subjects were discouraged to activate any wrist muscles during motions, jolting of the wrist during fast motions could have been subconsciously performed. On the other hand, it is envisaged that transradial amputees do not incur such wrist activation issues since motions are not physically performed.

While these inter-session results are promising, future work would need to look into the above-mentioned external causes of such between-session signal discrepancies to determine whether training data sets could be accumulated by intentionally varying such external variables.

7.4. Force Phase Estimation Results and Discussion

To quantitatively analyse the *Force Phase* intent interpretation system explained in Section 5.5, subject *S0* performed a testing session which required grasping contraction levels to be varied in specified time frames, as explained in Section 6.4. These consecutive force output levels, which have been termed as the estimated output signals, for the three different grasps are shown in Figure 7.33.

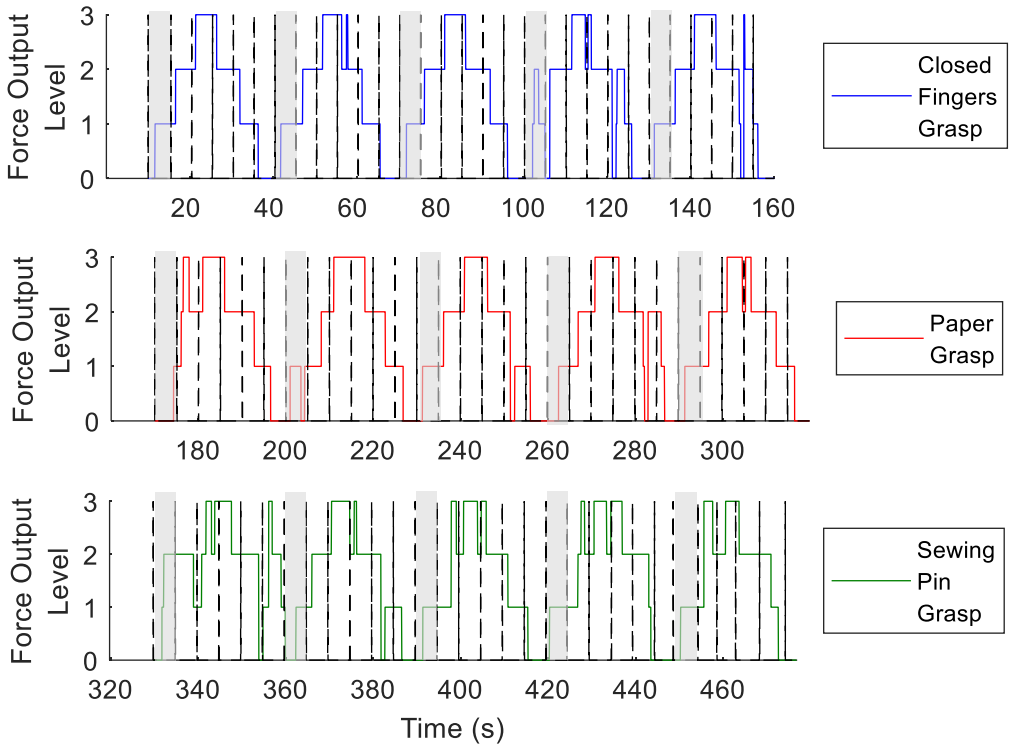

Figure 7.33 - The Force Output Levels which describe the five cycle Estimated signals, $y_{i,m}(s)$, obtained during the Real Time Force Estimation Testing Session where subject S0 performed contractions in the Closed Fingers Grasp, Paper Grasp and Sewing Pin Grasp, respectively. The dashed vertical lines show the instances where the subject was instructed to increase or decrease the Force Level. The shaded areas in grey are the first instance per cycle which cued the subject to reach a Low Force Level from a Rest Force Level. Every grey area suggests a new cycle start. Levels 0,1,2 and 3 refer to the Rest, Low, Medium and High Force Levels, respectively.

It is to be noted that due to the testing sequence design, the number of samples that were spent in the Rest and High force levels were half as much as that for the Low and Medium force levels. This permits an analysis on the estimated contraction levels which should follow a step-wise increase and decrease, accordingly.

As discussed in Section 6.4.2, an algorithm was followed such that grasp and cycle-dependent accuracy and delay values were obtained, leading to average grasp accuracies and delays. Figure 7.34 illustrates how for the first cycle of the Closed Fingers grasp, the ideal signal was aligned with the estimated signal in accordance to its first rising edge. This was done for all five cycles within the three grasp types, in accordance to the delay incurred between the initial cued cycle start and the actual change in estimated force level. The accuracy and delay values obtained per cycle as well as their average are provided in Table 7.5 and Table 7.6, respectively.

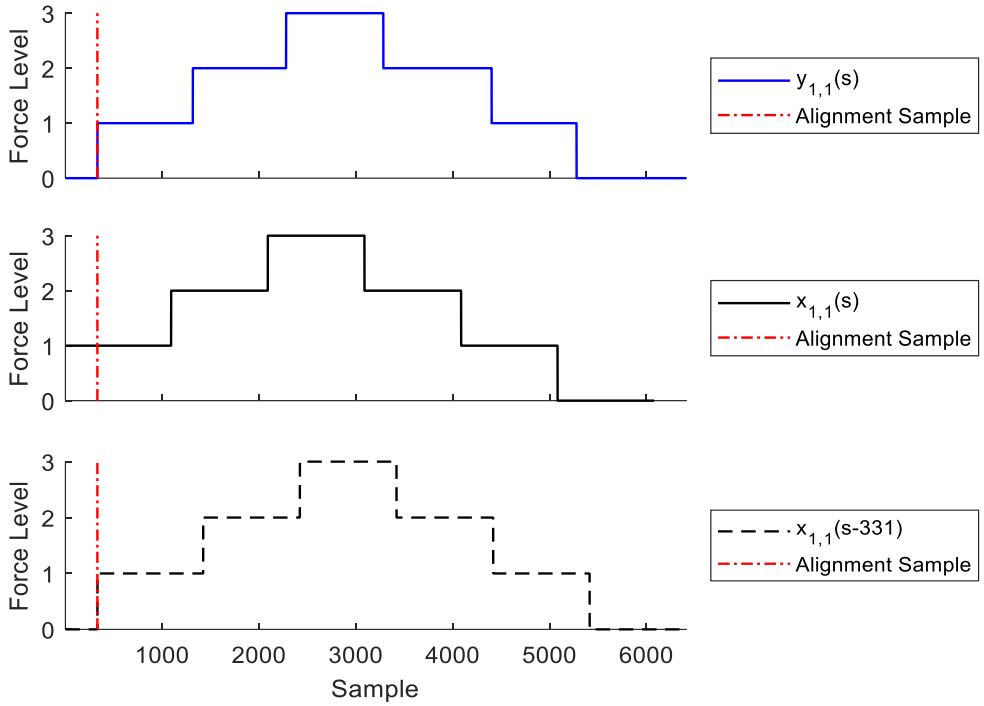

Figure 7.34 - The Estimated signal, $y_{1,1}(s)$, Ideal signal, $x_{1,1}(s)$ and Ideal signal shifted by the alignment sample value of 331, $x_{1,1}(s-331)$, for Cycle 1 of the Closed Fingers Grasp performed by subject S0. Levels 0,1,2 and 3 refer to the Rest, Low, Medium and High Force Levels, respectively. The sampling rate was 200Hz.

Table 7.5 - The Accuracy of the Estimated force levels in comparison to the Ideal force levels following signal alignment in accordance to the delays listed in Table 7.6 for the separate cycles for all three grasps, as well as the mean grasp Accuracy.

	$\boldsymbol{Accuracy_{i,1}}$ **(%)**	$\boldsymbol{Accuracy_{i,2}}$ **(%)**	$\boldsymbol{Accuracy_{i,3}}$ **(%)**	$\boldsymbol{Accuracy_{i,4}}$ **(%)**	$\boldsymbol{Accuracy_{i,5}}$ **(%)**	$\boldsymbol{\overline{Accuracy_i}}$ **(%)**
Closed Fingers Grasp $(\boldsymbol{i = 1})$	91.64	91.50	90.49	72.01	87.30	86.59
Paper Grasp $(\boldsymbol{i = 2})$	58.24	74.58	93.46	75.05	90.96	78.46
Sewing Pin Grasp $(\boldsymbol{i = 3})$	53.57	77.68	81.26	66.67	75.29	70.89

Table 7.6 - The Delay in number of samples incurred between the first rising edge of the Ideal signal per cycle and the first rising edge of the Estimated signal per cycle, also referred to as the alignment sample. The mean grasp Delay is also provided.

	$d_{i,1}$	$d_{i,2}$	$d_{i,3}$	$d_{i,4}$	$d_{i,5}$	$\overline{d_i}$
Closed Fingers Grasp ($i = 1$)	331	282	319	385	238	311
Paper Grasp ($i = 2$)	862	198	268	503	290	424.2
Sewing Pin Grasp ($i = 3$)	400	539	351	163	344	359.4

From Table 7.6, it can be deduced that for a sampling rate of 200Hz, the average grasp delays corresponded to 1555 ms, 2121 ms and 1797 ms for the Closed Fingers grasp, Paper grasp and Sewing Pin grasp, respectively. Since such long delays are user perceivable, it was important to factor out the sources of delay. Figure 7.35 shows the 331 sample delay between the initial cued instance of the first cycle of the Closed Fingers grasp and the first rising edge instance recorded from the estimated force level output. The normalized proportional control signal is shown since it provides the best visual representation of the subject's muscular efforts. From Figure 7.35, it is clear that the subject started to react to the sound cue at approximately 200 samples after the intended software cue, amounting to a delay of approximately one second. Since human response delay is only a fraction of this delay, typically approximate to 300 ms, the majority of this delay was traced back to an intrinsic delay within the *Matlab* software when instructed to perform the audio cue.

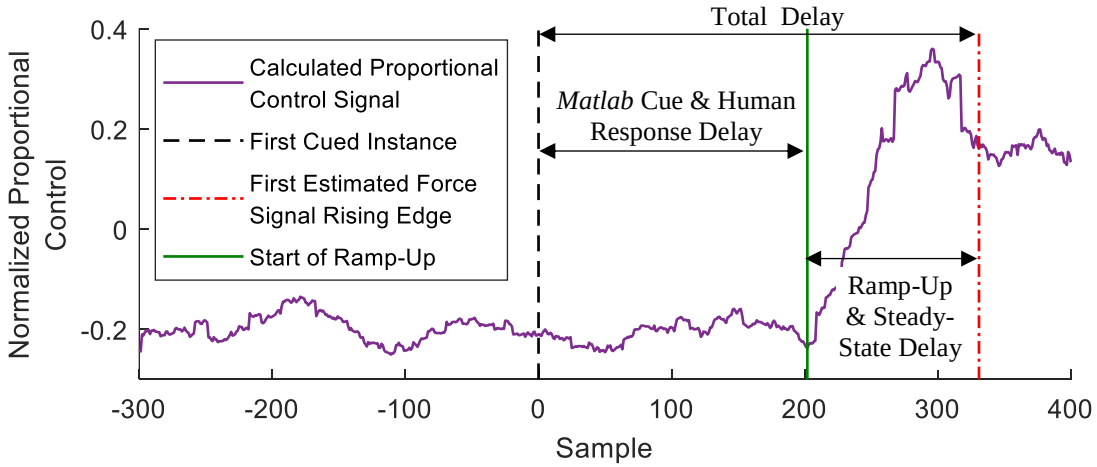

Figure 7.35 - A visualisation of the causes amounting to the long delays between the first intended cued instance for the first cycle of the Closed Fingers grasp and the actual instance of the first rising edge recorded from the estimated force level output.

The remaining delay of approximately 130 samples was caused by ramp-up and steady-state delay which was partly dependent on the subject's muscular control. This delay includes the algorithm specifications, including the smoothing of the proportional control signal and the 200 ms force level estimation steady-state requirement. Thus, it may be concluded that the delays obtained for each cycle were partly contributed by the delayed behaviour of the cued signal itself, muscular contraction ramping-up speed as well as system delays introduced for a more stable force level output.

Whilst the exact instance of the audio cue is unknown for all cycles, even in between the different levels of the cycles themselves, further work is required to determine the exact delays that are introduced when switching between the different force levels, by considering a more reliable cuing alternative.

The discrepancy between the delay and accuracy results obtained for all three grasps suggested that the subject had the best control over the force levels whilst in the Closed Fingers grasp, achieving the highest mean accuracy of 86.59% and the shortest average delay of 1555 ms. This muscular control proved to be tougher during the Paper grasp experiment in terms of delay, and tougher during the Sewing Pin grasp experiments in terms of force estimation accuracy. These difficulties may have been due to the subject having had a harder time ramping-up or ramping-down the muscular levels from the previous force levels whilst exerting steady muscular levels within the pre-defined activity bands for the set amount of time.

The accuracy results are also in line with what can be visually seen in Figure 7.33, with more force level overshoots occurring for the Sewing Pin grasp with much smoother and more stable transitions happening for the Closed Fingers grasp. This suggests that the set force level threshold values may need to be individually treated, specifying algorithm boundary values as well as hysteresis boundary levels in accordance to the grasp.

For a more in-depth analysis of the level of control that the subject had in the different grasps for the different force levels, sensitivity and specificity plots are shown in Figure 7.36 and Figure 7.37, respectively. These sensitivity and specificity values were obtained after taking all cycles within a grasp into consideration.

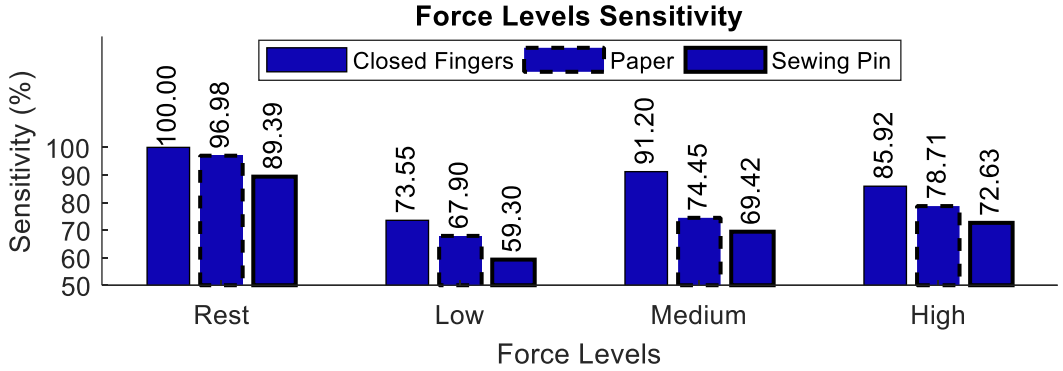

Figure 7.36 - The overall Sensitivity considering the four force levels for the aggregate of all five cycles for the Closed Fingers Grasp, Paper Grasp and Sewing Pin Grasp experiments, respectively.

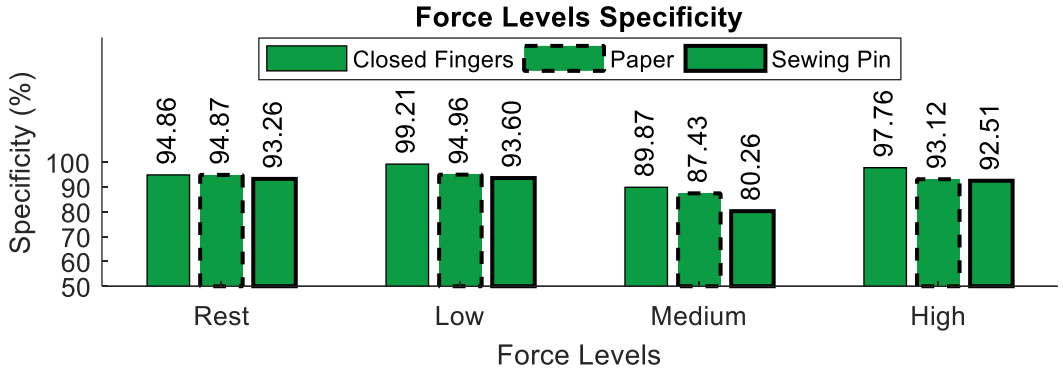

Figure 7.37 - The overall Specificity considering the four force levels for the aggregate of all five cycles for the Closed Fingers Grasp, Paper Grasp and Sewing Pin Grasp experiments, respectively.

From these figures, it is evident that the sensitivities for all levels followed the same pattern, such that the Closed Fingers grasp resulted in the highest sensitivities, followed by the Paper grasp and Sewing Pin grasp accordingly. This pattern was also noted for the specificities plot, except for slight differences in the Rest force level. The system was the least capable of detecting the Low force level for all three grasps with the highest number of FPs having been detected for the Medium force level, indicating that the threshold values for these two levels require the most attention and adjustments.

Scheme et al. [69] noted that wrist flexion/extension force control resulted in significantly better results when compared to other wrist and hand contractions. They discussed that this may be due to the physiological differences that comes about with the different contractions, such that the best performers are known to be driven by large muscles. Other gestures requiring larger combinations of deeper and smaller forearm muscles, which are more difficult to detect, resulted in poorer results. In this work, the large wrist muscles were not being used, only focusing on the detection of the wider range of deeper and smaller muscles, which may be the cause of the less

accurate (< 90%) force control. Whether this accuracy would increase with further rigorous training and system threshold tweaking would need to be studied in future work. Reducing the experienced delay for the best accuracy between grasps is also desirable.

Furthermore, since this test has only been performed by one subject, it is envisaged that for different subjects, different boundary feature values will need to be set, with the goal of setting realistic contraction ranges that are comfortable for the user to achieve, whilst also being distinguishable from the other force levels.

7.5. Final Results Discussion and Conclusion

From these results, different subjects have obtained different motion detection results, Proto-Motion identification measures, and overall accuracy rates, also showing diverse capabilities of the implemented system with detecting and differentiating between the four PMs and the Resting state. Nevertheless, whilst only subject *S0* had multiple training opportunities, the results have clearly shown that very high motion identification accuracies may still be obtained with very little training. The suitability of the designed *Movement Phase* intent interpretation system has also been confirmed from the results obtained by both upper limb amputees.

It has been discussed how the congenital amputee faced a bigger struggle with discriminating between the instructed motions, unlike subject *A2*, who felt comfortable performing the different motions, except for the Open Hand. Whilst this cannot be confirmed without further testing with a larger number of amputees, it is envisaged that congenital amputees, unlike non-congenital amputees, might have less success with operating such a control system, due to differences in their brain cortical mapping [155]. After all, due to their non-existent experience with performing such motions, the sense of intuition is essentially missing, requiring large amounts of training for successful results. Nevertheless, the results obtained from both subjects are very promising.

From statistical tests performed on LDA and SVM system results, it was concluded that the differences in mean measures obtained for the different *Movement Phase* stages were not statistically significant. Thus, there was no reason to believe that the non-parametric SVM classifiers were superior for the implemented intent interpretation systems in comparison to the less than ideal LDAs.

Continuous tests performed by subjects *S0* and *A2* also provided highly satisfactory results whilst inter-session reliability proved to be sufficient. Such reliability, however, is only satisfactory when electrode placement is done in accordance to the maximisation of results with the use of systems trained with previously recorded data.

Meanwhile, all results obtained in this work, including the inter-session results, were all based on data collected from ideal setups, such that the subjects were not fatigued whilst they remained in the same arm posture throughout the sessions. This was the scope of this work, with this design acting as the first step towards obtaining a system which may eventually be integrated with a mechanical prosthetic hand.

The *Force Phase* intent interpretation system was also tested by one subject and it was concluded that satisfactory performance rates were obtained for the three different grasps, for the four force levels. The Closed Fingers grasp resulted in the highest accuracy with the smallest delay, indicating that it was easier for the subject to control the force levels for this grasp, in comparison to the others. The large delays that were incurred per cycle were also broken down, such that it was also deduced that the *Matlab* software was introducing delays which were out of the experimenter's control. A more in-depth analysis is required in future work to determine whether algorithm boundaries and thresholds need to be set for the individual grasp types, with the participation of more subjects whilst also looking into further detail as to whether the subject and system dependent delays may be reduced.

8. Conclusion and Future Work

As has been identified in the introduction of this dissertation, the primary objective of this research project was to systematically develop a practical solution for the control of an artificial hand which best addresses the trade-off problem between simplicity, dexterity and usability. Due to this, these three attributes were defined, highlighting what prosthetic intent interpretation system capabilities would satisfy each and every attribute. Following a thorough literature review, the main elements that were to be considered for a successful solution were identified, leading to the development of the final implemented systems considering the *Movement Phases* and *Force Phases*, accordingly. The main findings and achievements of this work as well as suggested future work are discussed below.

8.1. Findings

From the reviewed literature, it was concluded that for this work, the sEMG phenomenon was to be used as the intuitive myoelectric mean to provide the user intent to the intent interpretation system for an upper limb prosthetic device. This review also led to choosing a pattern recognition system and a proportional control system for intent interpretation during *Movement Phases* and *Force Phases*, respectively, due to the advantages that they offered with respect to the three-attribute trade-off.

A disagreement found in the literature was whether transient signals provided discriminatory information as steady-state signals did. Since this work focussed on providing the user with the most intuitive solution for prosthetic control during both *Movement* and *Force Phases*, specific experiments were performed on the biceps muscle to determine whether both dynamic and static contractions contained discriminatory information. Whilst this was proved to be true, sEMG signals during both contraction types were characterised with respect to the exerted velocities and forces. It was concluded that the peak EMG RMS point during a dynamic contraction generally represents the maximal kinetics of the arm movement whilst the best characterisation of a steady state signal with respect to force is with every sample in time. These findings were then separately used in the *Movement Phase* and *Force Phase* intent interpretation strategies.

From these findings, the novel proposed system was devised such that the developed system is capable of tracking the natural flow of the user's intended motions, in

accordance to the transition between the initial and end grasp postures of the four chosen Proto-Motions.

Through the separation of transient and steady state EMG signals which are due to dynamic and static contractions, respectively, the system has also been designed to be more intuitively controlled. Motion detection and identification algorithms have therefore been solely based on the maxima values extracted from the transient portion of the sEMG signals generated through the motion itself. This implementation specifically targets the transient maxima, such that no classification post-processing is required, also reducing system delay. Meanwhile, continuously extracted steady-state sEMG features are utilised to estimate the force level of the three closing grasps.

The literature overwhelmingly proved that the LDA classifier was the most popular classifier in the upper limb prosthetic field, mostly due to its simplicity and high performance. The high performance of this classifier was also proved in this work, which was also compared to linear SVM classifiers in Section 7.1.6 such that no statistical significance was found between the two. While many different feature sets have been used in the literature for pattern recognition, the RMS feature proved to also obtain good results, even though it was not used in conjunction with other features. The extraction of the RMS feature from a sliding window of 250 ms with a single sample displacement of 5 ms was also found to be successful.

From this work, it was also concluded that the errors that may be introduced with continuous class classification as implemented in some literature, could be reduced by the introduction of the *Movement Detection Stage*. An additional conclusion was that the search for the RMS maxima in the *Movement Identification Stage* following the *Movement Detection Stage* was optimally done within a time-window WL_M of 200 ms.

This work has also highlighted the fact that congenital and non-congenital amputees may have different abilities and may require different training regimes in comparison to each other. It was also determined that amputees may also achieve high performance values, similar or better than normal limbed subjects, as was the case for subject *A2*. Nevertheless, the amputee pool in this work was very small and statistical conclusions could not be reached.

From inter-session tests, it was concluded that changes between the signals on different recording days are the cause of decline in system performance. However, the results obtained from both subjects *S0* and *A2* showed that inter-session success is possible.

From the *Force Phase* tests, it was noted that large delays were present between the first cued instance to the first rising edge of the estimated force signal. In Section 7.4, this was deduced to be a culmination of *Matlab* delays in performing the audio cue, human reaction delays, ramping-up delays as well as steady-state contraction delays. Whilst the latter two were partly subject controlled, also having been affected by the implementation of the algorithm, the others were not. These delays are to be considered for future system improvements.

8.2. Achievements

One of the main achievements is that the designed intent interpretation framework satisfies the trade-off between the simplicity, dexterity and usability attributes. Simplicity has been satisfied through the use of the sEMG phenomenon, utilising eight different sEMG electrodes, symmetrically placed around the forearm, to continuously detect the user's intentions. In the meantime, dexterity has been satisfied through the use of a multi-class linear pattern recognition system (LDA/SVM) which is capable of discriminating between the four chosen Proto-Motions, as well as the resting state. Meanwhile, usability has been satisfied through the introduction of a *Movement Detection* stage in the *Movement Phase* intent interpretation system, such that reliability is increased with less class predictions required to be made. Further usability was also introduced through the utilisation of sEMG amplitudes to estimate the force levels of the grasps, in real-time. This resemblance to human hand functionality helps users to more readily accept the device, leading to a more usable system.

Thus, the system was designed in such a way such that it successfully maximised the trade-off between the simplicity, dexterity and usability attributes. The natural human sense of intuition was exploited while still providing the user with the capability of performing a vast majority of activities of daily living, in a reliable and practical way. It was also important that the design resembled human hand operation in all its different aspects. This successful trade-off is in comparison to the prosthetic devices and systems listed in Chapter 2 such as the highly simple on/off controlled prosthetics which then offer minimal dexterity, or the highly dexterous hands listed in Table 2.1, which require unintuitive and less than simple control commands.

For offline *Movement Phase* systems using LDA classifiers, *Movement Detection* sensitivities exceeded 95% for all seven subjects. Meanwhile, class sensitivities, class specificities and class accuracies for the *Proto-Motion Identification Stage* varied per

subject. Overall accuracies encapsulating the results from the two stages resulted in a mean accuracy value of 92.31% ± 6.57% for the normal-limbed subjects and overall accuracies of 67.22% and 91.94% for amputee subjects *A1* and *A2*, respectively. Overall, subject *S0*, who had the most training experience out of all the subjects, achieved the highest accuracy rates. Considering the fact that subject *A1* was a congenital amputee with minimal experience of missing limb muscular activation, all the results achieved are highly satisfactory. These results proved to be satisfactory also in comparison to the literature, as discussed in Section 7.1.5.

Continuous tests performed by subjects *S0* and *A2* resulted in comparable results to the episodic tests, indicating high performance of the system in real-time. Meanwhile, inter-session analysis concluded that the overall accuracy of the *Movement Phase* system has been found to decrease when trained with data acquired on a different day, as was expected. Nevertheless, the results were still satisfactory when the EMG electrodes were placed as close as possible to the optimal positions which guaranteed high signal repeatability in comparison to previous data acquisition.

From the *Force Phase* experiments performed by subject *S0*, a mean accuracy larger than 70% was achieved for all the three tested grasps. It was also concluded that the subject had more control over the Closed Fingers grasp than over the other two grasps, resulting in a higher accuracy and a smaller mean delay than the Paper grasp and the Sewing Pin grasp.

In order to achieve the results presented in this work, a lot of work was required in order to design and program all the different algorithms within different stages of the project. These algorithms included different signal processing techniques, especially with the various experimental protocols. Other specific algorithms were also implemented in order to post-process all the data that was recorded, to finally obtain meaningful results. All algorithmic work was programmed on *Matlab*, which also required interfacing with the third party *Myo* band SDK for real-time EMG data collection. Interfacing was also done with the *Unity* software through the Internet protocol suite (TCP/IP) in order to provide the subjects with real-time feedback of the hand simulation developed by my MAProHand colleague.

The work done on the biceps in Chapter 4 also required further training on how to use the different sensors as well as how to synchronise them using BIOPAC's

AcqKnowledge data acquisition and analysis software. Training was also required to use the Vicon system, and its software.

One of the largest achievements in this work was the success of recruiting subjects, albeit the challenges caused by the global pandemic. This was especially challenging due to the small pool of transradial amputees on the island, which resulted to be even smaller once it was decided that only those amputees below the COVID at-risk age would be made eligible. The promise of keeping a safe environment for all subjects who willingly participated in this work was always kept, ensuring safe practise.

The biggest achievement of this work, however, was the fact that the amputee subject *A2* enjoyed experiencing real-time feedback of his performed motions during his second testing session. Through the *Unity* interface, the subject could feel, even if for a short while, that his missing limb was actually functioning the way he intended it to, even though it was physically absent.

8.3. Future Work

Whilst the work done on this project was substantial, further work is required in order to have a more reliable and successful system to be used in conjunction with a prosthetic hand in the real world.

In future work, the *Movement Phase* and *Force Phase* intent interpretation systems need to be combined, as was briefly explained in Section 5.3, such that a complete system could be fully integrated with a mechanical prosthesis. Such an integration would allow the system to be tested in a real-life setup where the subjects are required to perform ADLs in specified amounts of time. This would determine how well the system operates with changes in arm posture, longer times of the system in use, muscle fatigue and contraction variations, amongst others. Furthermore, the determination of the cause(s) of EMG signal differences between sessions is required so that attempts can be made to minimize them.

This system has only been implemented by considering one signal feature, the RMS and by implementing linear classifiers, LDAs and SVMs. In order to determine whether any accuracy improvements may be made to the intent interpretation framework, different combinations of features and (linear and non-linear) classifiers would also need to be analysed, such that the ideal combination could be determined. The detection of the movement detection false positives also needs further analysis

such that the analysis could then be fairly done in accordance to whether such instances were classifier misclassifications or actual uncued movements.

A more in-depth analysis on the *Force Phase* intent interpretation system is also to be done such that it is determined whether different algorithmic threshold levels are required to be set for the different grasps. Since the *Force Phase* system analysis was only done on one subject, the implemented algorithm is to be tested on more subjects, especially including amputees.

Since the end use of such a system is for amputees, a longitudinal study is to be done with a larger pool of amputee subjects, including both congenital and non-congenital amputees to determine whether improvements over muscular contractions are in fact possible with further training. Further discussions with amputees are also to be held in order to better determine what results in the most natural action intent system since it was especially noted that the amputee subjects found it challenging to rest in the end grasp after performing any of the Proto-Motions, which was not the case for the normal-limbed subjects.

In conclusion, while it is clear that a lot of future work is still required in order to determine whether the designed system is in fact reliable to use in a real-time setup, the results that have been obtained in this dissertation have been satisfactory for use in an ideal laboratory setup. Furthermore, such results were obtained from a system which was specifically designed to successfully balance the trade-off between the simplicity, dexterity and usability attributes. This is the first step towards obtaining a finalised system which may eventually be used by amputees, in conjunction with the physical minimal anthropomorphic hand currently under design, to achieve the end objective of MAProHand.

References

[1] F. Cordella, A. L. Ciancio, R. Sacchetti, A. Davalli, A. G. Cutti, E. Guglielmelli and L. Zollo, "Literature Review on Needs of Upper Limb Prosthesis Users," *Frontiers in Neuroscience,* vol. 10, p. 209, 2016.

[2] A. Ciancio, F. Cordella, E. Guglielmelli and L. Zollo, "Current Achievements and Future Directions of Hand Prostheses Controlled via Peripheral Nervous System," in *The Hand - Perception, Cognition, Action*, Cham, Springer International Publishing, 2017, pp. 75-95.

[3] A. Fougner, Ø. Stavdahl, P. J. Kyberd, Y. G. Losier and P. A. Parker, "Control of Upper Limb Prostheses: Terminology and Proportional Myoelectric Control—A Review," *IEEE Transactions on Neural Systems and Rehabilitation Engineering,* vol. 20, no. 5, pp. 663 - 677, 2012.

[4] M. Atzori and H. Müller, "Control Capabilities of Myoelectric Robotic Prostheses by Hand Amputees: A Scientific Research and Market Overview," *Frontiers in Systems Neuroscience,* vol. 9, no. 162, 2015.

[5] D. Dalli and M. A. Saliba, "Addressing Simplicity, Dexterity and Usability of Compact, Multi-Degree-of-Freedom Mechatronic Devices," in *IEEE International Conference on Advanced Intelligent Mechatronics (AIM)*, Alberta, 2016.

[6] D. Dalli and M. A. Saliba, "The University of Malta Minimal Anthropomorphic Robot (UM-MAR) Hand II," in *IEEE International Conference on Advanced Intelligent Mechatronics (AIM),* Alberta, 2016.

[7] M. A. Saliba, "MAProHand Project Proposal," University of Malta, 2018 (unpublished).

[8] P. Parker, K. Englehart and B. Hudgins, "Control Of Powered Upper Limb Prostheses," in *Electromyography: Physiology, Engineering, and Noninvasive Applications,* Hoboken, John Wiley & Sons, Inc., 2004, pp. 453-475.

[9] M. R. Dawson, J. P. Carey and F. Fahimi, “Myoelectric training systems,” *Expert Review of Medical Devices,* vol. 8, no. 5, pp. 581-589, 2011.

[10] P. Konrad, The ABC of EMG - A Practical Introduction to Kinesiological Electromyography, Scottsdale: Noraxon INC. USA., 2005.

[11] E. Criswell, Cram's Introduction To Surface Electromyography, Second Edition, Sudbury: Jones and Bartlett Publishers, 2011.

[12] W. Gaine, C. Smart and M. Bransby-Zachary, “Upper Limb Traumatic Amputees,” *Journal of Hand Surgery,* vol. 22B, no. 1, pp. 73-76, 1997.

[13] E. Vasluian, C. K. van der Sluis, A. J. van Essen, J. E. H. Bergman, P. U. Dijstra, H. A. Reinders-Messelink and H. E. K. de Walle, “Birth prevalence for congenital limb defects in the northern Netherlands: a 30-year population-based study,” *BMC Musculoskeletal Disorders,* vol. 14, no. 323, pp. https://doi.org/10.1186/1471-2474-14-323, 2013.

[14] A. Esquenazi, “Upper Limb Amputation, Rehabilitation, & Prosthetic Restoration,” in *CURRENT Diagnosis & Treatment: Physical Medicine & Rehabilitation*, Pennsylvania, McGraw-Hill Education, 2015, pp. 453-459.

[15] M. H. Mohd Zaini, S. A. Ahmad, M. H. Marhaban and W. Z. Wan Hasan, “UPM prosthetic hand system design - preliminary results,” in *IEEE Student Conference on Research and Development*, Cyberjaya, 2011.

[16] R. Beasley, “General considerations in managing upper limb amputations,” *Orthopaedic Clinics of North America,* vol. 12, no. 4, pp. 743-749, 1981.

[17] Ottobock, “Info for upper limb amputees & their families,” Ottobock, 2013. [Online]. Available: https://www.ottobock.co.uk/prosthetics/info-for-amputees/information-for-upper-limb-amputees-and-their-families/. [Accessed 24 January 2021].

[18] P. Geethanjali, “Myoelectric control of prosthetic hands: State-of-the-art review,” *Medical Devices: Evidence and Research,* vol. 9, no. 1, pp. 247-255, 2016.

[19] Ottobock, “Passive arm prostheses,” Ottobock, [Online]. Available: https://www.ottobockus.com/prosthetics/upper-limb-prosthetics/solution-overview/passive-arm-prostheses/. [Accessed 25 January 2021].

[20] T. Inc., “Volleyball Barrage,” Bold City Agency LLC & Brian Brown Designs, [Online]. Available: https://www.trsprosthetics.com/product/vollyeball-barrage/. [Accessed 14 August 2021].

[21] R. Pursley, “Harness patterns for upper-extremity prostheses,” *Artificial Limbs,* vol. 2, no. 3, pp. 26-60, 1955.

[22] A. Bottomley, “Myo-Electric Control Of Powered Prostheses,” *The Journal Of Bone And Joint Surgery,* vol. 47B, no. 3, pp. 411-415, 1965.

[23] P. Parker, K. Englehart and B. Hudings, “Myoelectric signal processing for control of powered limb prostheses,” *Journal of Electromyography and Kinesiology,* vol. 16, no. 6, pp. 541-548, 2006.

[24] C. Castellini, R. Kõiva, C. Pasluosta, C. Viegas and B. M. Eskofier, “Tactile Myography: An Off-Line Assessment of Able-Bodied Subjects and One Upper-Limb Amputee,” *Technologies,* vol. 6, no. 2, p. 38, 2018.

[25] N. Jaquier, M. Connan, C. Castellini and S. Calinon, “Combining Electromyography and Tactile Myography to Improve Hand and Wrist Activity Detection in Prostheses,” *Technologies,* vol. 5, no. 4, p. 64, 2017.

[26] A. Dwivedi, Y. Kwon, A. J. McDaid and M. Liarokapis, “EMG Based Decoding of Object Motion in Dexterous, In-Hand Manipulation Tasks,” in *7th IEEE International Conference on Biomedical Robotics and Biomechatronics (Biorob),* Enschede, 2018.

[27] B. Popov, “The Bio-Electrically Controlled Prosthesis,” *The Journal of Bone and Joint Surgery. British volume,* Vols. 47-B, no. 3, pp. 421-424, 1965.

[28] D. Lovely, “Signals and Signal Processing for Myoelectric Control,” in *Powered Upper Limb Prostheses: Control, Implementation and Clinical Application*, Berlin, Springer-Verlag, 2004, pp. 35-54.

[29] C. Battye, A. Nightingale and J. Whillis, “The Use Of Myo-Electric Currents In The Operation Of Prostheses,” *The Journal Of Bone And Joint Surgery,* vol. 37B, no. 3, pp. 506-510, 1955.

[30] H. H. Sears and J. Shaperman, “Proportional Myoelectric Hand Control: An Evaluation,” *American Journal Of Physical Medicine & Rehabilitation,* vol. 70, no. 1, pp. 20-28, 1991.

[31] C. Cipriani, F. Zaccone, S. Micera and M. C. Carrozza, “On the Shared Control of an EMG-Controlled Prosthetic Hand: Analysis of User–Prosthesis Interaction,” *IEEE Transactions On Robotics,* vol. 24, no. 1, pp. 170-184, 2008.

[32] B. Hudgins, P. Parker and R. N. Scott, “A New Strategy for Multifunction Myoelectric Control,” *IEEE Transactions On Biomedical Engineering,* vol. 40, no. 1, pp. 82-94, 1993.

[33] Össur, “i-Limb® Quantum,” Össur, [Online]. Available: https://www.ossur.com/en-us/prosthetics/arms/i-limb-quantum. [Accessed 23 January 2021].

[34] Ottobock, “Axon-Bus® Prosthetic System,” Ottobock, [Online]. Available: https://shop.ottobock.us/Prosthetics/Upper-Limb-Prosthetics/Michelangelo-Axon-Bus-System/Michelangelo-Hand-AxonHook/Axon-Bus%C2%AE-Prosthetic-System/p/8K5000. [Accessed 23 January 2021].

[35] Ottobock, “bebionic,” Ottobock, [Online]. Available: https://www.ottobockus.com/prosthetics/upper-limb-prosthetics/solution-overview/bebionic-hand/. [Accessed 23 January 2021].

[36] V. S. GmbH, “VINCENTevolution2,” Vincent Systems GmbH, [Online]. Available: https://www.vincentsystems.de/evolution2. [Accessed 23 January 2021].

[37] G. Kanitz, C. Cipriani and B. B. Edin, “Classification of Transient Myoelectric Signals for the Control of Multi-Grasp Hand Prostheses,” *IEEE Transactions on Neural Systems and Rehabilitation Engineering,* vol. 26, no. 9, pp. 1756-1764, 2018.

[38] D. Yang, J. Zhao, L. Jiang and H. Liu, “Dynamic Hand Motion Recognition Based On Transient And Steady-State EMG Signals,” *International Journal of Humanoid Robotics,* vol. 9, no. 1, p. 1250007 (18 pages), 2012.

[39] L. Hargrove, Y. Losier, B. Lock, K. Englehart and B. Hudgins, “A Real-Time Pattern Recognition Based Myoelectric Control Usability Study Implemented in a Virtual Environment,” in *29th Annual International Conference of the IEEE EMBS*, Lyon, 2007.

[40] K. Englehart and B. Hudgins, “A Robust, Real-Time Control Scheme for Multifunction Myoelectric Control,” *IEEE Transactions on Biomedical Engineering,* vol. 50, no. 7, 2003.

[41] A. Radmand, E. Scheme, P. Kyberd and K. Englehart, “Investigation of optimum pattern recognition methods for robust myoelectric control during dynamic limb movement,” in *36th Canadian Medical and Biological Engineering Conference*, Ottawa,Ontario, 2013.

[42] Ottobock, “Myo Plus pattern recognition,” Ottobock, [Online]. Available: https://www.ottobockus.com/prosthetics/upper-limb-prosthetics/solution-overview/myo-plus/myo-plus.html. [Accessed 25 January 2021].

[43] N. Jiang, S. Dosen, K.-R. Muller and D. Farina, “Myoelectric Control of Artificial Limbs - Is There a Need to Change Focus?,” IEEE Signal Processing Magazine, 152, 2012.

[44] E. Scheme and K. Englehart, “Electromyogram pattern recognition for control of powered upper-limb prostheses; State of the art and challenges for clinical use,” *Journal of Rehabilitation Research & Development,* vol. 48, no. 6, pp. 643-660, 2011.

[45] T. R. Farrell and R. F. Weir, “A Comparison of the Effects of Electrode Implantation and Targeting on Pattern Classification Accuracy for Prosthesis Control,” *IEEE Transactions On Biomedical Engineering,* vol. 55, no. 9, pp. 2198-2211, 2008.

[46] M. Ortiz-Catalan, R. Branemark and B. Hakansson, “BioPatRec: A modular research platform for the control of artificial limbs based on pattern recognition algorithms,” *Source Code for Biology and Medicine,* vol. 8, no. 11, 2013.

[47] Doctorlib, “Atlas of Anatomy: 22 Neurovasculature,” Doctorlib, 2015-2019. [Online]. Available: https://doctorlib.info/medical/anatomy/24.html. [Accessed 29 May 2020].

[48] E. N. Marieb and K. Hoehn, Human Anatomy & Physiology : Eleventh Edition, Hoboken, New Jersey: Pearson Education Inc., 2019.

[49] A. J. Young, L. J. Hargrove and T. A. Kuiken, “Improving Myoelectric Pattern Recognition Robustness to Electrode Shift by Changing Interelectrode Distance and Electrode Configuration,” *IEEE Transaction on Biomedical Engineering,* vol. 59, no. 3, pp. 645-652, 2012.

[50] C. Kendell, E. D. Lemaire, Y. Losier, A. Wilson, A. Chan and B. Hudgins, “A novel approach to surface electromyography: an exploratory study of electrode-pair selection based on signal characteristics,” *Journal of NeuroEngineering and Rehabilitation,* vol. 9, no. 24, pp. 1-8, 2012.

[51] J. Keating, “Relating Forearm Muscle Electrical Activity to Finger Forces,” Worcester Polytechnic Institute, Worcester, 2014.

[52] A. Gailey, P. Artemiadis and M. Santello, “Proof of Concept of an Online EMG-Based Decoding of Hand Postures and Individual Digit Forces for Prosthetic Hand Control,” *Frontiers in Neurology*, vol. 8, no. 7, pp. 1-15, 2017.

[53] M. Ortiz-Catalan, R. Branemark and B. Hakansson, “Biologically Inspired Algorithms Applied to Prosthetic Control,” in *BioMed 2012*, Innsbruck, Austria, 2012.

[54] G. Li, A. E. Schultz and T. A. Kuiken, “Quantifying Pattern Recognition - Based Myoelectric Control of Multifunctional Transradial Prostheses,” *IEEE Transactions On Neural Systems and Rehabilitation Engineering,* vol. 18, no. 2, pp. 185-192, 2010.

[55] A. M. Simon, L. J. Hargrove, B. A. Lock and T. A. Kuiken, “The Target Achievement Control Test: Evaluating real-time myoelectric pattern

recognition control of a multifunctional upper-limb prosthesis," *The Journal of Rehabilitation Research and Development,* vol. 48, no. 6, pp. 619-627, 2011.

[56] L. J. Hargrove, K. Englehart and B. Hudgins, "A Comparison of Surface and Intramuscular Myoelectric Signal Classification," *IEEE Transactions On Biomedical Engineering,* vol. 54, no. 5, pp. 847-853, 2007.

[57] SENIAM. [Online]. Available: http://www.seniam.org/. [Accessed 27 02 2020].

[58] N. V. Iqbal, K. Subramaniam and S. Asmi P., "A Review on Upper-Limb Myoelectric Prosthetic Control," *IETE Journal of Research,* vol. 64, no. 6, pp. 740-752, 2018.

[59] A. J. Young, L. H. Smith, E. J. Rouse and L. J. Hargrove, "A comparison of the real-time controllability of pattern recognition to conventional myoelectric control for discrete and simultaneous movements," *Journal of NeuroEngineering and Rehabilitation,* vol. 11, no. 5, 2014.

[60] R. C. Gopura, S. V. Bandara and M. Pamuditha, "Recent Trends in EMG-Based Control Methods for Assistive Robots," in *Electrodiagnosis in New Frontiers of Clinical Research,* Croatia, InTech, 2013, pp. 237-268.

[61] A. Dellacasa Bellingegni, E. Gruppioni, G. Colazzo, A. Davalli, R. Sacchetti, E. Guglielmelli and L. Zollo, "NLR, MLP, SVM, and LDA: a comparative analysis on EMG data from people with trans-radial amputation," *Journal of NeuroEngineering and Rehabilitation,* vol. 14, no. 82, 2017.

[62] M. Zia ur Rehman, A. Waris, S. O. Gilani, M. Jochumsen, I. K. Niazi, M. Jamil, D. Farina and E. N. Kamavuako, "Multiday EMG-Based Classification of Hand Motions with Deep Learning Techniques," *Sensors,* vol. 18, no. 2497, 2018.

[63] F. Leone, C. Gentile, A. L. Ciancio, E. Gruppioni, A. Davalli, R. Sacchetti, E. Guglielmelli and L. Zollo, "Simultaneous sEMG Classification of Hand/Wrist Gestures and Forces," *Frontiers in Neurorobotics,* vol. 13, no. 42, 2019.

[64] F. Bian, L. Ruifeng and P. Liang, “SVM Based Simultaneous Hand Movements Classification Using sEMG Signals,” in *IEEE International Conference on Mechatronics and Automation*, Takamatsu, 2017.

[65] P. Shenoy, K. Miller, B. Crawford and R. Rao, “Online electromyographic control of a robotic prosthesis,” *IEEE Transactions on Biomedical Engineering*, vol. 55, no. 3, pp. 1128-1135, 2008.

[66] O. MA and H. H, “Support vector machine-based classification scheme for myoelectric control applied to upper limb,” *IEEE Transactions on Biomedical Engineering*, vol. 55, no. 8, pp. 1956-1965, 2008.

[67] J. J. A. Mendes Junior, M. L. Freitas, H. V. Siqueira, A. E. Lazzaretti, S. F. Pichorim and S. L. Stevan Jr., “Feature selection and dimensionality reduction: An extensivecomparison in hand gesture classification by sEMG in eight channelsarmband approach,” *Biomedical Signal Processing and Control*, vol. 59, pp. 1-11, 2020.

[68] C. Cipriani, C. Antfolk, M. Controzzi, G. Lundborg, B. Rosen and M. Carrozza, “Online myoelectric control of a dexterous hand prosthesis by transradial amputees,” *IEEE Transactions On Neural Systems And Rehabilitation Engineering*, vol. 19, no. 3, pp. 260-270, 2011.

[69] E. Scheme, B. Lock, L. Hargrove, W. Hill, U. Kuruganti and K. Englehart, “Motion Normalized Proportional Control for Improved Pattern Recognition-Based Myoelectric Control,” *IEEE Transactions on Neural Systems and Rehabilitation Engineering*, vol. 22, no. 1, pp. 149-157, 2014.

[70] Y. Li, Q. Zhang, J. Chen and Q. Zhang, “Discrete Hand Motion Intention Decoding Based on Transient Myoelectric Signals,” *IEEE Access*, vol. 7, no. 10.1109/ACCESS.2019.2923455, pp. 81630-81639, 2019.

[71] H. U. Kuriki, F. M. de Azevedo, L. S. O. Takahashi, E. M. Mello, R. d. F. N. Filho and N. Alves, “The Relationship Between Electromyography and Muscle Force,” in *EMG Methods for Evaluating Muscle and Nerve Function* , Rijeka, InTech, 2012, pp. 31-54.

[72] J. Basmajian and D. L. CJ, Muscles Alive (5th edition), Baltimore: Williams and Wilkins, 1985.

[73] B. Mustard and R. Lee, "Relationship between EMG patterns and kinematic properties for flexion movements at the human wrist," *Experimental Brain Research,* vol. 66, no. 2, pp. 247-256, 1987.

[74] C. Disselhorst-Klug, T. Schmitz-Rode and G. Rau, "Surface electromyography and muscle force: limits in sEMG-force relationship and new approaches for applications," *Clinical Biomechanics,* vol. 24, no. 3, pp. 225-235, 2009.

[75] C. J. De Luca, "The Use of Surface Electromyography in Biomechanics," *Journal of Applied Biomechanics,* vol. 13, no. 2, pp. 135-163, 1997.

[76] J. Z. Liu, R. W. Brown and G. H. Yue, "A Dynamical Model of Muscle Activation, Fatigue, and Recovery," *Biophysical Journal,* vol. 82, no. 5, pp. 2344-2359, 2002.

[77] C. De Luca, A. Adam, R. Wotiz, L. Gilmore and S. Nawab, "Decomposition of surface EMG signals," *Journal of neurophysiology,* vol. 96, no. 3, pp. 1646-1657, 2006.

[78] C. J. De Luca, R. S. LeFever, M. P. McCue and A. P. Xenakis, "Behaviour of human motor units in different muscles during linearly varying contractions," *The Journal of Physiology,* vol. 329, pp. 113-128, 1982.

[79] R. S. LeFever and C. J. De Luca, "A Procedure for Decomposing the Myoelectric Signal Into Its Constituent Action Potentials - Part I: Technique, Theory, and Implementation," *IEEE Transactions on Biomedical Engineering,* vol. 29, no. 3, pp. 149-157, 1982.

[80] N. Nazmi, M. A. Abdul Rahman, S.-I. Yamamoto, S. A. Ahmad, H. Zamzuri and S. A. Mazlan, "A Review of Classification Techniques of EMG Signals during Isotonic and Isometric Contractions," *Sensors,* vol. 16, no. 1304, 2016.

[81] J.-J. Luh, G.-C. Chang, C.-K. Cheng, J.-S. Lai and e.-S. Kuo, "Isokinetic elbow joint torques estimation from surface EMG and joint kinematic data: using an

artificial neural network model," *Journal of Electromyography and Kinesiology,* vol. 9, pp. 173-183, 1999.

[82] E. Hanif, "Isokinetic Exercises: The Science, Examples and How You Can Benefit?," Squat Wolf, [Online]. Available: https://squatwolf.com/blog/isokinetic-exercises/. [Accessed 24 02 2020].

[83] J. R. Cram and G. S. Kasman, "The Basics of Surface Electromyography," in *Cram's Introduction to Surface Electromyography, Second Edition*, Sudbury, Jones and Bartlett Publishers, LLC, 2011, pp. 3-171.

[84] J. Basmajian, Muscles Alive, Their Functions Revealed By Electromyography, Second Edition, Baltimore: The Williams & Wilkins Company, 1967.

[85] A. F. Ruiz-Olaya, "Modeling the Human Elbow Joint Dynamics from Surface Electromyography," in *Applications, Challenges, and Advancements in Electromyography Signal Processing*, Hershey, IGI Global, 2014, pp. 114 - 128.

[86] M. Reaz, M. Hussain and F. Mohd-Yasin, "Techniques of EMG signal analysis: detection, processing, classification and applications," *Biological Proceedings Online*, vol. 8, no. 1, pp. 11-35, 2006.

[87] C. De Luca, "Electromyography," in *Encyclopedia of Medical Devices and Instrumentation*, Hoboken, John Wiley Publisher, 2006, pp. 98-109.

[88] N. U. Ahamed, K. Sundaraj, M. Alqahtani, O. Altwijri, M. A. Ali and M. A. Islam, "EMG-force relationship during static contraction: Effects on sensor placement locations on biceps brachii muscle," *Technology and health care: official journal of the European Society for Engineering and Medicine,* vol. 22, no. 4, pp. 505-513, 2014.

[89] H. Cao, S. Boudaoud, F. Marin and C. Marque, "Surface EMG-force modelling for the biceps brachii and its experimental evaluation during isometric isotonic contractions," *Computer Methods in Biomechanics and Biomedical Engineering*, vol. 18, no. 9, pp. 1014-1023, 2014.

[90] J. Vredenbregt and G. Rau, “Surface Electromyography in Relation to Force, Muscle Length and Endurance,” *New Developments in Electromyography and Clinical Neurophysiology,* vol. 1, pp. 607-622, 1973.

[91] E. P. Doheny, M. M. Lowery, D. P. FitzPatrick and M. J. O'Malley, “Effect of elbow joint angle on force–EMG relationships in human elbow flexor and extensor muscles,” *Journal of Electromyography and Kinesiology,* vol. 18, pp. 760-770, 2008.

[92] S. Shankar, R. Gander and B. Brandell, “Changes in the myoelectric signal (MES) power spectra during dynamic contractions,” *Electroencephalography and Clinical Neurophysiology,* vol. 73, no. 2, pp. 142-50, 1989.

[93] J. Miller, R. Croce, W. Smith and M. Horvat, “Contraction Intensity and Velocity on Vastus Lateralis SEMG Power Spectrum and Amplitude,” *Perceptual and Motor Skills,* vol. 114, no. 3, pp. 847-856, 1 6 2012.

[94] M. L. Latash, Neurophysiological Basis of Movement, Champaign: Human Kinetics, 1998.

[95] S. Bouisset and F. Goubel, “Integrated electromyographical activity and muscle work,” *Journal of Applied Physiology,* vol. 35, no. 5, pp. 695-702, 1973.

[96] A. C. Sy and N. T. Bugtai, “Velocity and Acceleration Induced Response to Bicep EMG Signal Threshold for Motion Intention Detection,” in *7th IEEE International Conference Humanoid, Nanotechnology, Information Technology Communication and Control, Environment and Management (HNICEM)*, Palawan, 2014.

[97] C. J. De Luca, “Surface Electromyography: Detection and Recording,” DelSys Incorporated, Natick, 2002.

[98] A. Phinyomark, P. Phukpattaranont and C. Limsakul, “Feature reduction and selection for EMG signal classification,” *Expert Systems with Applications,* vol. 39, no. 8, pp. 7420-7431, 2012.

[99] C. Gielen, K. van den Oosten and F. Pull ter Gunne, “Relation Between EMG Activation Patterns and Kinematic Properties of Aimed Arm Movements,” *Journal of Motor Behavior,* vol. 17, no. 4, pp. 421-442, 1985.

[100] M.-1. Corporation, *Data Sheet Advanced Digital Force Gauges Series 5,* Copiague.

[101] I. BIOPAC Systems, *Goniometers & Torsiometers Product Sheet,* Goleta, 2014.

[102] AURION, “ZEROWIRE MULTICHANNEL ELECTROMYOGRAPHY USER MANUAL,” 04 10 2005. [Online]. Available: https://fccid.io/VH6ZWTX07/User-Manual/User-Manual-903877#downloa1d. [Accessed 24 02 2020].

[103] V. M. S. Ltd., “Vicon T-Series, The world’s next generation motion capture camera,” [Online]. Available: http://www.helmar-ms.pl/helmar-ms/plik/vicon_t-series_nn4244.pdf. [Accessed 25 02 2020].

[104] I. BIOPAC Systems, “MP150 SYSTEMS PRODUCT SHEET,” 17 3 2016. [Online]. Available: https://www.biopac.com/. [Accessed 24 2 2020].

[105] I. BIOPAC Systems, “INTERFACE MODULES PRODUCT SHEET,” 25 6 2016. [Online]. Available: www.biopac.com. [Accessed 24 2 2020].

[106] I. BIOPAC Systems, “DA100C - DIFFERENTIAL AMPLIFIER MODULE PRODUCT SHEET,” 25 3 2019. [Online]. Available: www.biopac.com. [Accessed 24 2 2020].

[107] B.-M. Instruments, “Covidien Kendall Disposable Surface EMG/ECG/EKG Electrodes 1" (24mm) 50pkg,” [Online]. Available: https://bio-medical.com/covidien-kendall-disposable-surface-emg-ecg-ekg-electrodes-1-24mm-50pkg.html. [Accessed 27 02 2020].

[108] H. J. Hermens, B. Freriks, C. Disselhorst-Klug and G. Rau, “Development of recommendations for SEMG sensors and sensor placement procedures,” *Journal of Electromyography and Kinesiology,* vol. 10, no. 5, pp. 361-374, 2000.

[109] A. Patla, B. Hudgins, P. Parker and R. Scott, “Myoelectric signal as a quantitative measure of muscle mechanical output,” *Medical and Biological Engineering and Computing,* vol. 20, no. 3, pp. 319-328, 1982.

[110] E. Criswell, Cram's Introduction To Surface Electromyography, Second Edition, MA: Jones and Bartlett Publishers, 2011.

[111] B. Bigland and O. Lippold, “The Relation Between Force, Velocity And Integrated Electrical Activity In Human Muscles,” *The Journal of Physiology,* vol. 123, no. 1, pp. 214-224, 1954.

[112] A. H. Al-Timemy, R. N. Khushaba, G. Bugmann and J. Escudero, “Improving the Performance Against Force Variation of EMG Controlled Multifunctional Upper-Limb Prostheses for Transradial Amputees,” *IEEE Transactions on Neural systems and Rehabilitation Engineering,* vol. 24, no. 6, pp. 650-661, 2016.

[113] D. Stegeman and H. Hermens, “Standards for surface electromyography: the European project "Surface EMG for non-invasive assessment of muscles (SENIAM)”,” 2007.

[114] A. S. P. Sousa and J. M. R. S. Tavares, “Surface electromyographic amplitude normalization methods: A review,” in *Electromyography: New Developments, Procedures and Applications,* Nova Science Publishers, Inc., 2012, pp. 85-102.

[115] C. J. Payton and R. M. Bartlett, Biomechanical Evaluation of Movement in Sport and Exercise: The British Association of Sport and Exercise Sciences Guidelines, Cornwall: TJ International Ltd.,, 2008.

[116] P. W. Hodges and B. H. Bui, “A comparison of computer-based methods for the determination of onset of muscle contraction using electromyography,” *Electroencephalography and clinical Neurophysiology,* vol. 101, pp. 511-519, 1996.

[117] S. H. Brown and J. Cooke, “Amplitude- and Instruction- Dependent Modulation of Movement-related Electromyogram Activity in Humans,” *The Journal of Physiology,* vol. 316, pp. 97-107, 1981.

[118] J. Lawrence and C. De Luca, “Myoelectric signal versus force relationship in different human muscles,” *Journal of Applied Physiology,* vol. 54, no. 6, pp. 1653-1659, 1983.

[119] D. A. Winter, BIiomechanics And Motor Control Of Human Movement, Fourth Edition, New Jersey: John Wiley & Sons, Inc., 2009.

[120] Y. Aquilina, “Development of the mechanical framework for a minimal anthropomorphic prosthetic hand,” Ph.D. thesis, University of Malta, In Progess.

[121] N. Inc., “North,” [Online]. Available: https://www.bynorth.com/. [Accessed 17 February 2021].

[122] P. Visconti, F. Gaetani, G. Zappatore and P. Primiceri, “Technical Features and Functionalities of Myo Armband: An Overview on Related Literature and Advanced Applications of Myoelectric Armbands Mainly Focused on Arm Prostheses,” *International Journal on Smart Sensing and Intelligent Systems,* vol. 0, no. 0, pp. 1-25, 2018.

[123] S. Pizzolato, L. Tagliapietra, M. Cognolato, M. Reggiani, H. Müller and M. Atzori, “Comparison of six electromyography acquisition setups on hand movement classification tasks,” *PLoS One,* vol. 12, no. 10, 2017.

[124] A. L. A. Calado, *Comparison between Low-Cost and High-End sEMG Sensors for the Control of a Transradial Myoelectric Prosthesis,* Lisbon: University of Lisbon, November 2017.

[125] P. U. Murillo, R. J. Moreno and O. F. Avilés S, “Individual Robotic Arms Manipulator Control Employing Electromyographic Signals Acquired by Myo Armbands,” *International Journal of Applied Engineering Research,* vol. 11, no. 23, pp. 11241-11249, 2016.

[126] M. Tomaszewski, “Myo SDK MATLAB MEX Wrapper,” 19 October 2017. [Online]. Available: https://github.com/mark-toma/MyoMex. [Accessed 8 February 2021].

[127] C. M. Bishop, Pattern Recognition and Machine Learning, New York: Springer Science+Business Media, LLC, 2006.

[128] R. O. Duda, P. E. Hart and D. G. Stork, Pattern Classification, New York: John Wiley & Sons, Inc., 2001.

[129] C. van Meegen, S. Schnackenberg and U. Ligges, "Unequal Priors in Linear Discriminant Analysis," *Journal of Classification,* vol. 37, no. DOI: 10.1007/s00357-019-09336-2, pp. 598-615, 2020.

[130] C. J. Huberty, Applied Discriminant Analysis, New York: Wiley-Interscience, 1994.

[131] Y. Guo, T. Hastie and R. Tibshirani, "Regularized linear discriminant analysis and its application in microarrays," *Biostatistics,* vol. 8, no. 1, pp. 86-100, 2007.

[132] MathWorks, "fitcdiscr," [Online]. Available: https://www.mathworks.com/help/stats/fitcdiscr.html. [Accessed 11 February 2021].

[133] M. A. Oskoei and H. Hu, "Myoelectric control systems - A survey," *Biomedical Signal Processing and Control,* vol. 2, pp. 275-294, 2007.

[134] M. Hakonen, H. Piitulainen and A. Visala, "Current state of digital signal processing in myoelectric interfaces and related applications," *Biomedical Signal Processing and Control,* vol. 18, no. http://dx.doi.org/10.1016/j.bspc.2015.02.009, pp. 334-359, 2015.

[135] S. Zhou, D. L. Lawson, W. E. Morrison and I. Fairweather, "Electromechanical delay in isometric muscle contractions evoked by voluntary, reflex and electrical stimulation," *European Journal of Applied Physiology and Occupational Physiology,* vol. 70, no. 2, pp. 138-145, 1995.

[136] C. M. Smith, T. J. Housh, E. C. Hill, G. O. Johnson and R. J. Schmidt, "Dynamic versus isometric electromechanical delay in non-fatigued and fatigued muscle: A combined electromyographic, mechanomyographic, and force approach," *Journal of Electromyography and Kinesiology,* vol. 33, no. DOI: 10.1016/j.jelekin.2017.01.008, pp. 34-38, 2017.

[137] T. Hastie, R. Tibshirani and J. Friedman, The Elements of Statistical Learning: Data Mining, Interference, and Prediction, New York: Springer-Verlag, 2009.

[138] K. Mardia, "Measures of Multivariate Skewness and Kurtosis with Applications," *Biometrika,* vol. 57, no. 3, pp. 519-530, 1970.

[139] B. G. E. P., "A General Distribution Theory for a Class of Likelihood Criteria," *Biometrika,* vol. 36, no. 3/4, pp. 317-346, 1949.

[140] R. G. Brereton, "The chi squared and multinormal distributions," *Journal of Chemometrics,* vol. 29, pp. 9-12, 2015.

[141] V. N. Vapnik, The Nature of Statistical Learning Theory, New York: Springer, 1995.

[142] C. J. Burges, "A Tutorial on Support Vector Machines for Pattern Recognition," *Data Mining and Knowledge Discovery,* vol. 2, no. 2, pp. 121-167, 1998.

[143] MathWorks, "fitcsvm," MathWorks, [Online]. Available: https://www.mathworks.com/help/stats/fitcsvm.html#bt7nhte-3. [Accessed 15 April 2021].

[144] T. G. Dietterich and G. Bakiri, "Solving Multiclass Learning Problems via Error-Correcting Output Codes," *Journal of Artificial Intelligence Research,* vol. 2, pp. 263-286, 1995.

[145] E. L. Allwein, R. E. Schapire and Y. Singer, "Reducing Multiclass to Binary: A Unifying Approach for Margin Classifiers," *Journal of Machine Learning Research,* vol. 1, pp. 113-141, 2000.

[146] MathWorks, "fitcecoc," MathWorks, [Online]. Available: https://www.mathworks.com/help/stats/fitcecoc.html. [Accessed 15 April 2021].

[147] A. M. Simon, K. Stern and L. J. Hargrove, "A Comparison of Proportional Control Methods for Pattern Recognition Control," in *33rd Annual International conference of the IEEE EMBS*, Boston, Massachusetts, 2011.

[148] A. T. Belyea, K. B. Englehart and E. J. Scheme, “A proportional control scheme for high density force myography,” *Journal of Neural Engineering,* vol. 15, no. 4, pp. 10.1088/1741-2552/aac89b, 2018.

[149] T. H. Inc., “Typhoon HIL Documentation,” Typhoon HIL Inc., [Online]. Available: https://www.typhoon-hil.com/documentation/typhoon-hil-software-manual/References/hysteresis_function.html. [Accessed 15 February 2021].

[150] M. Stone, “Cross-Validatory Choice and Assessment of Statistical Predictions,” *Journal of the Royal Statistical Society: Series B (Methodological),* vol. 36, no. 2, pp. 111-147, 1974.

[151] M. Sokolova, N. Japkowicz and S. Szpakowicz, “Beyond Accuracy, F-Score and ROC: A Family of Discriminant Measures for Performance Evaluation,” in *AI 2006: Advances in Artificial Intelligence*, Hobart, 2006.

[152] MathWorks, “boxplot,” Mathworks, [Online]. Available: https://www.mathworks.com/help/stats/boxplot.html. [Accessed 26 February 2021].

[153] Student, “The Probable Error of a Mean,” *Biometrika,* vol. 6, no. 1, pp. 1-25, 1908.

[154] G. R. Quinn and M. J. Keough, Experimental Design and Data Analysis for Biologists, Cambridge, UK: Cambridge University Press, 2002.

[155] K. T. Reilly, C. Mercier, M. H. Schieber and A. Sirigu, “Persistent hand motor commands in the amputees' brain,” *Brain*, vol. 129, no. 8, pp. 2211-2223, 2006.